

RL-TR-96-91
In-House Report
June 1996



NUMERICAL FM DEMODULATION ENHANCEMENTS

Andrew J. Noga

APPROVED FOR PUBLIC RELEASE; DISTRIBUTION UNLIMITED.

19960730 117

**Rome Laboratory
Air Force Materiel Command
Rome, New York**

PRINTS QUALITY IMPROVED 1

This report has been reviewed by the Rome Laboratory Public Affairs Office (PA) and is releasable to the National Technical Information Service (NTIS). At NTIS it will be releasable to the general public, including foreign nations.

RL-TR-96-91 has been reviewed and is approved for publication.

APPROVED:



RONALD W. CWIRKO
Chief, Signal Intelligence Division
Intelligence & Reconnaissance Directorate

FOR THE COMMANDER:



JOSEPH CAMERA
Technical Director
Intelligence & Reconnaissance Directorate

If your address has changed or if you wish to be removed from the Rome Laboratory mailing list, or if the addressee is no longer employed by your organization, please notify Rome Laboratory/IRAP, Rome, NY 13441. This will assist us in maintaining a current mailing list.

Do not return copies of this report unless contractual obligations or notices on a specific document require that it be returned.

REPORT DOCUMENTATION PAGE

Form Approved
OMB No. 0704-0188

Public reporting burden for this collection of information is estimated to average 1 hour per response, including the time for reviewing instructions, searching existing data sources, gathering and maintaining the data needed, and completing and reviewing the collection of information. Send comments regarding this burden estimate or any other aspect of this collection of information, including suggestions for reducing this burden, to Washington Headquarters Services, Directorate for Information Operations and Reports, 1215 Jefferson Davis Highway, Suite 1204, Arlington, VA 22202-4302, and to the Office of Management and Budget, Paperwork Reduction Project (0704-0188), Washington, DC 20503.

1. AGENCY USE ONLY (Leave Blank)		2. REPORT DATE June 1996	3. REPORT TYPE AND DATES COVERED In-House 1 Apr 94 - 1 Apr 96
4. TITLE AND SUBTITLE NUMERICAL FM DEMODULATION ENHANCEMENTS		5. FUNDING NUMBERS PE - 62702F PR - 4594 TA - 15 WU - A1	
6. AUTHOR(S) Andrew J. Noga		8. PERFORMING ORGANIZATION REPORT NUMBER RL-TR-96-91	
7. PERFORMING ORGANIZATION NAME(S) AND ADDRESS(ES) Rome Laboratory/IRAP 32 Hangar Road Rome, NY 13441-4114		9. SPONSORING/MONITORING AGENCY NAME(S) AND ADDRESS(ES) Rome Laboratory/IRAP 32 Hangar Road Rome, NY 13441-4114	
11. SUPPLEMENTARY NOTES Rome Laboratory Project Engineer: Andrew J. Noga/IRAP, (315) 330-4581		10. SPONSORING/MONITORING AGENCY REPORT NUMBER	
12a. DISTRIBUTION/AVAILABILITY STATEMENT Approved for public release, distribution unlimited.		12b. DISTRIBUTION CODE	
13. ABSTRACT (Maximum 200 words) An analysis of the backward difference numerical FM demodulation process is presented. Both theoretical and simulated results are given. A method of enhancing the performance of the demodulator in specific receive-signal conditions using frequency feedback techniques is developed and evaluated. The receive-signal conditions that are addressed are frequency deviations that are large relative to the bandwidth of the message signal, a low uniform sample rate resulting from decimation, and noise strengths that yield values of input carrier-to-noise ratio of the order of ten (10) db or more.			
14. SUBJECT TERMS Numerical FM demodulation, frequency feedback demodulation, discrete-time signal processing			15. NUMBER OF PAGES 196
			16. PRICE CODE
17. SECURITY CLASSIFICATION OF REPORT UNCLASSIFIED	18. SECURITY CLASSIFICATION OF THIS PAGE UNCLASSIFIED	19. SECURITY CLASSIFICATION OF ABSTRACT UNCLASSIFIED	20. LIMITATION OF ABSTRACT U/L

TABLE OF CONTENTS

List of Figures	v
List of Abbreviations	xi
List of Conventions	xiii
1 Introduction	1
1.1 Research Objectives and Methodology	2
1.2 Background	3
1.3 Overview	7
2 Complex Numbers and the Generalized Pre-envelope	11
2.1 The Geometric Interpretation of Complex Numbers	12
2.1.1 Further Considerations of the Phase Angle α	15
2.2 Processing Considerations in the Utilization of Complex Numbers	17
2.2.1 Implicit Versus Explicit Addition of Phase Angles	18
2.3 The Discrete-Time Bandpass Signal Representation and Generation of the Corresponding Complex Envelope	21
2.3.1 A Method of Complex Envelope Generation: The Numerical Quadrature Downconversion Process	21
2.3.2 A Method of Complex Envelope Generation: The Complex Bandpass Filter	26
2.4 The Generalized Pre-envelope	30

3 Analysis of a Class of Numerical FM Discrimination Methods Amenable to Real-Time Implementation	33
3.1 The Ideal Discrete-Time FM (DTFM) Signal	34
3.2 Numerical FM Discrimination (Demodulation) Techniques	36
3.2.1 The Direct and Indirect Methods of Numerical FM Discrimination	38
3.2.1.1 Direct Numerical FM Discrimination	38
3.2.1.2 Indirect Numerical FM Discrimination	41
3.2.2 Arcsine Numerical FM Discrimination	42
3.2.3 Arccosine Numerical FM Discrimination	47
3.2.4 Principal-Value Arctan Numerical Discrimination	48
3.2.5 Standard Numerical FM Discrimination	50
3.2.6 Discrimination Method Comparison	56
3.2.6.1 Selection of a Baseline Numerical Discrimination Technique	59
3.3 Sampling Rate Considerations	61
3.3.1 Sampling Rate Requirements of the Ideal Complex DTFM Signal	66
3.3.2 Instantaneous Frequency Aliasing and the Generalized Pre-envelope	73
4 Backward Difference Numerical Discrimination in the Presence of Additive White Gaussian Noise	77
4.1 Phase Modulation Recovery and Phase Domain Performance Measures	78
4.1.1 The Phase Noise Probability Density Function	82

4.1.2 The Phase Cycle-Slip	86
4.1.3 The Phase Noise and Phase Cycle-Slip Performance Statistics	88
4.2 Recovery of the Sheet Sequence, $r(nT_s)$, in the Presence of AWGN	93
4.2.1 Case I: The Unmodulated Carrier and Perfectly Tuned Receiver	96
4.2.2 Case II: The Unmodulated Carrier and Off-tuned Receiver	102
4.2.3 Case III: The Angle Modulated Carrier and Off-tuned Receiver	108
4.3 The Mean-Square Phase Noise Performance Measure, \hat{E}_p	117
4.4 Relating Instantaneous Frequency Aliasing and the Phase Cycle-Slip	123
4.5 Concluding Remarks	124
5 Simulation of a Method of Discriminator Performance Enhancement for Efficient Processing of Large β DTFM Signals at Low Input CNR	125
5.1 Objective	126
5.1.1 The FM with Feedback (FMFB) Demodulator	128
5.1.2 The Numerical FM with Feedback Demodulator	129
5.2 The Reconstituted Numerical FM with Feedback (RNFMFB) Demodulator	134
5.2.1 The Implemented RNFMFB Demodulator Phase-Domain Model	138
5.3 RNFMFB Demodulation Performance Simulation Results	143
6 Conclusions and Areas of Future Research	149
6.1 Conclusions	150
6.2 Areas of Future Research	152

APPENDIX A - The Backward Difference Approximation to Time Differentiation	155
A.1 Acquisition of a Bandlimited Signal and its Corresponding Derivative	156
A.2 The Frequency Response of the Time Derivative Process	156
A.3 The Frequency Response of the Backward Difference Approximation	160
A.4 The Equivalent Distortion Response	162
APPENDIX B - The Backward Difference Phase Estimate Representation	165
B.1 The Effects of the Presence of Phase Noise	166
References	171

LIST OF FIGURES

<u>Figure</u>	<u>Title</u>	<u>Page</u>
(2-1)	The geometric interpretation of a nonrandom complex valued constant, $C = C_R + jC_I$, as a point in two-dimensional space.	12
(2-2)	The vector interpretation of a nonrandom complex valued constant, $C = C_R + jC_I$, referenced to the origin.	13
(2-3)	The process $g[\alpha]$.	18
(2-4)	The numerical quadrature downconverter.	23
(2-5)	A set of representative signal magnitude spectrum plots: a) Representative input signal magnitude spectrum; b) The frequency shifted and pre-filtered signal magnitude spectrum; c) The magnitude spectrum of the resulting complex envelope estimate.	25
(2-6)	A set of signal magnitude spectrum plots which are representative of the complex bandpass filter method of complex envelope generation: a) Representative input signal magnitude spectrum; b) The result of filtering this input signal with the complex bandpass filter; c) The magnitude spectrum of the resulting complex envelope estimate.	30
(3-1)	a) The conventional analog discriminator. b) Representative magnitude frequency response of the slope-circuit.	51
(3-2)	The discrete-time slope-circuit derived from the backward difference filter.	53
(3-3)	The Standard numerical FM discrimination method.	55

(3-4)	Bandpass signal pre-acquisition processing. a) A representative magnitude spectrum of a bandpass signal of bandwidth $B' < B$, centered at f_c Hz. b) The magnitude frequency response of the analog local oscillator used for frequency downconversion. c) The result of convolving the original spectrum with the local oscillator spectrum; $f_c = B/2$, $W = f_c + B'/2$. d) The representative spectrum of the desired signal, $s(t)$, prior to conversion from analog to discrete time.	62
(3-5)	Representative spectra depicting a special case of Bedrosian's product theorem. a) The magnitude spectrum of the real lowpass signal, $a(t)$. b) The magnitude spectrum of the approximately bandlimited signal, $\cos[\alpha(t)]$, where $\alpha(t) = 2\pi f_c t + \phi(t) - \theta$. c) The magnitude spectrum of the product, $a(t)\cos[\alpha(t)]$.	64
(3-6)	A set of signal magnitude spectrum depicting the decimation of the complex envelope by a factor of 2. a) $ \mathcal{J}\{\tilde{s}(nT_s)\} $ with F_s equal to the acquisition sample rate. b) $2 \mathcal{J}\{\tilde{s}(nT_s)\} $ with F_s equal to the decimated sample rate.	67
(3-7)	The geometric representation of the process $g[\alpha, f_o]$ as a rotation of the angle reference axes used in the modulo 2π process $g[\alpha]$. In this particular representation, a positive value of f_o is depicted.	75
(4-1)	The model of the ideal complex DTFM signal in the presence of bandlimited additive white Gaussian noise.	80
(4-2)	The phase plane representation of the phase noise, η , at an arbitrary time, $t = nT_s$.	84
(4-3)	The Middleton probability density function of the phase noise, η , at various values of the carrier-to-noise ratio, ρ .	86
(4-4)	Representative pdfs arising in the formation of $v(nT_s)$.	95
(4-5 a)	Analytically predicted number of <i>negative</i> phase cycle-slips vs. ρ ; Case I : The unmodulated carrier and perfectly tuned receiver.	100

(4-5 b)	Experimentally predicted number of <i>negative</i> phase cycle-slips vs. ρ (4 simulation runs); Case I : The unmodulated carrier and perfectly tuned receiver.	100
(4-5 c)	Analytically predicted number of <i>positive</i> phase cycle-slips vs. ρ ; Case I : The unmodulated carrier and perfectly tuned receiver.	101
(4-5 d)	Experimentally predicted number of <i>positive</i> phase cycle-slips vs. ρ (4 simulation runs); Case I : The unmodulated carrier and perfectly tuned receiver.	101
(4-6 a)	Analytically predicted number of <i>negative</i> phase cycle-slips vs. ρ ; Case II : The unmodulated carrier and off-tuned receiver $(2\pi f_e T_s = \pi\delta_e = \pi/10)$.	106
(4-6 b)	Experimentally predicted number of <i>negative</i> phase cycle-slips vs. ρ (4 simulation runs); Case II : The unmodulated carrier and off-tuned receiver $(2\pi f_e T_s = \pi\delta_e = \pi/10)$.	106
(4-6 c)	Analytically predicted number of <i>positive</i> phase cycle-slips vs. ρ ; Case II : The unmodulated carrier and off-tuned receiver $(2\pi f_e T_s = \pi\delta_e = \pi/10)$.	107
(4-6 d)	Experimentally predicted number of <i>positive</i> phase cycle-slips vs. ρ (4 simulation runs); Case II : The unmodulated carrier and off-tuned receiver $(2\pi f_e T_s = \pi\delta_e = \pi/10)$.	107
(4-7 a)	Analytically predicted number of <i>negative</i> phase cycle-slips vs. ρ ; Case III : The angle modulated carrier and off-tuned receiver $(2\pi f_e T_s = \pi\delta_e = \pi/10, \text{with sinusoidal modulation, } \gamma = 17.067,$ $\delta_m = 0.2930)$.	113
(4-7 b)	Experimentally predicted number of <i>negative</i> phase cycle-slips vs. ρ (4 simulation runs); Case III : The angle modulated carrier and off-tuned receiver $(2\pi f_e T_s = \pi\delta_e = \pi/10, \text{with sinusoidal modulation, } \gamma = 17.067, \delta_m = 0.2930)$.	113

(4-7 c)	Analytically predicted number of <i>positive</i> phase cycle-slips vs. ρ ; Case III : The angle modulated carrier and off-tuned receiver ($2\pi f_e T_s = \pi\delta_e = \pi/10$, with sinusoidal modulation, $\gamma = 17.067$, $\delta_m = 0.2930$).	114
(4-7 d)	Experimentally predicted number of <i>positive</i> phase cycle-slips vs. ρ (4 simulation runs); Case III : The angle modulated carrier and off-tuned receiver ($2\pi f_e T_s = \pi\delta_e = \pi/10$, with sinusoidal modulation, $\gamma = 17.067$, $\delta_m = 0.2930$).	114
(4-8 a)	Analytically predicted number of <i>negative</i> phase cycle-slips vs. ρ ; Case III : The angle modulated carrier and off-tuned receiver ($2\pi f_e T_s = \pi\delta_e = \pi/10$, with sinusoidal modulation, $\gamma = 17.067$, $\delta_m = 0.5859$).	115
(4-8 b)	Experimentally predicted number of <i>negative</i> phase cycle-slips vs. ρ (4 simulation runs); Case III : The angle modulated carrier and off-tuned receiver ($2\pi f_e T_s = \pi\delta_e = \pi/10$, with sinusoidal modulation, $\gamma = 17.067$, $\delta_m = 0.5859$).	115
(4-8 c)	Analytically predicted number of <i>positive</i> phase cycle-slips vs. ρ ; Case III : The angle modulated carrier and off-tuned receiver ($2\pi f_e T_s = \pi\delta_e = \pi/10$, with sinusoidal modulation, $\gamma = 17.067$, $\delta_m = 0.5859$).	116
(4-8 d)	Experimentally predicted number of <i>positive</i> phase cycle-slips vs. ρ (4 simulation runs); Case III : The angle modulated carrier and off-tuned receiver ($2\pi f_e T_s = \pi\delta_e = \pi/10$, with sinusoidal modulation, $\gamma = 17.067$, $\delta_m = 0.5859$).	116
(4-9 a)	Analytically predicted output phase SNR in the message bandwidth; (sinusoidal modulation, $\gamma = 17.067$).	119
(4-9 b)	Experimentally predicted output phase SNR in the message bandwidth; (sinusoidal modulation, $\gamma = 17.067$).	119
(4-10 a)	Analytically predicted number of <i>negative</i> phase cycle-slips vs. ρ ; Case III : The angle modulated carrier and off-tuned receiver ($2\pi f_e T_s = \pi\delta_e = \pi/10$, with sinusoidal modulation, $\gamma = 17.067$, $\delta_m = 0.8203$).	121

(4-10 b)	Experimentally predicted number of <i>negative</i> phase cycle-slips vs. ρ (4 simulation runs); Case III : The angle modulated carrier and off-tuned receiver ($2\pi f_e T_s = \pi\delta_e = \pi/10$, with sinusoidal modulation, $\gamma = 17.067$, $\delta_m = 0.8203$).	121
(4-10 c)	Analytically predicted number of <i>positive</i> phase cycle-slips vs. ρ ; Case III : The angle modulated carrier and off-tuned receiver ($2\pi f_e T_s = \pi\delta_e = \pi/10$, with sinusoidal modulation, $\gamma = 17.067$, $\delta_m = 0.8203$).	122
(4-10 d)	Experimentally predicted number of <i>positive</i> phase cycle-slips vs. ρ (4 simulation runs); Case III : The angle modulated carrier and off-tuned receiver ($2\pi f_e T_s = \pi\delta_e = \pi/10$, with sinusoidal modulation, $\gamma = 17.067$, $\delta_m = 0.8203$).	122
(5-1)	The continuous-time (analog) FM with feedback (FMFB) demodulator.	128
(5-2)	A numerical implementation of the FMFB demodulator.	130
(5-3)	The Type I reconstituted numerical FM with feedback demodulator.	135
(5-4)	Implemented Type II reconstituted numerical FM with feedback demodulator.	137
(5-5)	The phase-domain model of the implemented Type II RNFMB demodulator.	139
(5-6 a)	Experimentally predicted number of <i>negative</i> phase cycle-slips vs. ρ (4 simulation runs); <u>Backward Difference Discriminator</u> , ($2\pi f_e T_s = \pi\delta_e = \pi/10$, with sinusoidal modulation, $\gamma = 17.067$, $\delta_m = 0.8203$).	145
(5-6 b)	Experimentally predicted number of <i>negative</i> phase cycle-slips vs. ρ (4 simulation runs); <u>RNFMB Demodulator</u> , ($2\pi f_e T_s = \pi\delta_e = \pi/10$, with sinusoidal modulation, $\gamma = 17.067$, $\delta_m = 0.8203$).	145

(5-6 c)	Experimentally predicted number of <i>positive</i> phase cycle-slips vs. ρ (4 simulation runs); <u>Backward Difference Discriminator</u> , ($2\pi f_e T_s = \pi \delta_e = \pi/10$, with sinusoidal modulation, $\gamma = 17.067$, $\delta_m = 0.8203$).	146
(5-6 d)	Experimentally predicted number of <i>positive</i> phase cycle-slips vs. ρ (4 simulation runs); <u>RNFMFB Demodulator</u> , ($2\pi f_e T_s = \pi \delta_e = \pi/10$, with sinusoidal modulation, $\gamma = 17.067$, $\delta_m = 0.8203$).	146
(5-7 a)	Experimentally predicted output phase SNR in message bandwidth; <u>Backward Difference Discriminator</u> (sinusoidal modulation, $\gamma = 17.067$, $\delta_m = 0.8203$).	147
(5-7 b)	Experimentally predicted output phase SNR in message bandwidth; <u>RNFMFB Demodulator</u> (sinusoidal modulation, $\gamma = 17.067$, $\delta_m = 0.8203$).	147
(A-1)	Two methods of acquiring a bandlimited signal, $x(t)$, and its corresponding time derivative. a) A continuous-time method employing an analog time derivative and synchronized Analog to Discrete-time Converter (ADC) pair. b) The discrete-time backward difference approximation, employing a single ADC and difference of consecutive samples.	157
(A-2)	A discrete-time filter which has the same frequency response as System B shown in Figure (A-1).	162
(A-3)	One period of the magnitude frequency responses, $T_s H_A(e^{j\omega T_s}) $ and $T_s H_B(e^{j\omega T_s}) $.	164
(A-4)	One period of the frequency response of the distortion, $H_D(e^{j\omega T_s})$.	164

LIST OF ABBREVIATIONS

AFC	Automatic Frequency Control
AWGN	Additive (bandlimited) White Gaussian Noise
BPF	Bandpass Filter
CNR	Carrier-to-Noise (power) Ratio
DPLL	Digital Phase Lock Loop
DSP	Digital Signal Processing; Digital Signal Processor
DTFM	Discrete-Time Frequency Modulation; Discrete-Time Frequency-Modulated
DTL	Digital Tanlock Loop
FM	Frequency Modulation; Frequency-Modulated
FMFB	Frequency Modulation with Feedback
IF	Intermediate Frequency
LPF	Lowpass Filter
NCO	Numerically Controlled Oscillator
PLL	Phase Lock Loop
RNFMFB	Reconstituted Numerical Frequency Modulation with Feedback
VCO	Voltage Controlled Oscillator

LIST OF CONVENTIONS

some specific notation:

$ A_+(t) $	(positive) envelope of the noise-contaminated, modulated complex exponential signal
$ A_+(t)_{BPF} $	(positive) envelope of the bandpass filtered, noise-contaminated, modulated complex exponential signal
a	positive constant amplitude of the modulated complex exponential signal
$a(t)$	positive time-varying amplitude of the modulated complex exponential signal
$\alpha(t)$	true phase modulation (in radians)
δ	DTFM modulation index
δ_m	DTFM message index
δ_e	DTFM tuning-error index
$\delta(f)$	Dirac delta function
$\delta(nT_s)$	impulse sequence, equal to 1 at index $n = 0$, and equal to 0 for all other indices (Kronecker delta function)
$\eta(t)$	the Middleton distributed phase noise (in radians)
f_c	center frequency (in Hertz) of the positive half of the Nyquist interval, equal to $F/4$
f_o	an arbitrary frequency (in Hertz), positive or negative, in the Nyquist interval
$g[\alpha]$	a modulo 2π process applied to α , as defined in text
$g[\alpha, f_o]$	
nT_s	product of the integer index, n , and the sample time interval, T_s , identifying a set of time instants or a specific time instant, as taken in context (in seconds)

$\Omega = \omega T_s$	normalized radian frequency (in radians) equal to the product of $\omega = 2\pi f$ radians per second, and the interval T_s seconds
$\phi(t)$	true phase message (in radians)
$\hat{\phi}_d(t)$	estimate (in radians) of the true phase message, derived from the backward difference estimate of the derivative of the phase
$\tilde{\phi}_d(t)$	estimate (in radians) of the noise contaminated true phase message, derived from the backward difference estimate of the derivative of the noise contaminated phase
$\phi_i(t)$	instantaneous true phase message (in radians), as defined in text
$\hat{\phi}_i(t)$	instantaneous estimate of the true phase message (in radians), as defined in text
$\tilde{\phi}_i(t)$	instantaneous estimate of the noise-contaminated true phase message (in radians), as defined in text
ρ	input CNR, equal to $a^2/(2\sigma^2)$
$2\sigma^2$	variance of the input (complex) Gaussian noise
$s_+(t, f_o)$	complex-valued generalized pre-envelope sequence equal to the product of the complex envelope sequence, and the complex sequence $\exp[j2\pi f_o t]$
t	real variable representative of continuous time (in seconds), or a specific value of time as taken in context
$X_+(t, f_o)$	complex-valued, noise-contaminated, generalized pre-envelope sequence

some general notation:

$\{.\}_{\text{modulo } 2\pi}$	the remainder of , after division by 2π
\hat{X}	an estimate of the true value, x , or a predicted value of x as taken in context
$x(t) _{t=nT_s}, x(nT_s)$	the sequence obtained from uniform sampling of the signal, $x(t)$, equal to $x(nT_s) = \sum_{k=-\infty}^{\infty} x(kT_s) \cdot \delta([n - k]T_s)$, or a specific value of $x(t)$ at time $t = nT_s$, as taken in context

$E\{X\}$	expected value of the random variable X
$R_{xx}(\tau)$	autocorrelation function of the (wide sense stationary) random process, $X(t)$, found as $E\{X(t_1)X^*(t_2)\}$, $\tau = t_1 - t_2$
$S_{xx}(f)$	the power spectral density, $\mathcal{J}\{R_{xx}(\tau)\}$
$V\{X\}$	variance of the random variable X

continuous-time Fourier transforms: $\mathcal{J}\{x(t)\} = X(f) = \int_{-\infty}^{\infty} x(t)e^{-j2\pi ft} dt$

$$\mathcal{J}^{-1}\{X(f)\} = x(t) = \int_{-\infty}^{\infty} X(f)e^{j2\pi ft} df$$

discrete-time Fourier transforms: $\mathcal{J}\{x(nT_s)\} = X(e^{j\Omega}) = \sum_{n=-\infty}^{\infty} x(nT_s)e^{-j\Omega \cdot n}$

$$\mathcal{J}^{-1}\{X(e^{j\Omega})\} = x(nT_s) = \frac{1}{2\pi} \int_{-\pi}^{+\pi} X(e^{j\Omega})e^{j\Omega \cdot n} d\Omega$$

spectral periodic convolution property:

Let $y(nT_s) = x(nT_s) \cdot h(nT_s)$, then

$$Y(e^{j\Omega}) = X(e^{j\Omega}) \otimes H(e^{j\Omega}) = \frac{1}{2\pi} \int_{-\pi}^{+\pi} X(e^{j\Omega_o})H(e^{j(\Omega-\Omega_o)})d\Omega_o .$$

linear convolution:

$$y(nT_s) = x(nT_s) * h(nT_s) = \sum_{k=-\infty}^{\infty} x(kT_s)h([n-k]T_s)$$

ACKNOWLEDGMENTS

This research has been performed in partial fulfillment of the requirements of the Ph.D. degree in Electrical Engineering at Syracuse University. It is with great appreciation that I acknowledge the contributions others have made to this research. In particular I am thankful to my advisor in this work, Professor Tapan K. Sarkar, who fosters and encourages independence, while keeping research on track with his constructive guidance. Acknowledgment and thanks are also given to Professor Donald D. Weiner, who initially served as advisor pro tem and gave valuable guidance in meeting degree requirements.

Further acknowledgment is given to the management of Rome Laboratory including Mr. Ronald Cwirko and Mr. Joseph Camera who made this opportunity possible, and to Dr. Michael Wicks, Dr. James Michels and Dr. Darryl Greenwood of Rome Laboratory for their guidance.

CHAPTER 1

Introduction

1.1 Research Objectives and Methodology

This research addresses the need to accurately analyze the performance of a particular class of frequency-modulation (FM) numerical demodulation techniques that are amenable to real-time implementation. The class of demodulators to be analyzed are those which apply the backward difference estimate of the time derivative of the phase to produce instantaneous frequency estimates. The receive-signal conditions used for performance analysis purposes are that of a single, discrete-time, constant envelope, frequency-modulated complex exponential in the presence of additive, spectrally uniform, Gaussian noise. With the performance of the backward difference numerical FM demodulator as an established baseline, a further objective is to address the performance enhancement of this demodulator in specific receive-signal conditions, by employing frequency feedback techniques. In this case, the receive-signal conditions of interest are frequency deviations that are large relative to the bandwidth of the message signal, a low sample rate resulting from decimation, and noise strengths that yield values of input carrier-to-noise ratio (CNR) of the order of 10 dB or more.

The performance analysis methodology is a combination of theoretical analyses and experimental verifications via non-real-time computer simulations. More correctly, it is the noise-contaminated complex signal that is simulated and used as input to the demodulation processes, for performance measurements and comparisons. The demodulation processes themselves are direct floating-point implementations, and are more appropriately described as being experimental (although non-real-time) in nature.

1.2 Background

Since the pioneering work of Armstrong [1], Carson, and Fry [2], a wealth of research has been conducted in the theory and applications of analog FM communication systems. In particular, previous research has included various analyses of the effects of noise on the received signal, such as the work presented by Middleton [3, 4], Stumpers [5], and Rice [6]. More recently, with the advent of high speed digital circuitry and programmable signal processors, interest has turned toward discrete-time implementations of the FM demodulation process.

Various methods have been proposed for performing discrete-time FM demodulation. These include zero-crossing interval averaging for signals where the deviation of the instantaneous frequency from the carrier is small, and iterative recovery techniques using zero-crossings as proposed by Wiley, Schwarzlander and Weiner [7] where large frequency deviations exist. In contrast to these techniques, the research to be presented addresses the problem of numerical demodulation of uniformly sampled discrete-time signals, using the complex analytic signal. An example of this type of system is the discrete-time FM receiver proposed by Kammeyer [8], in which sampled in-phase and quadrature signals are derived from the received analog signal and used to produce a linear estimate of the original message modulation. The processing proposed by Kammeyer is consistent with the continuous-time definition given by Cramer and Leadbetter [9] of instantaneous frequency, as the derivative (with respect to time) of the recovered phase component of the analytic signal.

The earliest work employing the Hilbert transform for generation of the complex signal is commonly attributed to Gabor [10]. Among the quality references on the generation and use of the discrete-time analytic signal are the works presented by Urkowitz [11], and Oppenheim and Schafer [12]. Consistent with Nuttall's work [13], Urkowitz correctly avoids the previously held notion that the modulated signal must have a bandwidth which is much smaller than the intermediate frequency (IF) at which demodulation takes place within the receive chain. This notion is also quite contrary to the common usage of what are referred to as "zero-IF" receivers employing in-phase and quadrature signals, where such a bandwidth to IF ratio becomes infinite. Practical generation of the sampled analytic signal is presented by Schussler and Weith [14], Regalia and Mitra [15], and Rosenkranz [16] using Hilbert transform techniques. Schussler and Weith present a design method for a causal recursive Hilbert transformer. The work by Regalia and Mitra allows for the use of known half-band filter design techniques in designing Hilbert transform systems. Rosenkranz presents an alternate sampling-based method to the more commonplace quadrature downconversion process presented in [11].

In addition to the reception and demodulation of man-made FM signals, research is also being conducted on the concept of instantaneous frequency as applied to the analysis of "naturally" occurring signals, such as animal vocalizations and human voice. Much of this work also relies on the generation of the sampled analytic signal for estimation of the discrete-time instantaneous frequency. Among the more revealing references for the concept of the instantaneous frequency of a discrete-time signal is the work by Boashash, Jones and O'Shea [17]. Although the central difference is used rather than the backward

difference for approximating the time derivative, this work is an example where modulo 2π processing is applied to the instantaneous frequency estimate of "monocomponent" signals, taking into account the circular nature of the Fourier transform of discrete-time signals. (As defined by the authors, a monocomponent signal is one "where there is only one frequency or a narrow range of frequencies varying as a function of time".) Their presented applications include the detection of harmonically related signals, and time-varying filtering.

Included in work since that performed by Armstrong, Carson and Fry has been a considerable amount of effort in the design and analysis of receive systems employing feedback techniques. Part of this previous research is the analysis of devices such as the phase-lock loop (PLL), commonly referenced in texts on communications theory, and the less well known FM with feedback (FMFB) demodulator. The FMFB demodulator as introduced by Chaffee [18] and furthered by Enloe [19] and others, effectively acts as a time-varying or tracking filter. However, rather than changing filter characteristics over time, this device translates the incoming signal in frequency to the fixed center of a bandpass filter. The purpose of the bandpass filter is to reject out of band noise, while passing the narrow range of frequencies centered about the instantaneous frequency of the input signal. Inconsistencies in earlier performance comparisons of the PLL and FMFB demodulators began to be reconciled with Develet's research [20], in which appropriate conditions lead to equivalent servo-mechanisms. Emphasis more recently has been on the discrete-time implementation of these devices.

The evolution of the PLL from continuous-time to various discrete-time implementations is readily apparent in the literature. For example, Rosenkranz [21] has presented a discrete-time approach to the PLL for numerical FM demodulation. The numerical implementation of a PLL is often referred to as a digital PLL (DPLL). The demodulator presented by Rosenkranz is a type of DPLL which is characterized by a non-linear phase detector. Continuous-time PLL devices with a nearly linear phase detector characteristic were studied by Robinson [22] and others, and were referred to as "tanlock loops". As the name implies, the characteristic of the phase detector in these devices approached the piece-wise linear phase characteristic of the arctangent. Research has been conducted on the numerical implementation of the tanlock loop, as evidenced by the work of Lee and Un [23]. Here, the authors present a non-uniform sampling device referred to as the digital tanlock loop (DTL). This numerical implementation is modeled using an exact piece-wise linear phase detector characteristic. As a more recent example, Ono, Aoyama, Hagiwara and Nakagawa [24] have presented a uniform sampling numerical PLL implementation with a linear phase detector. In this work and that of Lee and Un, we begin to see the appropriate trend to mathematically model the modulo 2π process, and include this process in subsequent phase-domain block diagrams and models.

Recently there has been much interest in time-frequency distribution theory and applications. Boashash and White [25] have employed methods of instantaneous frequency estimation to control a time-varying filter. Although the device is properly described as a tracking filter, the technique is more appropriately referred to as an open loop system.

1.3 Overview

As claimed within the work presented by Natali [26], there are relatively few publications pertaining to the automatic frequency control (AFC) loop, a form of tracking device employing frequency feedback. With Natali's research, we begin to see an interest in the performance analysis of numerical FM discriminators, as applied to the AFC loop. Even this work, however, does not include the use or performance analysis of a discrete-time FM discrimination device that has a linear characteristic over the entire Nyquist band. Thus it is evident that a need exists to properly characterize the performance of such discrete-time FM demodulation processes.

In view of the previously stated objectives of this research, we begin in Chapter 2 with the application of the concept of Riemann surfaces to the time-domain phase plane leading to the definition of a modulo 2π process, referred to as $g[\alpha]$. Here, α is a variable representative of an input argument value, and $g[\alpha]$ is the output result. This process is necessary for the proper definition of the instantaneous frequency of a modulated complex exponential sequence. It is also necessary for proper theoretical analysis of the discrete-time angle demodulation processes. This analysis leads to the accurate prediction of changes in the error in Riemann sheet identification at any particular sample instant, referred to as a "phase cycle-slip". We continue in Chapter 2 with the demonstration of the equivalence of the traditional quadrature downconverter and the complex bandpass filter, for generation of the in-phase and quadrature sequences from the original real-valued input sequence. This in turn leads to the concept of the "generalized pre-envelope", as presented and used throughout the research.

The concepts developed in Chapter 2 are subsequently used in Chapter 3 in the development and definition of the numerical FM discrimination process. In Chapter 3, we modify the Arcsine numerical FM demodulator presented by Kammeyer [8], to extend the linear phase detector characteristic to the complete Nyquist frequency band arising in complex-valued systems. We also introduce several other methods of numerical FM demodulation. These include the Arccosine, the Principal-Value Arctan (previously developed by the author), and the Standard numerical FM discriminator. The Standard numerical FM discriminator is derived from the conversion to discrete-time of a continuous-time FM discrimination process. Subsequent demonstration of the equivalence of the presented numerical FM demodulators to the Standard discriminator, and to the better known Direct and Indirect methods, allows us to refer to these devices as numerical FM *discriminators*. Chapter 3 concludes with the development of explicit sample rate requirements for frequency modulated complex exponential sequences. This leads to the definition of a pair of parameters which characterize the modulated complex exponential. These parameters are the relative message sampling rate, γ , and the discrete-time FM (DTFM) modulation index, δ . The definition of the process $g[\alpha]$ is then modified for use with the generalized pre-envelope.

In Chapter 4, an analysis is presented of the performance of the backward difference class of numerical FM demodulators in the presence of additive white (over the Nyquist band) Gaussian noise (AWGN). Both theoretical and experimental results obtained via computer simulations, are presented.

Finally, in chapter 5, we address the issue of performance enhancement of the numerical FM discriminator under specific modulation conditions, through the use of specific frequency feedback techniques. Here, the reconstituted numerical FM with feedback (RNFMFb) demodulator is introduced. Enhanced discriminator performance is demonstrated via computer simulation techniques.

CHAPTER 2

Complex Numbers and the Generalized Pre-envelope

2.1 The Geometric Interpretation of Complex Numbers

The purpose of the proceeding sections is to review the mechanism of the vector representation of complex numbers and complex valued time sequences [27]. A nonrandom complex number, C , can be represented mathematically in Cartesian (i.e., rectangular) coordinates as

$$C = C_R + jC_I , \quad (2-1)$$

where C_R is a real valued number representative of the real constituent of C , and C_I is a real valued number representative of the imaginary constituent of C . The variable j has the usual meaning of the square root of -1. Note that it is the association or pairing of C_R with C_I , combined with rules of complex arithmetic, which facilitate the processing of complex numbers on a computing device.

Geometrically, C can be interpreted as a point in a two-dimensional plane, whose location is determined by the ordered pair of real numbers, $\{C_R, C_I\}$, as depicted in Figure (2-1).

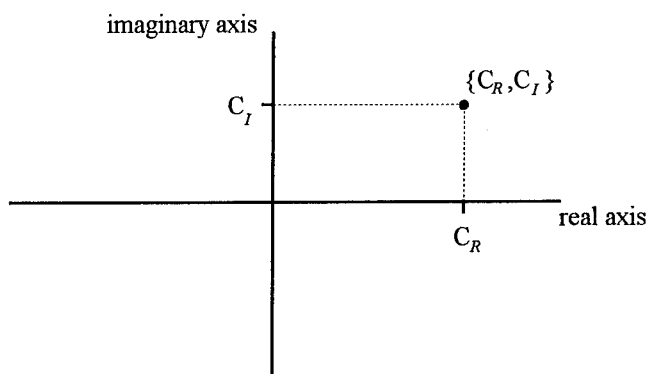


Figure (2-1). The geometric interpretation of a nonrandom complex valued constant, $C = C_R + jC_I$, as a point in two-dimensional space.

It is also apparent that this point in space is identifiable by a vector referenced to the origin with a particular length, L , and direction angle, α , as depicted in Figure (2-2)

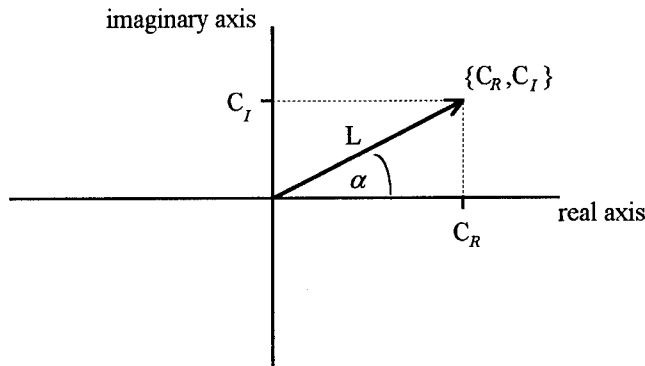


Figure (2-2). The vector interpretation of a nonrandom complex valued constant, $C = C_R + jC_I$, referenced to the origin.

The angle α is by convention measured from the positive real axis. This angle is considered positive when C_I is positive, and negative when C_I is negative. Also, α is zero when C_I is zero and C_R is positive. It is apparent that the ordered pair of real numbers, $\{L, \alpha\}$, is an alternate representation of the complex constant, C .

The values of L and α are readily determined from geometric considerations as

$$L = \sqrt{C_R^2 + C_I^2}, \quad (2-2)$$

and

$$\alpha = \text{Arctan}\left\{\frac{C_I}{C_R}\right\}. \quad (2-3)$$

Thus L is the radial distance of the point $\{C_R, C_I\}$ from the origin and is always non-negative. L is commonly referred to as the *envelope*, *modulus* or *magnitude* of the complex constant C , and is represented as $|C|$. The angle α is commonly referred to as the *phase* or *argument* of C , and is represented as $\angle C$. This phase angle can be defined either as

$$-\pi \leq \alpha < +\pi, \text{ i.e., } \alpha \in [-\pi, +\pi),$$

or alternatively as

$$-\pi < \alpha \leq +\pi, \text{ i.e., } \alpha \in (-\pi, +\pi],$$

for unambiguous representation. Special note is made of Equation (2-3), in which the first letter of the abbreviation for the arctangent is capitalized. This is to distinguish this arctangent of a ratio of two known real quantities, from the arctangent of a single known real quantity. In the latter case, an angle in the range $-\pi/2$ to $+\pi/2$ results, and is normally referred to as the *principal value*. In the case of the arctangent of the ratio of two quantities which are representative of the coordinates of a point in space, $\{C_R, C_I\}$, the signs of both C_R and C_I are necessary to determine whether to add or subtract π from the principal value resulting from the arctangent of the ratio of the coordinates. This in effect determines the phase quadrant in which the vector lies. Thus the complex constant, C , can be represented in *vector* or *polar* notational form as the pairing

$$C = |C| \angle C.$$

As with the ordered real pair $\{C_R, C_I\}$, complex arithmetic rules have been developed for the ordered real pair $\{|C|, \angle C\}$. These rules facilitate the processing of complex constants represented in polar form, on a computing device.

2.1.1 Further Considerations of the Phase Angle α

From further geometric considerations it is evident that the real component of C is

$$Re\{C\} = C_R = |C| \cos[\alpha], \quad (2-4)$$

and likewise the imaginary component is

$$Im\{C\} = C_I = |C| \sin[\alpha]. \quad (2-5)$$

Employing Euler's identity leads us to the *exponential* representation of the complex constant C , as the product

$$C = |C|e^{j\alpha}. \quad (2-6)$$

The exponential form places in evidence the fact that α need not be constrained to be less than π in magnitude. This is a consequence of the modulo 2π nature of the cosine and sine functions in Equations (2-4) and (2-5). Thus the exponential form leads to the concept of expanding the complex plane of Figure (2-2) into a continuum of "sheets" overlapping in a helical fashion, which can be likened to a spiraling staircase. We can

consider each angle α as resulting from the rotation of the vector C , starting from the phase angle zero. As the rotation progresses from slightly less than $+\pi$ to slightly greater than $+\pi$, the vector representing C is said to progress from sheet 0 to sheet 1. Likewise, for any progression across the negative real axis, the vector is considered as progressing to the next sheet. (This helical surface is a particular example of what is referred to as a Riemann Surface [28].)

To allow for the placement of the complex constant on some particular sheet, r , the angle α is written explicitly in terms of its constituents as

$$\alpha = \alpha_0 + 2r\pi, r \in \text{integers}, \alpha_0 \in (-\pi, +\pi] . \quad (2-7)$$

In so doing, the various complex constants represented by Equation (2-6) become unique *via knowledge of the integer r* . This integer is representative of the number of angular rotations of the vector C through an entire 2π cycle as referenced to the positive real axis, and corresponds to the sheet number on which the vector lies. For example, with a phase angle of -1.1π , the vector C lies on sheet -1, and r is -1.

Note that in many situations, the integer r may not be known. In this case, determination of the phase angle via Equation (2-3) from the ordered pair $\{C_R, C_I\}$, will yield α_0 rather than α . Thus in general, the ordered triplet $\{C_R, C_I, r\}$ is required for a "complete" representation of the complex constant C . Likewise, the ordered triplet $\{|C|, \alpha_0, r\}$ will be referred to as a complete representation.

2.2 Processing Considerations in the Utilization of Complex Numbers

In many situations where complex numbers are represented and processed on a computing device, the representation is either intentionally or necessarily incomplete in the sense that the integer r is not used or not known. For example, in representing the discrete-time counterpart of a continuous-time bandpass signal, the initial value of r is either unknown or assigned the value zero. In fact if r , as a result of processing, takes on another value other than zero, it is often re-assigned the value zero. In such a case, the process is utilizing α_0 rather than α . This prompts us to define the function, or more correctly, the process $g[]$ as

$$\begin{aligned} g[\alpha] &= \{\alpha + \pi \cdot \text{sgn}(\alpha)\}_{\text{modulo } 2\pi} - \pi \cdot \text{sgn}(\alpha), \quad \{\alpha + \pi \cdot \text{sgn}(\alpha)\}_{\text{modulo } 2\pi} \neq 0, \\ &= +\pi, \quad \{\alpha + \pi \cdot \text{sgn}(\alpha)\}_{\text{modulo } 2\pi} = 0, \\ \text{sgn}(b) &= +1, \quad b > 0 \\ &= 0, \quad b = 0 \\ &= -1, \quad b < 0. \end{aligned} \tag{2-8}$$

A plot of $g[\alpha]$ versus α is shown in Figure (2-3). The process $g[\alpha]$ is simply representative of the information loss in going from the ordered pair $\{|C|, \alpha\}$, triplet $\{|C|, \alpha_0, r\}$ or triplet $\{C_R, C_I, r\}$ representation of C , to the ordered pair $\{|C|, \alpha_0\}$ or $\{C_R, C_I\}$. Likewise, it is representative of the modulo 2π nature of the quantity $e^{j\alpha}$. Note for example that

$$\alpha_0 = g[\alpha_0] = g[\alpha], \tag{2-9}$$

demonstrating that all phase angles are mapped to sheet 0 , by the process $g[\alpha]$.

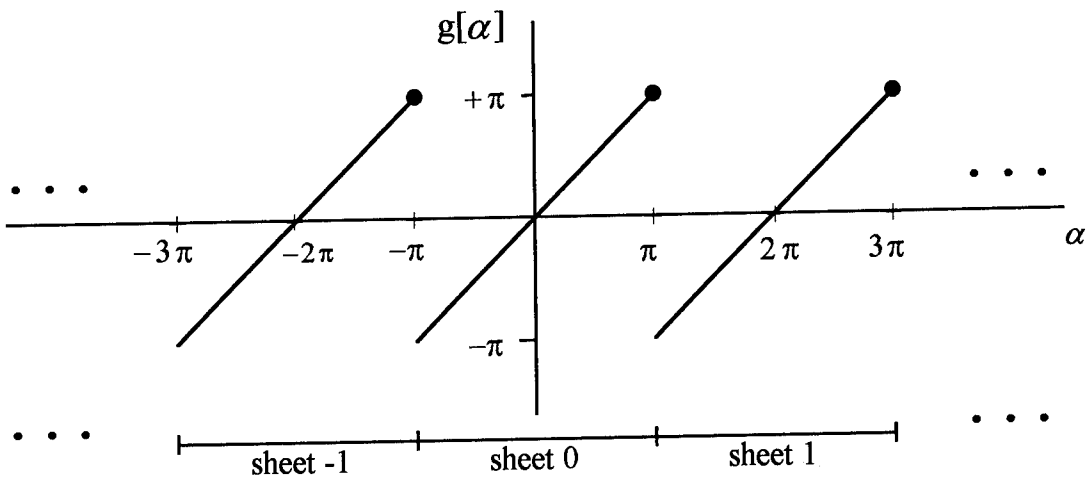


Figure (2-3). The process $g[\alpha]$.

From Equation (2-9) it is also readily apparent that

$$\begin{aligned} e^{j\alpha_0} &= e^{jg[\alpha_0+2r\pi]} \\ &= e^{jg[\alpha_0]} \end{aligned} \quad (2-10)$$

Thus for the incompletely specified complex number C represented as $\{C_R, C_I\}$, the equivalent exponential form of C is $|C|e^{jg[\alpha]}$.

2.2.1 Implicit Versus Explicit Addition of Phase Angles

We are now able to make a distinction between the *implicit* and the *explicit* addition of the phase angles of complex numbers. The addition of two phase values which were obtained via independent applications of Equation (2-3), is considered to be an explicit addition. The result of this addition ranges from -2π to $+2\pi$ radians, since each of

the phases being summed ranges from $-\pi$ to $+\pi$. More generally, if M such phase angles from sheet 0 are added together, the result ranges from $-M\pi$ to $+M\pi$ radians. Note that explicit phase angle addition results in a phase angle that is associated with a resulting complex number which may require a complete representation; i.e., the integer r associated with the resultant complex number may be non-zero.

An alternate method of implementing the addition of the phase angles of a set of complex numbers is to do so implicitly, via complex multiplication. For example, consider the resultant product, C , of the complex numbers A and B , where

$$A = |A| e^{jg[\alpha_{0a} + 2r_a\pi]}$$

and

$$B = |B| e^{jg[\alpha_{0b} + 2r_b\pi]} .$$

Here, the phase angles α_{0a} and α_{0b} and the integers r_a and r_b are such that

$$\alpha_{0a} = g[\alpha_a] \text{ and } \alpha_{0b} = g[\alpha_b] , \text{ with } \alpha_a = \alpha_{0a} + 2r_a\pi \text{ and } \alpha_b = \alpha_{0b} + 2r_b\pi .$$

The product is formed as

$$\begin{aligned} C &= A \cdot B \\ &= \{A_R, A_I\} \cdot \{B_R, B_I\} \\ &= \{A_R \cdot B_R - A_I \cdot B_I, A_I \cdot B_R + A_R \cdot B_I\} \\ &= \{C_R, C_I\}. \end{aligned} \tag{2-11}$$

The resulting phase, α_{0c} , is found using Equation (2-3). Equivalently we can write

$$\begin{aligned}
 C &= A \cdot B \\
 &= |A|e^{jg[\alpha_a]} \cdot |B|e^{jg[\alpha_b]} \\
 &= |A| \cdot |B|e^{jg[g[\alpha_a] + g[\alpha_b]]} \\
 &= |C|e^{j\alpha_{0c}}
 \end{aligned} \tag{2-12}$$

Note that even if r_a and r_b are known, r_c is not identifiable using the implicit method of phase additions. Note also that if phase differencing is desired, the difference can be performed implicitly by first forming the conjugate of B as

$$B^* = \{B_R, -B_I\},$$

and subsequently forming the product $A \cdot B^*$.

If it is desired to obtain the implicit result using explicit phase additions, the process $g[\alpha]$ can be applied to the explicit result. It will become evident as this research progresses that the distinction between implicit and explicit phase additions is needed to be able to properly analyze the numerical FM discrimination process.

2.3 The Discrete-Time Bandpass Signal Representation and Generation of the Corresponding Complex Envelope

We turn our attention now to the representation and processing of signal waveforms that are essentially bandlimited in frequency, such that these continuous-time signals can be uniformly sampled in time with tolerable destructive aliasing. For samples equally spaced in time (i.e., uniform sampling,) the Nyquist sample rate requirement implies that a lowpass signal of bandwidth W Hz can be sampled at time intervals of $\Delta t = T_s < 1/(2W)$ seconds, to prevent (destructive) aliasing of frequency constituents. This translates to selecting a sample rate, $F_s = 1/T_s$, greater than twice the lowpass signal bandwidth, W . For bandpass signals of approximate bandwidth B' Hz, and originally centered at some carrier frequency f_c Hz, sampling can be performed as above by first downconverting to a new center frequency of $f_c > B'/2$ Hz, with $W = f_c + B'/2$. In this manner, we have not violated the requirement that the bandpass bandwidth relative to f_c must be less than 200% [11]. Further details of this process are deferred to Chapter 3.

By sampling such a bandpass, continuous-time signal $s(t)$ at integer multiples of $\Delta t = T_s$, we obtain the discrete-time sequence $s(nT_s)$, where the index n is an integer which identifies a particular sample of the newly obtained sequence.

2.3.1 A Method of Complex Envelope Generation: The Numerical Quadrature Downconversion Process

The numerical or digital quadrature downconversion process [11] is presented as a model of the processing which is required to generate the *in-phase* (i) data corresponding to the real constituent of the complex envelope sequence, and the

quadrature (q) data corresponding to the imaginary constituent of the complex envelope sequence, from the real sequence, $s(nT_s)$. As will be seen in Section 3.3, a properly downconverted and sampled angle modulated signal can be considered to be a discrete-time bandpass process. We represent this input signal, $s(nT_s)$, as

$$s(nT_s) = a(nT_s) \cos[2\pi f_c nT_s + \phi(nT_s)] , \quad a(nT_s) > 0 , \quad (2-13)$$

where $a(nT_s)$ is the time varying *amplitude* of $s(nT_s)$, and $\phi(nT_s)$ represents the *phase* or *angle* modulation imposed on the signal. In this research, f_c is defined as the *true center frequency after analog downconversion* (immediately prior to sampling), which is considered to be close to the center of the Nyquist bandwidth. Thus for a sampling rate of F_s samples per second, f_c is about half way between 0 and $F_s/2$ Hz, i.e., $f_c \approx F_s/4$ Hz. As seen in Figure (2-4), the input signal, $s(nT_s)$, is replicated and mixed with two local oscillator frequencies which are in phase quadrature relative to each other, and at the tuning frequency, f_l . This tuning frequency is set to exactly (within the numerical accuracy of the processing device) one-quarter of the sampling frequency, since this is our best estimate of the true center frequency, f_c . The mixing (numerical multiplication) process generates in the i and q channels, frequency components centered around both $(f_c + f_l)$ and $(f_c - f_l)$. The role of the (identical) lowpass filters is to remove the unwanted components centered around $(f_c + f_l)$. Further insight into the workings of the numerical quadrature downconverter is arrived at by analyzing the channels simultaneously using complex signal representation.

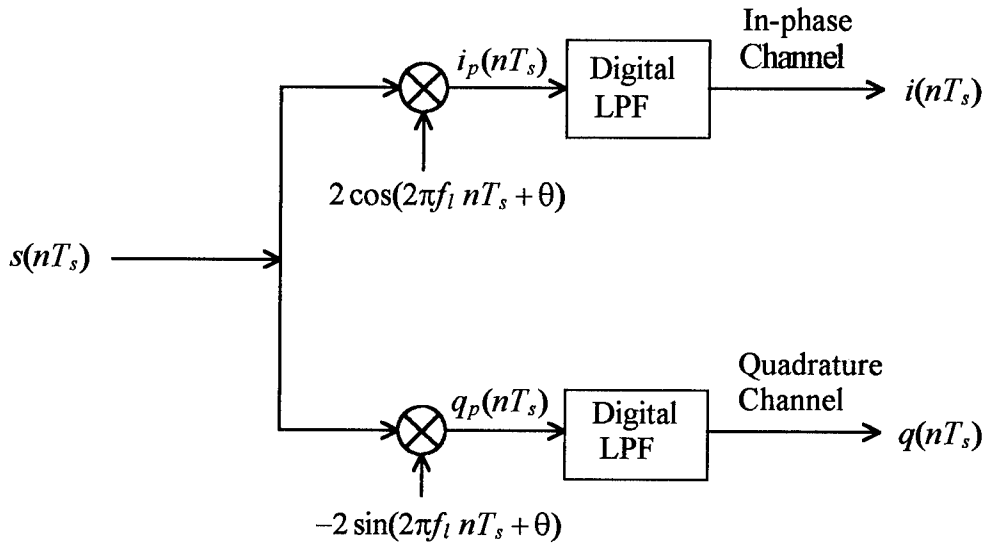


Figure (2-4). The numerical quadrature downconverter.

The rules of complex arithmetic justify the interpretation of the overall mixing process as the multiplication of the real input signal by the complex exponential

$$2e^{-j\alpha_{l0}(nT_s)} = 2 \cos[\alpha_{l0}(nT_s)] - j \cdot 2 \sin[\alpha_{l0}(nT_s)] , \quad (2-14)$$

where

$$\alpha_{l0}(nT_s) = g[2\pi f_l nT_s + \theta] . \quad (2-15)$$

The result is the circular (i.e., periodic) convolution of the periodic spectrum of the input signal with the periodic spectrum of the complex exponential of Equation (2-14). In effect, the original signal spectrum, $S(e^{j2\pi f T_s})$, is circularly rotated down in frequency by

the amount f_l . This is a direct consequence of the discrete-time modulation or windowing theorem [12].

Figure (2-5) shows a representative set of resulting magnitude spectra, at various stages in the numerical quadrature downconversion process. The pair of digital or discrete-time lowpass filters can be interpreted as a single real filter operating on complex data, with the desired magnitude response as seen in the figure. Thus after multiplication by the complex exponential, but prior to the filtering, we have the pre-filtered complex signal

$$s_p(nT_s) = i_p(nT_s) + jq_p(nT_s) , \quad (2-16)$$

where

$$i_p(nT_s) = 2 \cdot s(nT_s) \cos[2\pi f_l nT_s + \theta] \quad (2-17)$$

and

$$q_p(nT_s) = -2 \cdot s(nT_s) \sin[2\pi f_l nT_s + \theta] . \quad (2-18)$$

After application of trigonometric identities and lowpass filtering, we obtain the approximation to the sampled *complex envelope*, $\tilde{s}(nT_s)$, as

$$\tilde{s}(nT_s) \cong i(nT_s) + jq(nT_s) , \quad (2-19)$$

where

$$i(nT_s) \cong a(nT_s) \cos[2\pi f_e nT_s + \phi(nT_s) - \theta] \quad (2-20)$$

and

$$q(nT_s) \cong a(nT_s) \sin[2\pi f_e nT_s + \phi(nT_s) - \theta]. \quad (2-21)$$

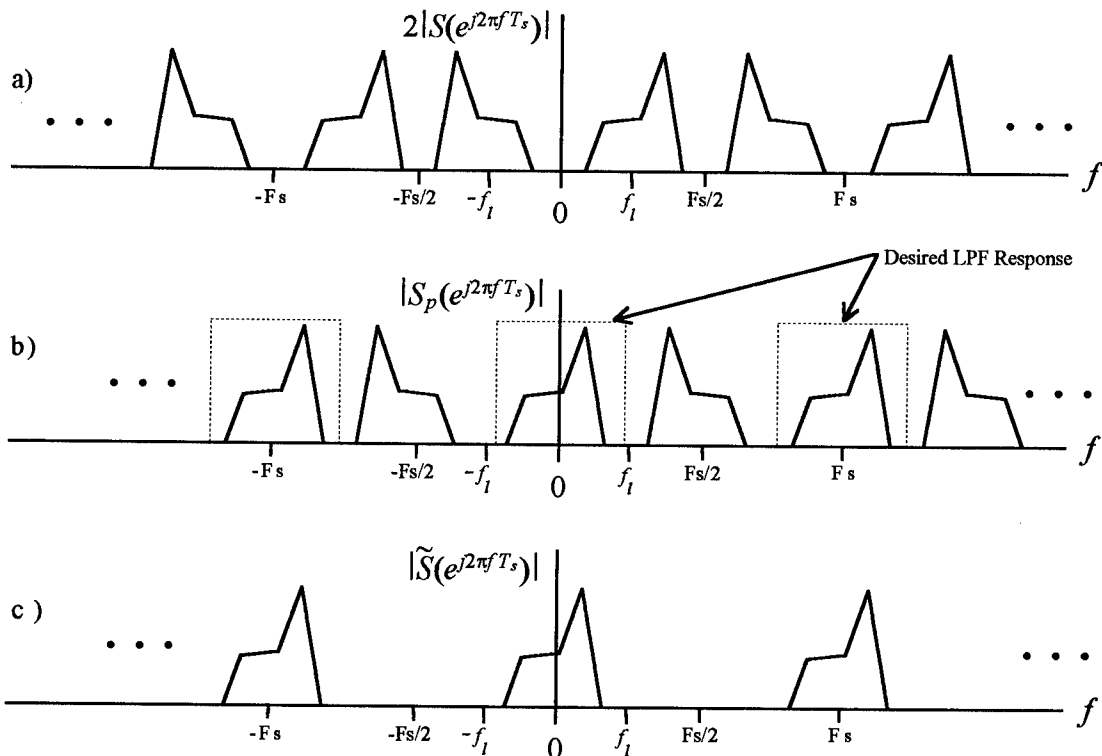


Figure (2-5). A set of representative signal magnitude spectrum plots: a) Representative input signal magnitude spectrum; b) The frequency shifted and pre-filtered signal magnitude spectrum; c) The magnitude spectrum of the resulting complex envelope estimate.

Here, f_e is the error in the estimate of the true center frequency, i.e., $f_e = (f_c - f_i)$. This error is a consequence of the noncoherent nature of the quadrature downconversion process, and can be either negative or positive. In the absence of a tuning error, the remaining error accounted for by the above approximations, is due to the non-ideal nature of the lowpass filters. The quadrature downconverter therefore generates the sequence of ordered pairs, $\{i(nT_s), q(nT_s)\}$ as a time-ordered series of Cartesian coordinates, available for subsequent processes.

2.3.2 A Method of Complex Envelope Generation: The Complex Bandpass Filter

The processing of the sequence $s(nT_s)$ by the numerical quadrature downconverter as presented in Figure (2-4) and described in Section 2.3.1, will be shown to be equivalent to linearly convolving $s(nT_s)$ with a complex bandpass filter with impulse response

$$h_{eq}(nT_s) = h_i(nT_s) + jh_q(nT_s), \quad (2-22)$$

and subsequently (circularly) rotating the result in frequency by the amount $-f_i$ Hz. To determine this impulse response, we first consider the complex output, $i(nT_s) + jq(nT_s)$. From Figure (2-4), it is readily apparent that

$$i(nT_s) + jq(nT_s) = 2e^{-j0} \cdot \{s(nT_s) \cdot e^{-j2\pi f_i nT_s}\} * h_{lp}(nT_s). \quad (2-23)$$

(Note that for the present discussion, to simplify analysis we will use the standard approach to the representation of the complex exponential, by not explicitly identifying the

process $g[]$ in our equations.) Here, $h_{lp}(nT_s)$ is the real-valued impulse response of the lowpass filters of the quadrature downconverter. Indicating spectral periodic convolution as \otimes , the right-hand side of Equation (2-23) has the discrete-time Fourier transform

$$2e^{-j\theta} \{S(e^{j2\pi(f+f_l)T_s})\} \cdot H_{lp}(e^{j2\pi f T_s}) = 2e^{-j\theta} \{S(e^{j2\pi f T_s}) \cdot H_{lp}(e^{j2\pi(f-f_l)T_s})\} \otimes \sum_{m=-\infty}^{\infty} \delta(f + f_l + mF_s),$$

$$\frac{-F_s}{2} < f_l \leq \frac{F_s}{2}, \quad m \in \text{integers}. \quad (2-24)$$

Taking the inverse Fourier transform of the right-hand side of Equation (2-24) and applying Equation (2-23) we find that

$$i(nT_s) + jq(nT_s) = 2e^{-j\theta} \{s(nT_s) * [h_{lp}(nT_s) \cdot e^{j2\pi f_l n T_s}]\} \cdot e^{-j2\pi f_l n T_s}. \quad (2-25)$$

Thus Equations (2-23) and (2-25) demonstrate that the quadrature downconversion process of Figure (2-4) is equivalent to convolving $s(nT_s)$ with a complex impulse response, $h_{eq}(nT_s)$, and subsequently multiplying the result by the complex sequence,

$$2e^{-j\theta} e^{-j2\pi f_l n T_s}$$

The complex impulse response is identified as

$$h_{eq}(nT_s) = h_{lp}(nT_s) \cdot e^{j2\pi f_l n T_s}$$

$$= h_{lp}(nT_s) \cdot \cos[2\pi f_l n T_s] + j h_{lp}(nT_s) \cdot \sin[2\pi f_l n T_s]. \quad (2-26)$$

From Equations (2-22) and (2-26) we have

$$h_i(nT_s) = h_{lp}(nT_s) \cos[2\pi f_l nT_s] , \quad (2-27)$$

and

$$h_q(nT_s) = h_{lp}(nT_s) \sin[2\pi f_l nT_s] . \quad (2-28)$$

This establishes the impulse response of the complex bandpass filter. We now turn our attention toward identifying the complex bandpass filter coefficients.

Consider the lowpass filter impulse response, $h_{lp}(nT_s)$, and its z-transform, $H_{lp}(z)$.

For $H_{lp}(z)$ of the form

$$H_{lp}(z) = \frac{\sum_{k=0}^M b_k \cdot z^{-k}}{1 - \sum_{k=1}^N a_k \cdot z^{-k}} , \quad (2-29)$$

the impulse response, $h_{lp}(nT_s)$, is determined by the $M+1+N$ real coefficients b_k , $k=0,1,2,\dots,M$ and a_k , $k=1,2,3,\dots,N$. The z-transform of $h(nT_s)$ is by definition

$$H(z) = \sum_{n=-\infty}^{\infty} h(nT_s) \cdot z^{-n} . \quad (2-30)$$

Therefore, the complex sequence,

$$h_{lp}(nT_s) e^{+j2\pi f_l nT_s} ,$$

has the z-transform

$$h_{lp}(nT_s)e^{+j2\pi f_l nT_s} \stackrel{z}{\Leftrightarrow} H_{lp}(z \cdot e^{-j2\pi f_l T_s}) = H_{eq}(z). \quad (2-31)$$

Thus for filters of the form presented in Equation (2-29) we have

$$\begin{aligned} H_{eq}(z) &= \frac{\sum_{k=0}^M b_k \{z \cdot e^{-j2\pi f_l T_s}\}^{-k}}{1 - \sum_{k=1}^N a_k \{z \cdot e^{-j2\pi f_l T_s}\}^{-k}} \\ &= \frac{\sum_{k=0}^M \{b_k e^{+j2\pi f_l k T_s}\} z^{-k}}{1 - \sum_{k=1}^N \{a_k e^{+j2\pi f_l k T_s}\} z^{-k}} \quad . \end{aligned} \quad (2-32)$$

Equation (2-32) implies that any filter with the response as indicated in Equation (2-29) can be circularly rotated in frequency by the amount f_l , by multiplying the finite length real coefficient sequences a_k and b_k by the complex exponential sequence,

$$e^{+j2\pi f_l k T_s}$$

Thus we can transform the lowpass filter of the quadrature downconverter into a complex bandpass filter, and subsequently linearly convolve the input sequence with this complex filter. The result of this convolution can then be circularly rotated down in frequency as implied in Equation (2-25), to yield the complex envelope identified in Section 2.3.1. This process is depicted in Figure (2-6).

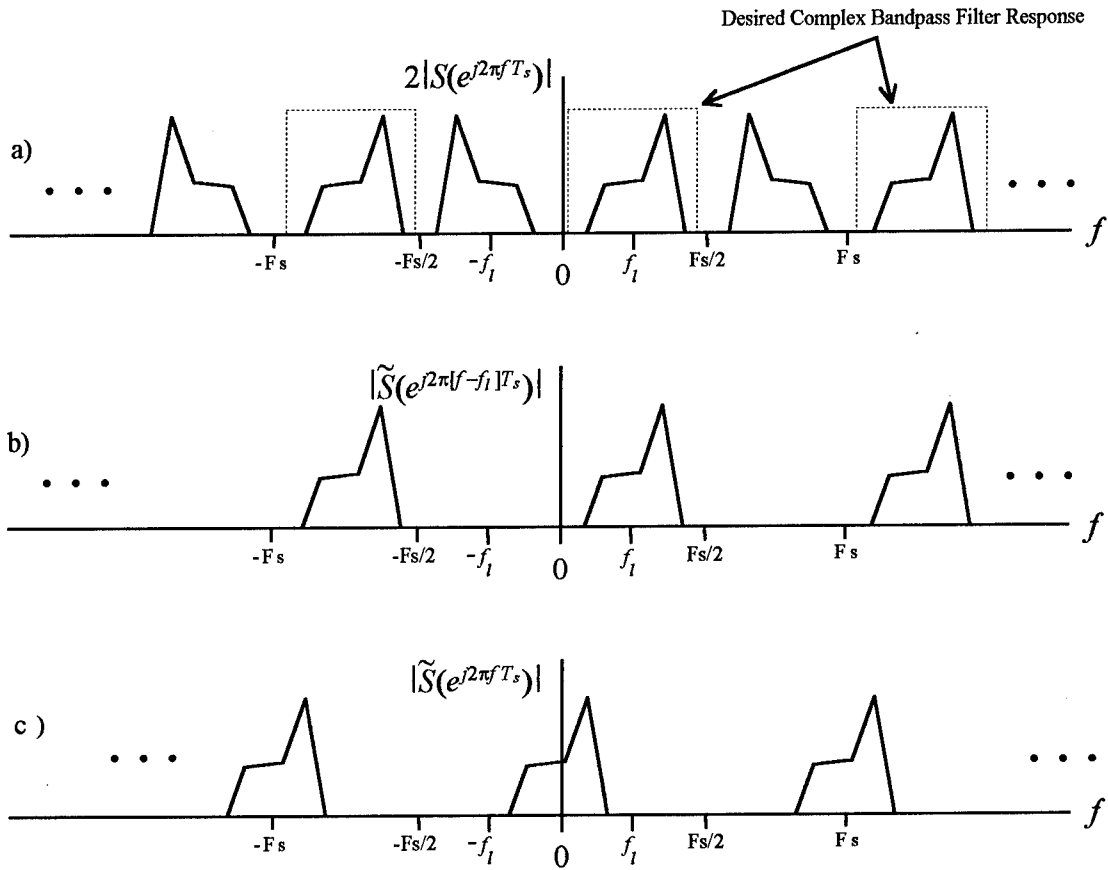


Figure (2-6). A set of signal magnitude spectrum plots which are representative of the complex bandpass filter method of complex envelope generation: a) Representative input signal magnitude spectrum; b) The result of filtering this input signal with the complex bandpass filter; c) The magnitude spectrum of the resulting complex envelope estimate.

2.4 The Generalized Pre-envelope

In light of the equivalence of the numerical quadrature downconversion method described in Section 2.3.1 and the complex bandpass filter / downconversion method described in Section 2.3.2, the *generalized pre-envelope* is introduced. Normally the term "analytic signal" and the notation $s_+(nT_s)$ is reserved for the *pre-envelope*,

$$\tilde{s}(nT_s) \cdot e^{+j2\pi f_c nT_s},$$

to identify the complex signal prior to downconversion [29]. This is the signal whose spectrum is depicted in Figure (2-6 b). In this research, however, it will become evident that the discrete-time FM demodulation methods to be described need not rely on whether downconversion is explicitly implemented as in the previously described methods. Therefore, it is convenient to define the generalized pre-envelope as

$$s_+(nT_s, f_o) \equiv \tilde{s}(nT_s) e^{+j2\pi f_o nT_s}, \quad -\frac{F_s}{2} < f_o \leq \frac{+F_s}{2}. \quad (2-33)$$

The pre-envelope and the complex envelope are simply the special cases where $f_o = f_c$, and $f_o = 0$ respectively. Thus the generalized pre-envelope sequence, is simply the complex envelope sequence circularly rotated in frequency to an arbitrary frequency, f_o . For the case where an unknown tuning error, f_e , exists as previously described, for notational simplicity we will adopt the convention

$$s_+(nT_s) = s_+(nT_s, f_e).$$

Note that the real phase sequence extracted from the complex generalized pre-envelope is

$$\alpha_0(nT_s, f_o) = g[\alpha(nT_s, f_o)], \quad (2-34)$$

where

$$\alpha(nT_s, f_o) = 2\pi f_o n T_s + \phi(nT_s) - \theta . \quad (2-35)$$

The demodulation methods to be described in Chapter 3 require as input the complex envelope, as generated by the preceding techniques or their equivalents. More generally it will be seen that the generalized pre-envelope can also be processed to estimate the original message.

CHAPTER 3

Analysis of a Class of Numerical FM Discrimination Methods

Amenable to Real-Time Implementation

3.1 The Ideal Discrete-Time FM (DTFM) Signal

In Chapter 2, methods were introduced for generating the discrete-time generalized pre-envelope, $s_+(nT_s)$, from the discrete-time bandpass signal, $s(nT_s)$. It is readily apparent that these techniques are approximate or non-ideal in light of the fact that the required ideal lowpass (or complex bandpass) filter cannot be realized [12]. In fact there are numerous distortions of the original message and the modulated signal, which have taken place in all stages of the transmit/receive process. It is therefore not the intent of this research to address the various issues regarding the generation of the pre-envelope with regard to its accuracy in representing the intended modulated signal. However, it is the intent of this research to establish a baseline numerical FM demodulation method, to which other methods can be compared. To accomplish this objective, the analyses and simulations throughout this research will utilize what is considered to be the *ideal* generalized pre-envelope,

$$s_+(nT_s) = i(nT_s) + jq(nT_s) , \quad (3-1)$$

where

$$i(nT_s) = a(nT_s)\cos[2\pi f_e nT_s + \phi(nT_s) - \theta] \quad (3-2)$$

and

$$q(nT_s) = a(nT_s)\sin[2\pi f_e nT_s + \phi(nT_s) - \theta] . \quad (3-3)$$

The class of numerical FM discrimination methods to be described estimate the original message by processing the time sequence of ordered pairs, $\{i(nT_s), q(nT_s)\}$. Thus subsequent numerical discrimination methods can be fairly compared since all will be processing this same ideal generalized pre-envelope.

The envelope, $|a(nT_s)|$, for the present will not be restricted to being constant, but we will impose the constraint that $a(nT_s)$ be greater than 0, as indicated in Equation (2-13). As before, f_e is indicative of a frequency tuning error. The sampled phase angle term, $\phi(nT_s)$, is modeled as being the result of the frequency modulation process

$$\phi(nT_s) = \phi(t)|_{t=nT_s} = 2\pi\Delta f \int_0^{nT_s} m(t)dt , \quad (3-4)$$

where $m(t)$ is the original bandlimited message, that has been amplitude limited such that

$$-1 \leq m(t) \leq +1 ,$$

and is also zero mean in time. The complex signal defined by Equations (3-1) through (3-4) is representative of what will be referred to as the *ideal discrete-time FM* (DTFM) signal. The constant phase term, θ , is comprised of two sources of constant phase offset. The first is the arbitrary but unknown phase offset between the carrier and the local oscillator frequencies of the numerical downconversion process. The second is the constant phase resulting from the integration of the modulating signal, including time t less than 0. Both sources of constant phase offset are taken into account via the arbitrary but constant phase, θ .

The discrete-time *true instantaneous frequency*, $y(nT_s)$, is defined as

$$y(nT_s) = \phi'(nT_s) = \phi'(t)|_{t=nT_s} = 2\pi\Delta f \cdot m(t)|_{t=nT_s}, \quad (3-5)$$

in units of radians per second. This is obtained by direct differentiation of Equation (3-4). (The prime in Equation (3-5) indicates differentiation with respect to time.) Thus, in all approaches, the goal is to estimate the sampled instantaneous frequency [30], which is found as the time rate of change of phase of the modulated complex signal, $s_+(nT_s)$.

3.2 Numerical FM Discrimination (Demodulation) Techniques

As already indicated, the numerical FM demodulation techniques to be described in this research are considered to be of the same class, in that each results in the backward difference approximation to the time derivative of the phase, as a method of recovering the modulating signal. The differentiation of a continuous function of time, $x(t)$, can be defined as

$$x'(t) = \frac{dx(t)}{dt} \equiv \lim_{\Delta t \rightarrow 0} \left[\frac{x(t) - x(t - \Delta t)}{\Delta t} \right]. \quad (3-6)$$

The backward difference approximation to the discrete-time signal, $x'(nT_s)$, resulting from this differentiation is [12]

$$x'(nT_s) \cong \frac{x(nT_s) - x([n-1]T_s)}{T_s} = F_s \cdot \{x(nT_s) - x([n-1]T_s)\}, \quad (3-7)$$

and is readily seen to be the (weighted) difference between the present and previous samples of the sequence, $x(nT_s)$. The weighting allows for the incorporation of the knowledge of the value of T_s into the approximation. Note that this approximation approaches our definition of the actual time derivative in Equation (3-6) as the sampling interval, T_s , decreases. It can be shown (see Appendix A) that this approximation to the time derivative has the magnitude frequency response

$$|H_B(e^{j\omega T_s})| = \frac{1}{T_s} \cdot \sqrt{2 - 2 \cos(\omega T_s)} , \quad (3-8)$$

which for small values of $|\omega|$ relative to the sampling rate, closely resembles the desired magnitude response of the time derivative.

These numerical demodulation techniques are presented in a progression of development beginning with what is considered to be the two most fundamental methods of this class, the *Direct* and the *Indirect* or *Implicit* numerical FM discriminators. Following these methods, the *Arcsine* method is arrived at by employing a mathematical analysis of the nearly equivalent continuous-time analogy, and subsequently compensating for distortions introduced by the sampling process. The *Arccosine* method is presented in a similar fashion. As will be seen, the *Principal-Value Arctan* approach is developed via an alternate compensation method applied to the first stages of the Arcsine approach. The last technique to be covered in this chapter will be referred to as the *Standard* numerical discriminator, since it is developed in an analogous fashion to the standard or conventional continuous-time FM discriminator.

3.2.1 The Direct and Indirect Methods of Numerical FM Discrimination

Before proceeding further with the descriptions of the Direct and Indirect methods of numerical FM discrimination, we must modify our definition of the backward difference approximation. Since we are applying this approximation to a sequence which is representative of sequential phase angles extracted from the generalized pre-envelope, we must take into account the modulo 2π nature of these angles. Thus we define the backward difference approximation to the desired discrete-time signal, $\alpha'(nT_s, f_o)$, as

$$\hat{\alpha}'(nT_s, f_o) \equiv \frac{g[\alpha_0(nT_s, f_o) - \alpha_0([n-1]T_s, f_o)]}{T_s} = F_s \cdot g[\alpha_0(nT_s, f_o) - \alpha_0([n-1]T_s, f_o)] , \quad (3-9)$$

where $\alpha_0(nT_s, f_o)$ is as presented in Equation (2-34). Equation (3-9) is the backward difference approximation to the rate of change of phase of the generalized pre-envelope, $s_+(nT_s, f_o)$. With this definition, we can now develop the Direct and Indirect numerical discrimination methods.

3.2.1.1 Direct Numerical FM Discrimination

Equations (3-1) through (3-3) represent $s_+(nT_s)$ evaluated at $f_o = f_e$ in Cartesian form, and can be converted to exponential form using Equations (2-2) and (2-3), resulting in

$$s_+(nT_s) = \sqrt{i^2(nT_s) + q^2(nT_s)} \cdot \exp\left\{j \cdot \text{Arctan}\left[\frac{q(nT_s)}{i(nT_s)}\right]\right\} . \quad (3-10)$$

From simple trigonometric considerations, it is readily seen that

$$\sqrt{i^2(nT_s) + q^2(nT_s)} = |a(nT_s)| \quad (3-11)$$

represents the envelope of the original signal, $s(nT_s)$, as previously described in Chapter 2. The *instantaneous phase message estimate*, $\hat{\phi}_i$, at time sample n is identified as

$$\hat{\phi}_i(nT_s) = \text{Arctan}\left[\frac{q(nT_s)}{i(nT_s)}\right] = g[2\pi f_e n T_s + \phi(nT_s) - \theta] = \alpha_0(nT_s), \quad (3-12)$$

which implies that

$$-\pi < \hat{\phi}_i \leq +\pi .$$

In other words, the instantaneous phase message estimate will lie on sheet 0 of our Riemann surface described in Chapter 2. In a straightforward fashion, Equation (3-12) shows that it is possible to obtain these estimates at any particular sample in time, by using the corresponding in-phase and quadrature samples. The Direct method of numerical discrimination is simply the implementation of Equation (3-9), using consecutive instantaneous phase message estimates. To distinguish between the explicitly required modulo 2π process $g[]$ in Equation (3-9), and the implicitly applied process $g[]$ indicated in Equation (3-12), the Direct method of discrimination is summarized as

$$\hat{y}_d(nT_s) = \hat{\phi}'_d(nT_s) = F_s \cdot g_E[\hat{\phi}_i(nT_s) - \hat{\phi}_i([n-1]T_s)] . \quad (3-13)$$

Here, the subscript E on the process $g[]$ is used to indicate that this process is being explicitly applied to the backward difference of instantaneous phase message estimates. These phase message estimates have been obtained via consecutive Arctan calculations, as in Equation (3-12).

Either the modulo 2π process, $g_E[]$, must be applied explicitly to the backward difference of consecutive instantaneous phase message samples, or a "phase-difference quadrant determination" algorithm is required as follows:

$$\begin{aligned}
 d(nT_s) &= \hat{\phi}_i(nT_s) - \hat{\phi}_i([n-1]T_s) \\
 \text{if} \{ d(nT_s) > +\pi \} \\
 d(nT_s) &= d(nT_s) - 2\pi \\
 \text{if} \{ d(nT_s) < -\pi \} \\
 d(nT_s) &= d(nT_s) + 2\pi \\
 \hat{y}(nT_s) &= F_s \cdot d(nT_s)
 \end{aligned} \tag{3-14}$$

Note that the above quadrant determination algorithm achieves the same result as Equation (2-8) only for the difference range

$$-2\pi < \{\hat{\phi}_i(nT_s) - \hat{\phi}_i(nT_s)\} < +2\pi ,$$

which is sufficient based on the range of phase message estimates returned by Equation (2-3). In the mathematically equivalent Indirect approach, it will become evident that this phase difference quadrant determination is not explicitly required.

3.2.1.2 Indirect Numerical FM Discrimination

The Indirect technique, commonly implemented in practice, utilizes the fact that multiplication of two complex numbers in exponential form is accomplished by real multiplication of the magnitudes, and addition of the corresponding phases. Since the goal is to determine the difference between consecutive phase samples as an instantaneous frequency estimate, it is possible to achieve this difference by multiplying the complex pre-envelope phasor (i.e., phase-vector) at time sample n , by the conjugate of the phasor at time sample $(n - 1)$. Thus we find that

$$s_+(nT_s) \cdot s_+^*([n-1]T_s) = a(nT_s) \cdot a([n-1]T_s) \exp\{j \cdot [2\pi f_e T_s + \phi(nT_s) - \phi([n-1]T_s)]\}, \quad (3-15)$$

and our Indirect instantaneous frequency estimate is found as the "phase" of the resultant vector in Equation (3-15),

$$\hat{y}_I(nT_s) = F_s \cdot g[2\pi f_e T_s + \phi(nT_s) - \phi([n-1]T_s)] \quad (3-16)$$

In units of radians/sec, the Indirect method of frequency modulation estimation is proportional to the backward difference approximation to the rate of change of phase, plus the bias term $2\pi f_e$. Rather than converting to exponential form, as indicated in Section 2.2.1 the multiplication can be performed in Cartesian form using implicit phase addition, since

$$s_+(nT_s) \cdot s_+^*([n-1]T_s) = [i(nT_s) + jq(nT_s)] \cdot [i([n-1]T_s) - jq([n-1]T_s)] = A + jB , \quad (3-17)$$

where

$$A = i(nT_s) \cdot i([n-1]T_s) + q(nT_s) \cdot q([n-1]T_s) \quad (3-18)$$

is the resulting real term, and

$$B = q(nT_s) \cdot i([n-1]T_s) - i(nT_s) \cdot q([n-1]T_s) \quad (3-19)$$

is the resulting imaginary term. Thus we obtain our frequency modulation estimate as

$$\hat{y}_I(nT_s) = F_s \cdot \text{Arctan}[\frac{B}{A}] . \quad (3-20)$$

Equations (3-18) through (3-20) summarize the Indirect numerical FM discrimination technique, given the in-phase and quadrature samples sequences, $i(nT_s)$ and $q(nT_s)$.

3.2.2 Arcsine Numerical FM Discrimination

The Arcsine method of numerical FM demodulation [8] is arrived at by first considering the continuous time analogy to Equation (3-12) which expresses the instantaneous phase message estimate as

$$\hat{\phi}_i(t) = \arctan\left[\frac{q(t)}{i(t)}\right] = g[2\pi f_e t + \phi(t) - \theta] . \quad (3-21)$$

The estimate of the rate of change of modulated phase, $\hat{\phi}'_i(t)$, is found by utilizing

$$\frac{d}{dt}[\arctan\{u(t)\}] = \frac{1}{1+u^2(t)} \cdot \frac{du}{dt} , \quad (3-22)$$

for the angle range

$$\frac{-\pi}{2} < \arctan\{u(t)\} < \frac{+\pi}{2} .$$

From Equations (3-21) and (3-22) it is apparent that

$$\hat{\phi}'_i(t) = \frac{1}{1 + \frac{q^2(t)}{i^2(t)}} \left[\frac{i(t) \cdot \frac{dq}{dt} - q(t) \cdot \frac{di}{dt}}{i^2(t)} \right] = \frac{i(t) \cdot \frac{dq}{dt} - q(t) \cdot \frac{di}{dt}}{i^2(t) + q^2(t)} , \quad (3-23)$$

for the instantaneous phase angle range

$$\frac{-\pi}{2} < \arctan\left\{\frac{q(t)}{i(t)}\right\} < \frac{+\pi}{2} .$$

In the methods of numerical FM discrimination being described, we have available to us sampled versions of the in-phase and quadrature signals, but do not have sampled versions of their corresponding time derivatives. The Arcsine method applies Equation (3-7), the backward difference approximation of this time derivative, to $i(nT_s)$ and $q(nT_s)$ to yield

$$\begin{aligned}
\hat{\phi}'_s(nT_s) &= \frac{i(nT_s) \cdot \{q(nT_s) - q([n-1]T_s)\} - q(nT_s) \cdot \{i(nT_s) - i([n-1]T_s)\}}{i^2(nT_s) + q^2(nT_s)} \\
&= \frac{q(nT_s) \cdot i([n-1]T_s) - i(nT_s) \cdot q([n-1]T_s)}{i^2(nT_s) + q^2(nT_s)} , \tag{3-24}
\end{aligned}$$

which can be scaled by F_s for our frequency modulation estimate.

By employing Equations (3-2) and (3-3) in Equation (3-24) we find that

$$\hat{\phi}'_s(nT_s) = \frac{a(nT_s)a([n-1]T_s)\{\sin C \cos D - \cos C \sin D\}}{a^2(nT_s)} , \tag{3-25}$$

where

$$C = 2\pi f_e n T_s + \phi(nT_s) - \theta \tag{3-26}$$

and

$$D = 2\pi f_e [n-1] T_s + \phi([n-1]T_s) - \theta . \tag{3-27}$$

Application of a trigonometric identity to Equation (3-25) along with Equations (3-26)

and (3-27) yields

$$\hat{\phi}'_s(nT_s) = \frac{a(nT_s)a([n-1]T_s)\sin(C-D)}{a^2(nT_s)}$$

$$= \frac{a(nT_s)a([n-1]T_s)\sin[2\pi f_e T_s + \phi(nT_s) - \phi([n-1]T_s)]}{a^2(nT_s)} \quad (3-28)$$

Under the condition that $a(nT_s) = a([n-1]T_s)$, we arrive at

$$\hat{\phi}'_s(nT_s) = \sin[2\pi f_e T_s + \phi(nT_s) - \phi([n-1]T_s)] , \quad (3-29)$$

which implies the need for an arcsine correction, to properly recover an estimate of the modulating waveform. Thus from Equations (3-24) and (3-29) we find that

$$\begin{aligned} \hat{y}_{as}(nT_s) &= F_s \cdot \arcsin[\hat{\phi}'_s(nT_s)] \\ &= F_s \cdot \arcsin\left[\frac{q(nT_s) \cdot i([n-1]T_s) - i(nT_s) \cdot q([n-1]T_s)}{i^2(nT_s) + q^2(nT_s)}\right] , \end{aligned} \quad (3-30)$$

can be used to estimate the time rate of change of phase for the phase difference range

$$\frac{-\pi}{2} < [2\pi f_e T_s + \phi(nT_s) - \phi([n-1]T_s)] < \frac{+\pi}{2}$$

In comparing the Arcsine method as summarized by Equation (3-30), to the previously described Direct and Indirect numerical FM discrimination methods, two very basic observations can be made. The first observation is with regard to the range of phase differences over which the message can be recovered. It would appear that we are limited to differences in the range $-\pi/2$ to $+\pi/2$ exclusively, to be able to utilize Equation (3-30). In actuality, we can use the sign of the numerator of the argument in Equation (3-30) and the sign of Equation (3-19) to decide whether to add $-\pi$, 0 , or $+\pi$ to the negated principal

value returned by the arcsine (prior to scaling by the sample rate, F_s). This new phase-difference quadrant determination algorithm required by the Arcsine method can be summarized by

$$\begin{aligned}
 d(nT_s) &= \arcsin \left[\frac{B}{i^2(nT_s) + q^2(nT_s)} \right] \\
 \text{if(} A < 0 \text{)} \\
 \quad \text{if(} B < 0 \text{)} \\
 \quad \quad d(nT_s) = -\pi - d(nT_s) \\
 \quad \text{else} \\
 \quad \quad d(nT_s) = +\pi - d(nT_s) \\
 \hat{y}_{as}(nT_s) &= F_s \cdot d(nT_s), \tag{3-31}
 \end{aligned}$$

where A and B are defined as in Equations (3-18) and (3-19). The second observation is that the Arcsine method is arrived at via the constraint that consecutive envelope samples are essentially equal (i.e., the signal has a constant modulus). Note that in the event that the constant modulus condition is not initially present, we can correct the envelope by normalizing the in-phase and quadrature signal components, thus imposing this condition. This would be done at the expense of the processing requirements of the extra square-root required for normalization as implied by Equation (3-11), and the extra divisions which would be required.

3.2.3 Arccosine Numerical FM Discrimination

Given the existence of the Arcsine numerical discrimination method and the Indirect method which requires an arctangent calculation, it is naturally expected that a discrimination method exists which requires an arccosine correction. Consider the ratio

$$\begin{aligned}\hat{\phi}'_c(nT_s) &= \frac{A}{i^2(nT_s)+q^2(nT_s)} \\ &= \frac{i(nT_s) \cdot i([n-1]T_s) + q(nT_s) \cdot q([n-1]T_s)}{i^2(nT_s)+q^2(nT_s)} .\end{aligned}\quad (3-32)$$

From Equations (3-2) and (3-3), the denominator of Equation (3-32) is

$$i^2(nT_s) + q^2(nT_s) = a^2(nT_s) .$$

Similarly, the numerator simplifies to

$$\begin{aligned}i(nT_s) \cdot i([n-1]T_s) + q(nT_s) \cdot q([n-1]T_s) &= a(nT_s)a([n-1]T_s)\{\cos C \cos D + \sin C \sin D\} \\ &= a(nT_s)a([n-1]T_s)\cos(C - D) \\ &= a(nT_s)a([n-1]T_s) \cdot \cos[2\pi f_e T_s + \phi(nT_s) - \phi([n-1]T_s)] .\end{aligned}$$

Here, C and D are as defined in Equations (3-26) and (3-27). With the above substitutions, the instantaneous frequency estimate is equivalent to

$$\hat{\phi}'_c(nT_s) = \frac{a(nT_s)a([n-1]T_s)\cos[2\pi f_e T_s + \phi(nT_s) - \phi([n-1]T_s)]}{a^2(nT_s)} .\quad (3-33)$$

For the constant modulus case, we define

$$\begin{aligned}\hat{y}_{ac}(nT_s) &= F_s \cdot \arccos[\hat{\phi}'_c(nT_s)] \\ &= F_s \cdot \arccos\left[\frac{A}{i^2(nT_s)+q^2(nT_s)}\right].\end{aligned}\quad (3-34)$$

The arccosine function will unambiguously yield a value between 0 and π radians. The phase-difference quadrant determination algorithm that is required is therefore simply

$$\begin{aligned}d(nT_s) &= \arccos\left[\frac{A}{i^2(nT_s)+q^2(nT_s)}\right] \\ \text{if } \{B < 0.\} \\ d(nT_s) &= -d(nT_s) \\ \hat{y}_{ac}(nT_s) &= F_s \cdot d(nT_s),\end{aligned}\quad (3-35)$$

where A and B are defined as in Equations (3-18) and (3-19). Thus, the Arccosine method of numerical discrimination is as summarized by Equation (3-34) and Algorithm (3-35).

3.2.4 Principal-Value Arctan Numerical FM Discrimination

The Principal-Value Arctan numerical demodulation method can be developed by partially utilizing the development of the Arcsine method, previously described. By making the observation that the backward difference approximation to the time derivative as defined by Equation (3-7) is most valid at time $t = [n - \frac{1}{2}]T_s$, or half way between

consecutive time samples (see Appendix A) it becomes apparent that Equation (3-24) can be modified as

$$\hat{\phi}'_t(nT_s) = \frac{q(nT_s) \cdot i([n-1]T_s) - i(nT_s) \cdot q([n-1]T_s)}{\left[\frac{i(nT_s) + i([n-1]T_s)}{2} \right]^2 + \left[\frac{q(nT_s) + q([n-1]T_s)}{2} \right]^2} . \quad (3-36)$$

Essentially, an attempt has been made to time-align the sampled in-phase and quadrature signals with their corresponding time derivative estimates, by substituting

$$\frac{1}{2} \{ i(nT_s) + i([n-1]T_s) \}$$

for $i(nT_s)$, and

$$\frac{1}{2} \{ q(nT_s) + q([n-1]T_s) \}$$

for $q(nT_s)$ respectively. As can be seen, the numerator in Equation (3-24) remains unchanged, and the denominator is an estimate of the square of the envelope at time $t = [n - \frac{1}{2}]T_s$.

By applying Equations (3-2) and (3-3) to Equation (3-36), we find that

$$\hat{\phi}'_t(nT_s) = \frac{4 \sin[2\pi f_e T_s + \phi(nT_s) - \phi([n-1]T_s)]}{\frac{a^2(nT_s) + a^2([n-1]T_s)}{a(nT_s)a([n-1]T_s)} + 2 \cos[2\pi f_e T_s + \phi(nT_s) - \phi([n-1]T_s)]} . \quad (3-37)$$

Again, under the condition that $a(nT_s) = a([n-1]T_s)$, it is found that

$$\hat{\phi}'_t(nT_s) = 2 \tan\left[\frac{2\pi f_e T_s + \phi(nT_s) - \phi([n-1]T_s)}{2}\right] , \quad (3-38)$$

after application of a trigonometric identity. The modulating signal can be recovered as

$$\hat{y}_{pv}(nT_s) = 2F_s \cdot \arctan\left[\frac{1}{2}\hat{\phi}'_t(nT_s)\right], \quad (3-39)$$

where $\hat{\phi}'_t(nT_s)$ is as defined in Equation (3-32).

Note that the arctangent required in Equation (3-39) is different from that required in Equation (3-20) since the range of the obtained sampled phase differences has been reduced by a factor of 1/2, i.e.,

$$\frac{-\pi}{2} \leq \frac{1}{2}\hat{\phi}'_t(nT_s) \leq \frac{+\pi}{2},$$

as implied by Equation (3-38). Thus, the Principal-Value Arctan numerical FM demodulation method as summarized by Equations (3-36) and (3-39) requires neither phase quadrant determination as in the Direct and Indirect methods, nor phase-difference quadrant determination as in the Direct, Arcsine and Arccosine methods. Like the Arcsine and Arccosine methods, this numerical demodulation technique is best applied to constant modulus input signals.

3.2.5 Standard Numerical FM Discrimination

The conventional or standard *analog* FM discriminator [30] consists of a "slope-circuit" followed by an envelope detector, as shown in Figure (3-1 a). The frequency response of the slope-circuit is such that a constant-envelope frequency

modulated signal at the input results in an output signal with an envelope that is proportional to the original message. The slope circuit is designed to operate at a particular intermediate frequency, $f_{c'}$, as seen in the representative response in Figure (3-1 b). This response is approximately linear over the frequency interval

$$(f_{c'} - \Delta f) \leq |f| \leq (f_{c'} + \Delta f)$$

Typically, the constant envelope condition is imposed on the received FM signal via amplitude limiting circuitry, to remove any noise-/distortion-induced envelope variations. Thus the analog FM discriminator converts the instantaneous frequency variations into proportional amplitude variations, for subsequent envelope demodulation.

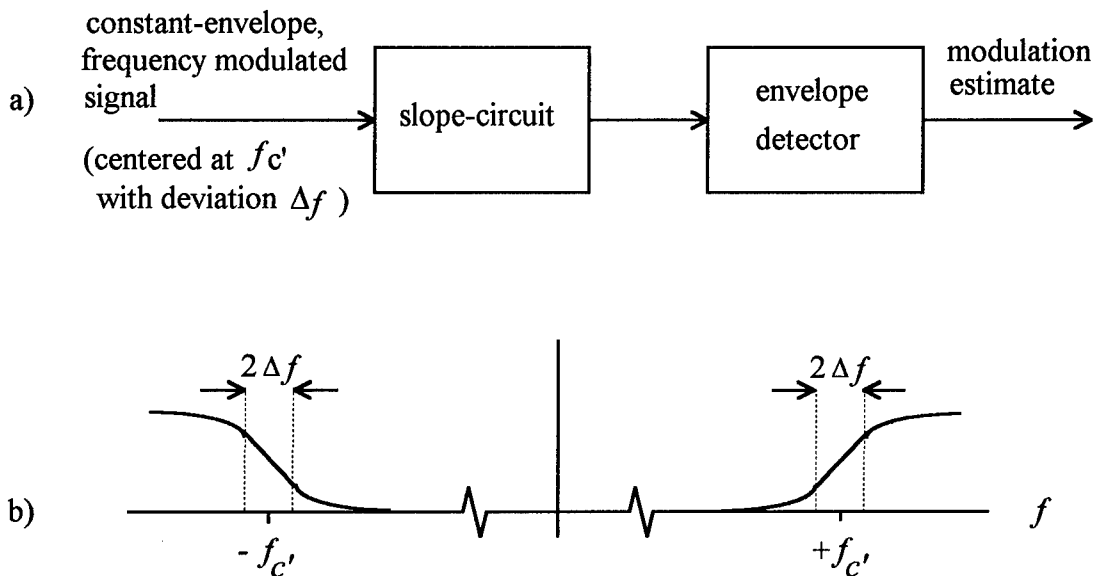


Figure (3-1). a) The conventional analog discriminator. b) Representative magnitude frequency response of the slope-circuit.

The Standard numerical FM discrimination method is the discrete-time implementation of the conventional analog device. In the discrete-time case, we will be processing the ideal generalized pre-envelope, $s_+(nT_s)$, centered at the frequency $f_o = f_e$, i.e., the slightly mis-tuned complex envelope. Of the various stages of processing required, it is the discrete-time counterpart to the slope-circuit which requires some detailed development.

We borrow upon previous developments in both Chapter 2 and Appendix A, to arrive at a numerical slope-circuit implementation. From Figure (A.3-2), it is apparent that the response of the backward difference identified as $H_B(e^{j\Omega})$ approximates that of an ideal slope-circuit, $H_A(e^{j\Omega})$, over the frequency interval 0 to $F_s/2$ Hz. It is also apparent that if the generalized pre-envelope were centered near $F_s/4$ Hz, it could be filtered using the (real) backward difference impulse response, to generate a signal with an envelope modulation which is proportional to the instantaneous frequency. Note that the allowable range on the instantaneous frequency is from 0 to $F_s/2$.

Rather than rotating the generalized pre-envelope from f_e Hz to $(f_e + F_s/4)$ Hz, the impulse response of the backward difference can be (circularly) rotated in frequency by the amount $-F_s/4$ Hz, using the methods described in Section 2.3.2. The result is a (complex) impulse response which can be used to directly filter the complex envelope, $s_+(nT_s)$. The impulse response of the backward difference filter is

$$\begin{aligned} T_s \cdot h_B(nT_s) &= +1, \quad n = 0, \\ &= -1, \quad n = -1, \\ &= 0, \quad \text{else}. \end{aligned} \tag{3-40}$$

Frequency rotation of these coefficients is accomplished by multiplying the sequence of Equation (3-40) by the complex exponential,

$$\begin{aligned}
 e^{-j[2\pi \cdot \frac{F_s}{4} \cdot n T_s]} &= \cos[2\pi \cdot \frac{F_s}{4} \cdot n T_s] - j \sin[2\pi \cdot \frac{F_s}{4} \cdot n T_s] \\
 &= \cos[\frac{\pi}{2} \cdot n] - j \sin[\frac{\pi}{2} \cdot n]. \tag{3-41}
 \end{aligned}$$

The result is the discrete-time slope-circuit complex impulse response,

$$\begin{aligned}
 T_s \cdot h_{sl}(n T_s) &= +1, \quad n = 0, \\
 &= +j, \quad n = -1, \\
 &= 0, \text{ else}. \tag{3-42}
 \end{aligned}$$

This discrete-time slope-circuit is implemented in a straightforward fashion as shown in Figure (3-2).

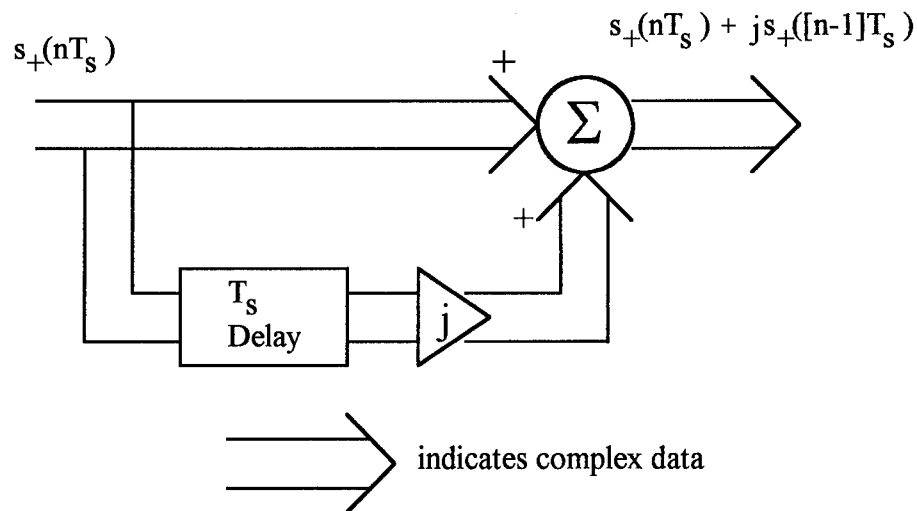


Figure (3-2). The discrete-time slope-circuit derived from the backward difference filter.

The output of this slope-circuit is

$$s_+(nT_s) + j \cdot s_+([n-1]T_s) = [i(nT_s) - q([n-1]T_s)] + j \cdot [q(nT_s) + i([n-1]T_s)] . \quad (3-43)$$

If we consider forming the square of the envelope of the signal of Equation (3-43), the result is

$$\begin{aligned} |s_+(nT_s) + j \cdot s_+([n-1]T_s)|^2 &= [i^2(nT_s) + q^2(nT_s)] + [i^2([n-1]T_s) + q^2([n-1]T_s)] \\ &\quad - 2 \cdot [i(nT_s) \cdot q([n-1]T_s) - q(nT_s) \cdot i([n-1]T_s)] . \end{aligned} \quad (3-44)$$

As already indicated, in the conventional analog discriminator, a constant envelope condition is imposed via amplitude limiting circuitry. In a similar fashion, a normalized envelope condition can be imposed on the complex envelope, prior to the slope-circuit. Under this condition, the first two terms in brackets in Equation (3-44) are each equal to unity. In this case Equation (3-44) simplifies to

$$|s_+(nT_s) + j \cdot s_+([n-1]T_s)|_{normalized}^2 = 2 \cdot [1 + q(nT_s) \cdot i([n-1]T_s) - i(nT_s) \cdot q([n-1]T_s)] . \quad (3-45)$$

By simply subtracting the constant term and scaling by a factor of 1/2, the Standard numerical FM discrimination estimate becomes

$$\hat{\phi}'_s(nT_s) = q(nT_s) \cdot i([n-1]T_s) - i(nT_s) \cdot q([n-1]T_s) . \quad (3-46)$$

Figure (3-3) summarizes the Standard numerical FM discrimination processing steps.

In comparing Equations (3-46) with the intermediate step in the Arcsine discrimination method of Equation (3-24), it is noted that under the normalized envelope condition, these equations are identical. It is then immediately evident that once again, an arcsine correction is required as indicated in Equation (3-30) to achieve a linear estimate of the original message. Likewise, to increase the range of allowable instantaneous frequency values to the entire (complex) Nyquist band, the phase-difference quadrant determination algorithm in (3-31) can be employed.

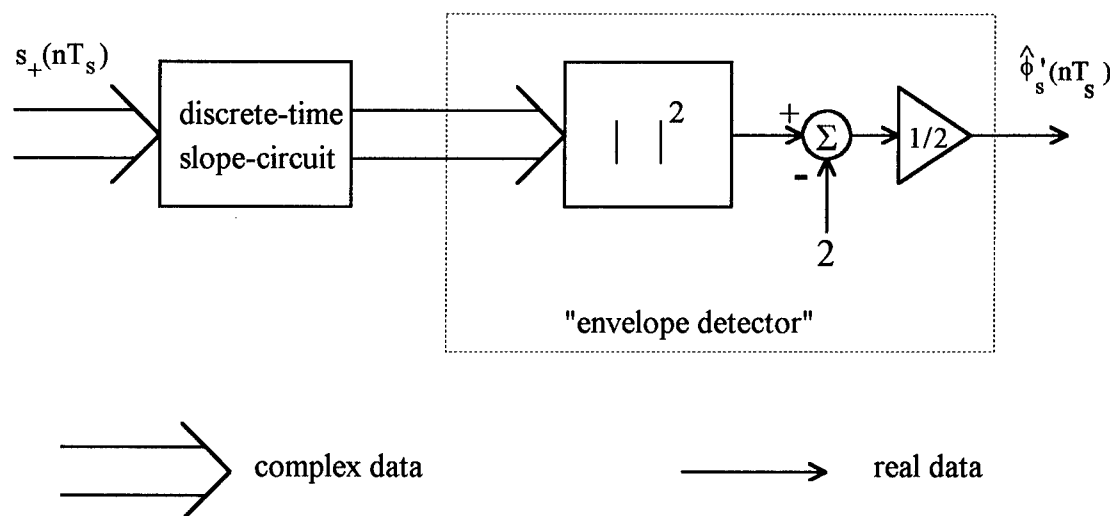


Figure (3-3). The Standard numerical FM discrimination method.

Thus, the Standard numerical FM discrimination method is found to be mathematically equivalent to an intermediate step in the Arcsine method. With the appropriate corrections previously described, the output of the Standard discrimination process will be equivalent to the output of the Arcsine method. This is interesting to note, given that the Arcsine and the Standard methods were developed using very distinct approaches. In fact, it will be demonstrated in the following section that the Direct, Indirect, Arcsine, Arccosine, Principal-Value Arctan and the (corrected) Standard methods of numerical FM demodulation are all mathematically equivalent.

3.2.6 Discrimination Method Comparison

In Section 3.2.5 it has been established that the distortion-corrected Standard numerical discriminator and the Arcsine numerical discriminator are mathematically equivalent. We will subsequently establish the additional result that the Arcsine method (and therefore the distortion-corrected Standard method) is also equivalent to the Direct, Indirect, Arccosine and Principal-Value Arctan discrimination techniques. Thus the numerical demodulation techniques presented in Section 3.2 are considered to be of the class of FM demodulators which employ the backward difference approximation to the time rate of change of phase, as the message estimate. Further, since these numerical demodulators include the distortion-corrected Standard discriminator, justification of the term "discriminator" for each member of this class is established. Each member is

therefore considered to be of the class of *backward difference numerical FM discriminators*.

We first consider the equivalence of the Direct and Indirect processing techniques. Equivalence can be established by demonstrating that the instantaneous frequencies specified by Equations (3-13) and (3-16) are the same. From Equation (3-12), this implies that we must demonstrate the equivalence of the Direct process,

$$\hat{y}_d(nT_s) = F_s \cdot g_E [g[2\pi f_e n T_s + \phi(nT_s) - \theta] - g[2\pi f_e [n-1] T_s + \phi([n-1]T_s) - \theta]] , \quad (3-47)$$

and the Indirect process,

$$\hat{y}_I(nT_s) = F_s \cdot g[2\pi f_e T_s + \phi(nT_s) - \phi([n-1]T_s)] . \quad (3-48)$$

Applying modulo arithmetic rules it can be shown that

$$g[\alpha_1 - \alpha_2] = g[g[\alpha_1] - g[\alpha_2]] , \quad (3-49)$$

which immediately demonstrates the equivalence of Equations (3-47) and (3-48), with α_1 identified as

$$\alpha_1 = 2\pi f_e n T_s + \phi(nT_s) - \theta ,$$

and α_2 identified as

$$\alpha_2 = 2\pi f_e [n-1] T_s + \phi([n-1]T_s) - \theta .$$

Thus we find that

$$\hat{y}_d(nT_s) = F_s \cdot g[2\pi f_e T_s + \phi(nT_s) - \phi(nT_s)] . \quad (3-50)$$

Consider now the Arcsine method as summarized by Equation (3-30) and the phase-difference quadrant determination of Algorithm (3-31). From Equations (3-29) and (3-30) along with Algorithm (3-31) we have

$$\hat{y}_{as}(nT_s) = F_s \cdot g[2\pi f_e T_s + \phi(nT_s) - \phi([n-1]T_s)] . \quad (3-51)$$

The process $g[]$ indicated in Equation (3-51) is a result of the phase-difference algorithm. This algorithm is simply a variant of the phase quadrant determination process required by the Arctan introduced in Equation (2-3) of Section 2.1. In comparing Equations (3-51) and (3-48), it is apparent that the Arcsine method of discrimination is mathematically equivalent to the Indirect (and therefore also to the Direct) method of instantaneous frequency estimation. Likewise for the Arccosine method, Equations (3-33), (3-34) and Algorithm (3-35) demonstrate that

$$\hat{y}_{ac}(nT_s) = F_s \cdot g[2\pi f_e T_s + \phi(nT_s) - \phi([n-1]T_s)] . \quad (3-52)$$

Finally, from the properties of the arctangent required in Equation (3-35) and the results of Equation (3-34), the Principal-Value Arctan method yields

$$\hat{y}_{pv}(nT_s) = F_s \cdot g[2\pi f_e T_s + \phi(nT_s) - \phi([n-1]T_s)] . \quad (3-53)$$

Thus the Arccosine and Principal-Value Arctan methods are also equivalent to each of the aforementioned techniques.

It has been demonstrated that the distortion-corrected Standard method, the Direct and Indirect methods, the Arcsine and Arccosine methods and the Principal-Value Arctan methods are all mathematically equivalent numerical FM demodulation techniques. Note however, that differences do exist in the processing requirements of each method. Therefore, one of the methods will be selected based on implementation considerations, as an "established baseline" for subsequent performance analysis comparisons.

3.2.6.1 Selection of a Baseline Numerical Discrimination Technique

Each of the previously described numerical FM demodulation techniques require, as a minimum, a single division and a trigonometric inversion. However, in view of the additional processing required by the Standard, Arcsine, Arccosine and Principal-Value Arctan discrimination methods to impose the constant modulus condition, these methods will not be considered further. It is acknowledged that depending on specific application requirements, any one of these methods may be considered "better" than the others. For example, if an application happens to require an envelope estimate in addition to the instantaneous frequency, the envelope calculation is no longer considered to be an extra processing burden. In this case, the Standard, Arcsine, Arccosine and Principal-Value Arctan methods become more attractive from an implementation viewpoint.

Since, for the purposes of this research, it is the instantaneous frequency which is of primary interest, the Direct and Indirect methods remain as baseline candidates due to their insensitivity to amplitude variations. Further still, due to its conceptual simplicity, the Direct method is arbitrarily selected as the chosen baseline numerical FM discriminator. It is pointed out, however, that since each of these methods are mathematically equivalent, subsequent performance analyses and simulations of the Direct method apply equally well to the remaining discrimination techniques.

3.3 Sampling Rate Considerations

The sampling theorem as put into general practice in the field of communications engineering by Nyquist [31] and formalized by Shannon [32], has become commonplace in the scientific and technical community. Simply stated the sampling theorem indicates that a real lowpass signal having spectral content limited to the frequency range 0 to W Hz, can be accurately represented by instantaneous samples of the amplitude of the signal taken at time intervals of $\Delta t = T_s < 1/(2W)$ seconds. Entire texts (e.g., [12]) have been devoted to the processing of the resulting discrete-time signal, and to the reconstruction into continuous time of the extracted information or control bearing signals. (In fact, generalized versions of the sampling theorem do not require uniformly time-spaced samples, and also includes, for example, sampling the signal and its derivatives to form a discrete-time representation [32][33].)

Shannon's presentation of the sampling theorem also allows for the conversion of a real bandpass (i.e., bandlimited) signal, centered at $f = f_c$, from continuous to discrete time by employing the proper frequency downconversion techniques as stated in Section 2.3. Reformulating this result, a real bandpass signal of approximate bandwidth B' Hz, and originally centered at some carrier frequency f_c Hz, can be sampled by first downconverting to a new center frequency of $f_c > B'/2$ Hz, with $W = f_c + B'/2$. An idealized version of this process is depicted in Figure (3-4).

As Slepian appropriately points out [34], strictly speaking, truly bandlimited lowpass/bandpass signals do not exist in reality, since this would imply that such a signal is present for all time. In light of this, he established the concept of essentially or *really*

bandlimited signals, to distinguish between exact mathematical models and models that are less restrictive for practical implementation. Urkowitz applied this result and correctly concludes that this *approximate* bandwidth of a real bandpass signal must be less than 200%, relative to its center frequency, f_c . This center frequency is, as implied, the center or midpoint of the signal frequency band.

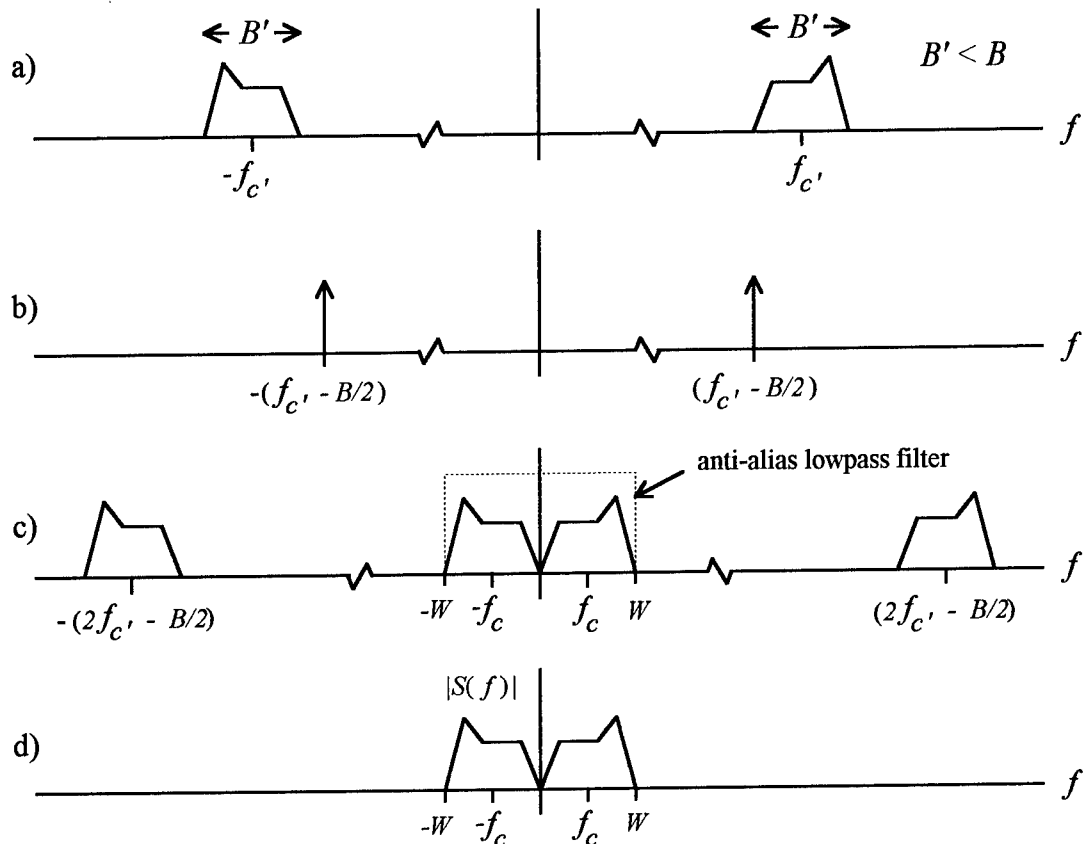


Figure (3-4). Bandpass signal pre-acquisition processing. a) A representative magnitude spectrum of a bandpass signal of bandwidth $B' < B$, centered at f_c Hz. b) The magnitude frequency response of the analog local oscillator used for frequency downconversion. c) The result of convolving the original spectrum with the local oscillator spectrum; $f_c = B/2$, $W = f_c + B'/2$. d) The representative spectrum of the desired signal, $s(t)$, prior to conversion from analog to discrete time.

Thus Shannon's previously presented method of preparing a bandpass signal for conversion from analog to discrete time, and Urkowitz's requirement as stated above, are consistent.

We now turn our attention to the representation of a bandpass signal, $s(t)$, as the product of the real lowpass signal, $a(t)$, and the real bandlimited signal, $\cos[2\pi f_c t + \phi(t) - \theta]$. As a consequence of Bedrosian's product theorem [35], in order for the signal, $s(t)$, modeled as

$$s(t) = a(t) \cdot \cos[2\pi f_c t + \phi(t) - \theta] \quad (3-54)$$

to be bandpass, it is required that

$$\begin{aligned} |A(f)| &= 0, \quad |f| > f_1, \\ |A(f)| &\geq 0, \quad |f| \leq f_1, \end{aligned} \quad (3-55)$$

and simultaneously that

$$\begin{aligned} |\mathcal{F}\{\cos[2\pi f_c t + \phi(t) - \theta]\}| &= 0, \quad |f| < f_2, \\ &\geq 0, \quad f_2 \leq |f| \leq f_3, \\ &= 0, \quad |f| > f_3, \end{aligned} \quad (3-56)$$

with $f_2 > f_1$. Here, $|A(f)| = |\mathcal{F}\{a(t)\}|$ is the magnitude spectrum of the real lowpass signal, $a(t)$. (Equality in Equations (3-55) and (3-56) can be interpreted as in the practical sense

developed by Slepian.) Figure (3-5) is representative of this application of Bedrosian's product theorem, for the case where f_2 approaches f_1 , and $a(t)$ is real. Note that in view of Slepian's results, this product theorem can be viewed both as a bandpass signal construction technique and as justification of bandpass signal representation, as applied to the signal $s(t)$ resulting from the pre-sampling process depicted in Figure (3-4).

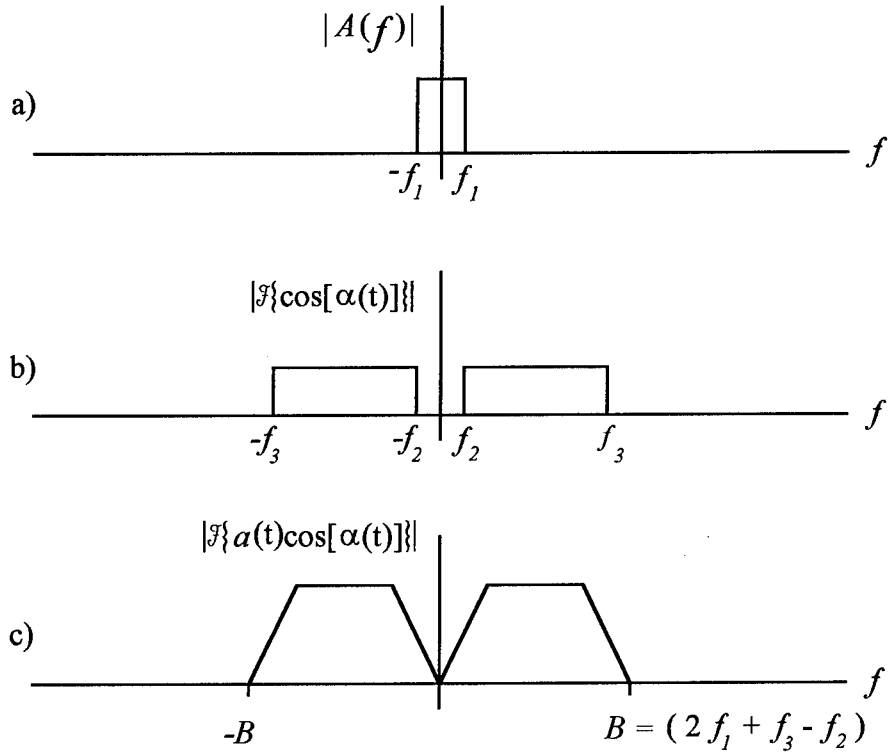


Figure (3-5). Representative spectra depicting a special case of Bedrosian's product theorem. a) The magnitude spectrum of the real lowpass signal, $a(t)$. b) The magnitude spectrum of the approximately bandlimited signal, $\cos[\alpha(t)]$, where $\alpha(t) = 2\pi f_c t + \phi(t) - \theta$. c) The magnitude spectrum of the product, $a(t)\cos[\alpha(t)]$.

We conclude that the pre-sampled signal, $s(t)$, resulting from the proper downconversion and anti-aliasing filtering of a bandpass signal centered at f_c Hz, retains the bandpass representation indicated in Equation (3-54). The resultant discrete-time signal, $s(nT_s)$, is therefore (within an arbitrary constant phase offset)

$$s(nT_s) = s(t)|_{t=nT_s} = a(nT_s) \cdot \cos[2\pi f_c nT_s + \phi(nT_s)] . \quad (3-57)$$

It is this real discrete-time "bandpass" signal which is processed as described in Sections 2.3.1 and 2.3.2 to generate the complex-valued generalized pre-envelope, $s_+(nT_s)$. Thus for the bandpass signal, $s(t)$, of bandwidth B Hz, the required *acquisition* sample interval is

$$T_s(\text{acquisition}) < \frac{1}{2B} \text{ seconds.} \quad (3-58)$$

Note that in additionally modeling this signal as being representative of the frequency modulation process as in Equation (3-4), it is further required that $a(nT_s) > 0$, as indicated in Equation (2-13). This condition prevents the sign of the amplitude, $a(nT_s)$, from distorting the instantaneous phase. This amplitude has initially been modeled as being time dependent to allow us to demonstrate the insensitivity of the Direct and Indirect numerical discrimination methods to these amplitude variations. However, in adopting this more general model, it has been necessary to address the previous bandpass representation considerations. In subsequent analyses we will adopt the more restrictive model in which

the amplitude is a constant, $a(nT_s) = a$. In this constant amplitude case, we can closely approximate the bandwidth, B , using Carson's rule [30],

$$B \cong 2 \cdot (\Delta f + f_m) \text{ Hz} . \quad (3-59)$$

Here, f_m is the highest significant frequency component in the message signal, $m(t)$.

3.3.1 Sampling Rate Requirements of the Ideal Complex DTFM Signal

Once generated, it is common practice to increase the sampling interval of the complex envelope by a factor of 2. Thus the sampling interval requirement for the complex envelope becomes

$$T_{s \text{ (decimated)}} = 2 \cdot T_{s \text{ (acquisition)}} , \quad (3-60)$$

which from Equation (3-58) becomes

$$T_{s \text{ (decimated)}} < \frac{1}{B} \text{ seconds.} \quad (3-61)$$

A set of signal spectra representative of this decimation or downsampling process is shown in Figure (3-6). The ability to do so is simply a consequence of the lack of signal energy in the frequency bands

$$\dots -\frac{3F_s}{4} < f < -\frac{F_s}{4} , \quad \frac{F_s}{4} < f < \frac{3F_s}{4} , \quad \frac{5F_s}{4} < f < \frac{7F_s}{4} \dots$$

where

$$F_s = \frac{1}{T_s(\text{acquisition})}$$

Therefore, increasing the sample interval by a factor of 2 by simply discarding every other sample, does not lead to destructive aliasing of frequency components in the resulting decimated complex envelope [12]. (As a consequence of decimation by a factor of 2, the resulting spectrum is 1/2 the amplitude prior to decimation, to be consistent with the discrete-time Fourier transform definition.)

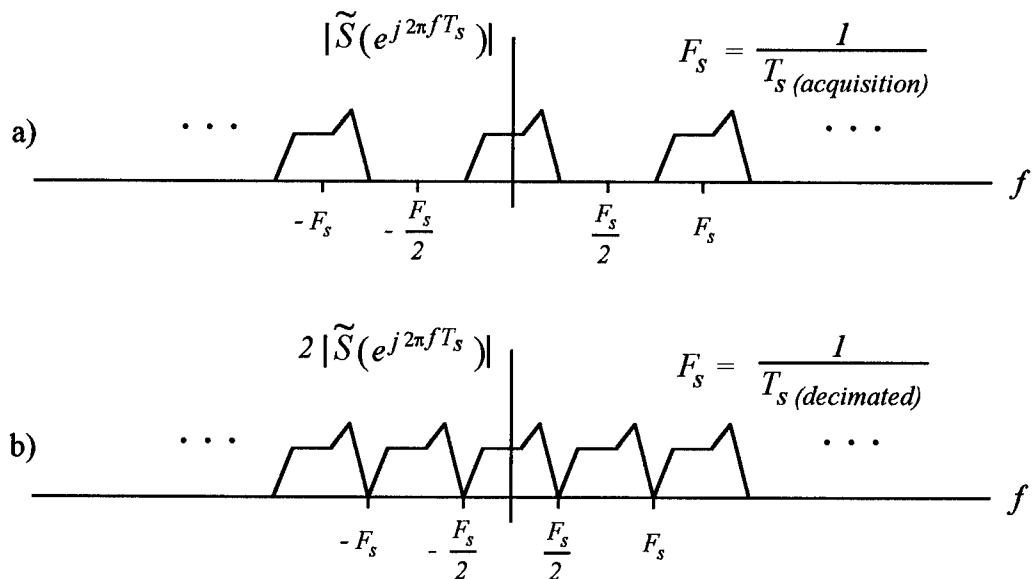


Figure (3-6). A set of signal magnitude spectrum depicting the decimation of the complex envelope by a factor of 2. a) $|\mathcal{F}\{\tilde{s}(nT_s)\}|$ with F_s equal to the acquisition sample rate. b) $2|\mathcal{F}\{\tilde{s}(nT_s)\}|$ with F_s equal to the decimated sample rate.

Likewise the generalized pre-envelope, once generated, can be properly represented by samples at time intervals of $T_{s(\text{decimated})}$. This is evident since circular frequency rotation can be performed either before or after the downsampling process, resulting in exactly the same time sequence of ordered pairs, $\{i(nT_s), q(nT_s)\}$. Note however that this and any further decimation in time must be done *after* generating the generalized pre-envelope sequence. Thus we do initially require a sample interval as defined in Equation (3-58), for the method of acquisition which has been defined.

The issue that needs to be addressed is the determination of the largest time interval, resulting from decimation, that can be allowed. We do so by considering the requirement to extract an estimate of the original message, $m(t)$. The message signal is modeled as being bandlimited such that

$$\begin{aligned} |M(j\omega)| &= |\mathcal{F}\{m(t)\}| \geq 0, \quad |\omega| \leq \omega_m, \\ &= 0, \quad |\omega| > \omega_m, \quad \omega_m = 2\pi f_m. \end{aligned} \quad (3-62)$$

For each ordered pair $\{i(nT_s), q(nT_s)\}$, backward difference numerical FM discrimination will result in the estimate

$$\hat{y}_d(nT_s) = \hat{\phi}'_d(nT_s) = F_s \cdot g[T_s \cdot h_B(nT_s) * \{2\pi f_e nT_s + \phi(nT_s) - \theta\}], \quad (3-63)$$

as implied by Equation (3-51). Here, $h_B(nT_s)$ is as defined in Equation (3-40) with the response indicated in Appendix A. (The subscript d can be thought of as representing either the *Direct* method specifically, or more generally, backward difference numerical *discrimination*.) From the results of Appendix A and Equation (3-5) we conclude that

$$\begin{aligned}\hat{y}_d(nT_s) &= F_s \cdot g[2\pi f_e T_s + T_s \cdot h_D(nT_s) * \phi'(nT_s)] \\ &= F_s \cdot g[2\pi f_e T_s + T_s \cdot h_D(nT_s) * \{2\pi \Delta f \cdot m(nT_s)\}]\end{aligned}\quad (3-64)$$

Here, $h_D(nT_s)$ is the impulse response of the distortion transfer function, $H_D(e^{j\Omega})$, due to the non-ideal nature of the backward difference approximation to the true time derivative. Equation (3-64) is a key result, in that it indicates the need to specify two distinct sample time-interval requirements for complex DTFM signals.

The first requirement is a result of applying Nyquist's criterion to the message signal, $m(t)$. Since the linear convolution internal to Equation (3-64) does not result in frequency components outside the range indicated in Equation (3-62), we have the requirement

$$T_s \text{ (decimated)} < \frac{1}{2f_m} . \quad (3-65)$$

Defining the ratio

$$\gamma = \frac{F_s}{2f_m} , \quad (3-66)$$

we have the equivalent requirement

$$\gamma > 1 . \quad (3-67)$$

We will refer to γ as the *relative message sampling rate*. The requirement identified in Equation (3-67) ensures that the discrete-time estimation of the original message, as identified in Equation (3-64), is sampled at a sufficient rate.

The second sample rate requirement is a consequence of the modulo 2π process, $g[]$, in Equation (3-64). We immediately conclude that this results in a mapping of all phase differences, to sheet 0 of the phase-difference plane. In order to unambiguously recover an estimate of the original message, it is additionally required that

$$-\pi < 2\pi f_e T_s + T_s \cdot h_D(nT_s) * \{2\pi \Delta f \cdot m(nT_s)\} \leq +\pi . \quad (3-68)$$

Since both f_e and $m(nT_s)$ can independently be either positive or negative, this translates into the requirement

$$T_s (\text{decimated}) < \frac{1}{2 \cdot \{|f_e| + \Delta f \cdot |h_D(nT_s) * m(nT_s)|\}} , \quad (3-69)$$

for all values of the index n . From Appendix A it is apparent that the gain of the distortion response, $|H_D(e^{j\Omega})|$, does not exceed unity at any particular frequency. In addition, by design $m(nT_s)$ does not exceed unity in magnitude. Therefore, in most modulation scenarios, Equation (3-69) simplifies to the requirement

$$T_s (\text{decimated}) < \frac{1}{2 \cdot \{|f_e| + \Delta f\}} . \quad (3-70)$$

In this form it is evident that this second sampling interval requirement ensures that the maximum deviation of the instantaneous frequency from 0 Hz, does not exceed $F_s/2$ in magnitude. Thus, this requirement prevents *instantaneous frequency aliasing*. Defining the ratio

$$\delta = \delta_e + \delta_m , \quad (3-71 \text{ a})$$

where

$$\delta_e = \frac{2 |f_e|}{F_s} , \quad (3-71 \text{ b})$$

and

$$\delta_m = \frac{2 \Delta f}{F_s} , \quad (3-71 \text{ c})$$

we equivalently require

$$\delta < 1 . \quad (3-72)$$

We will refer to δ as the *DTFM modulation index*, δ_m as the *DTFM message index*, and δ_e as the *DTFM tuning-error index*. Note that "overmodulation" (i.e., $\delta > 1$) translates into instantaneous frequency aliasing.

The DTFM modulation index, δ , and the relative message sampling rate, γ , can be related to the modulation index, β , of the continuous-time FM signal by considering the product

$$\gamma \cdot \delta = \frac{f_e}{f_m} + \frac{\Delta f}{f_m} . \quad (3-73)$$

The modulation index of the continuous-time FM signal is typically defined as [30]

$$\beta \equiv \frac{\Delta f}{f_m} . \quad (3-74)$$

Thus from Equations (3-73), (3-74), and previous results we obtain

$$\beta = \gamma \cdot \delta - \frac{f_e}{f_m} = \gamma \cdot \delta_m . \quad (3-75)$$

The sampling interval requirements summarized by Equations (3-65) and (3-70) for proper recovery of the message signal from the complex DTFM signal can be combined as

$$T_{s \text{ (decimated)}} < \min \left\{ \frac{1}{2f_m}, \frac{1}{2 \cdot \{|f_e| + \Delta f\}} \right\} . \quad (3-76)$$

Note that since we have modeled the DTFM signal as having a constant amplitude, the decimation process will not result in frequency aliasing in the envelope sequence.

3.3.2 Instantaneous Frequency Aliasing and the Generalized Pre-envelope

In representing our instantaneous frequency estimate as in Equation (3-64), it is implied that the input to the discrimination process is

$$s_+(nT_s, f_e) = a \cdot \{\cos[2\pi f_e nT_s + \phi(nT_s) - \theta] + j \sin[2\pi f_e nT_s + \phi(nT_s) - \theta]\}. \quad (3-77)$$

Consider the case where we have as input the generalized pre-envelope

$$s_+(nT_s, f_o) = a \cdot \{\cos[2\pi f_o nT_s + \phi(nT_s) - \theta] + j \sin[2\pi f_o nT_s + \phi(nT_s) - \theta]\},$$

$$\frac{-F_s}{2} < f_o \leq \frac{+F_s}{2}. \quad (3-78)$$

Analogous to Equation (3-64), this results in the instantaneous frequency estimate

$$\hat{y}_d(nT_s, f_o) = F_s \cdot g[2\pi f_o T_s + T_s \cdot h_D(nT_s) * \{2\pi \Delta f \cdot m(nT_s)\}]. \quad (3-79)$$

Note that for values of f_o near $\pm F_s/2$, even the slightest message signal amplitude can result in instantaneous frequency aliasing. Rather than discarding the discrimination result indicated in Equation (3-79), it is possible to correct the frequency rotation implied by the term, $2\pi f_o T_s$. Define the modulo 2π process, $g[\alpha, f_o]$, as

$$g[\alpha, f_o] \equiv g[\alpha - \frac{2\pi f_o}{F_s}], \quad (3-80)$$

where $g[]$ is as in Equation (2-8). By employing the property of modulo arithmetic indicated in Equation (3-49) along with Equations (3-79) and (3-80), it is readily apparent that

$$\hat{y}_d(nT_s, 0) = F_s \cdot g[T_s \cdot \hat{y}_d(nT_s, f_o), f_o]. \quad (3-81)$$

Thus in the case that the center frequency, f_o , is known exactly, the result of the backward difference discrimination process can always be corrected. In effect, the process $g[\alpha, f_o]$ changes the reference of the process $g[\alpha]$ from 0 radians, to $2\pi f_o / F_s$ radians, as depicted in Figure (3-7).

As indicated in Section 2.3.1, in practice the true center frequency, f_o , is not known exactly. This results in the tuning error, f_e , which is normally small relative to $F_s/2$. In this case, the instantaneous frequency estimate becomes

$$\begin{aligned} \hat{y}_d(nT_s) &= \hat{y}_d(nT_s, f_o) \\ &= F_s \cdot g[T_s \cdot \hat{y}_d(nT_s, f_o), f_o - f_e]. \end{aligned} \quad (3-82)$$

Thus the sampling rate requirements remain as in Section 3.3.1. The process indicated in Equation (3-82) will be referred to as a phase-difference "downwrapping", since in effect both frequency downconversion (or rotation) and phase-difference unwrapping or quadrant determination are performed simultaneously.

In conclusion, the generalized pre-envelope sequence, $s_+(nT_s, f_o)$, can be processed directly by the numerical discrimination techniques previously described. The resulting

sequence is subsequently processed as in Equation (3-82), to yield the desired instantaneous frequency estimate. Note that the discrimination and the downwrapping process can be performed on a sample by sample basis. Therefore, the class of backward difference numerical FM discriminators are particularly useful in real-time applications.

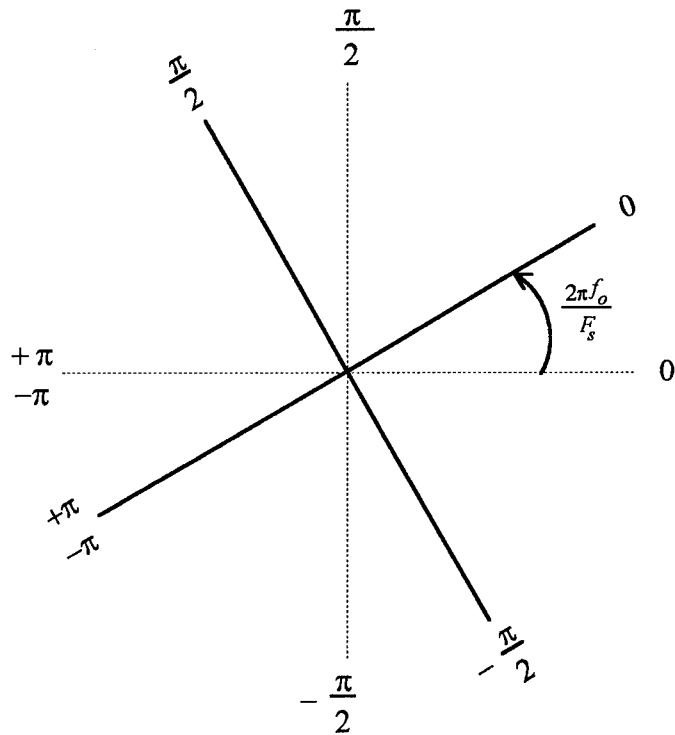


Figure (3-7). The geometric representation of the process $g[\alpha, f_o]$ as a rotation of the angle reference axes used in the modulo 2π process $g[\alpha]$. In this particular representation, a positive value of f_o is depicted.

CHAPTER 4

**Backward Difference Numerical Discrimination
in the Presence of Additive White Gaussian Noise**

4.1 Phase Modulation Recovery and Phase Domain Performance Measures

In Chapter 3, various approaches to the generation of the backward difference approximation of the rate of change of phase were introduced as instantaneous frequency estimates. From among these approaches the Direct method has been selected as a baseline numerical FM discrimination process for analysis purposes, although each of these approaches results in the same estimate. Therefore any reference made to the baseline numerical discrimination process will refer to the Direct method specifically, or more generally, to any one of these equivalent processes.

We summarize the baseline discriminator using Equations (3-12) and (3-13) as

$$\hat{\phi}'_d(nT_s) = F_s \cdot g_E[\hat{\phi}_i(nT_s) - \hat{\phi}_i([n-1]T_s)] \quad (4-1)$$

in units of radians per second, where

$$\hat{\phi}_i(nT_s) = \text{Arctan}\left[\frac{\text{Im}\{\text{complex envelope}\}}{\text{Re}\{\text{complex envelope}\}}\right]. \quad (4-2)$$

It is convenient to define the phase message estimate as the accumulation of the instantaneous frequency sequence of Equation (4-1). Thus in units of radians we define

$$\hat{\phi}_d(nT_s) = T_s \cdot \left\{ \sum_{k=0}^n \hat{\phi}'_d(kT_s) + \phi_d(-T_s) \right\} \quad (4-3)$$

as the *baseline discriminator phase message estimate*. Here, $\phi_d(-T_s)$ is an arbitrary initial phase value assigned to the phase at time $t = -T_s$. This is also the initial value assigned to the instantaneous phase at time $t = -T_s$ during the numerical discrimination process, i.e.,

$$\phi_d(-T_s) = \hat{\phi}_i(-T_s).$$

Usually the initial phase $\phi_d(-T_s)$ is assigned the value zero, such that it need not be retained for phase message recovery. Note that the accumulation process of Equation (4-3) is an inversion of the backward difference calculation [12] and has the transfer function $[H_B(e^{j\Omega})]^{-1}$. Thus we are motivated to work in the phase domain in subsequent performance analyses in that the distortion $H_D(e^{j\Omega})$ is no longer present and therefore not of concern.

In this chapter we will use both an analytical and an experimental approach to the prediction of the performance of backward difference numerical FM discrimination in the presence of additive white Gaussian noise (AWGN). The experimental aspect consists of computer simulations where finite length complex signal sequences consisting of the ideal DTFM signal and additive noise are generated and processed for performance measurement purposes. By calculating a pair of statistics to be described, an experimental performance measure is established for comparison to the analytically predicted results. It should be noted that in this research, the term "white" refers to the fact that the noise power spectral density is constant over the Nyquist frequency interval. In continuous time, it is common to refer to this noise as being "bandlimited white" noise.

The signal model to be used for both the analytical and experimental performance predictions is depicted in Figure (4-1). The model consists of the ideal complex DTFM signal sequence as described by Equations (3-1) through (3-4), in summation with a complex Gaussian noise sequence, both of which are represented in Cartesian form. The discrete-time noise sequence is the sampled bandpass noise process

$$\tilde{N}(nT_s) = N_i(nT_s) + j \cdot N_q(nT_s) , \quad (4-4)$$

where $N_i(nT_s)$ is the Gaussian distributed in-phase component sequence, and $N_q(nT_s)$ is the Gaussian distributed quadrature component sequence. The random processes $N_i(nT_s)$ and $N_q(nT_s)$ are real-valued independent and identically distributed processes of zero mean and variance σ^2 . This signal-plus-noise model is typical of that used in communication systems analyses [11, 36].

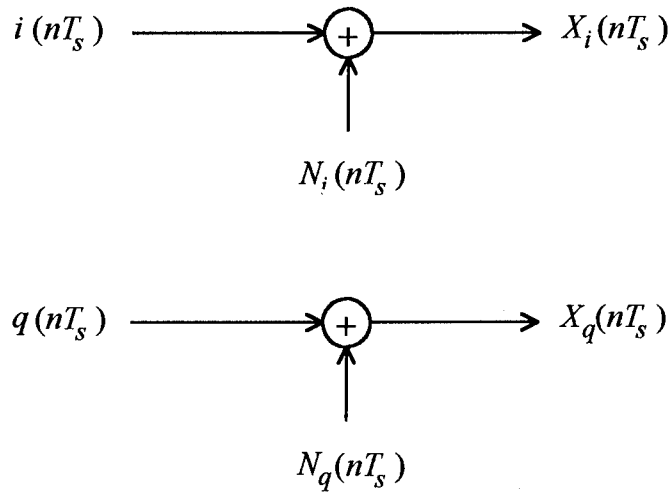


Figure (4-1). The model of the ideal complex DTFM signal in the presence of bandlimited additive white Gaussian noise.

Prior to sampling, we consider the power spectral density of the noise, $S_{\tilde{N}\tilde{N}}(f)$, as being uniformly distributed over the frequency interval $-W/2 < f \leq +W/2$, and of density $2N_0$ Watts/Hz. The corresponding autocorrelation sequence, $R_{\tilde{N}\tilde{N}}(\tau)$, found as the inverse Fourier transform of the power spectral density, is

$$R_{\tilde{N}\tilde{N}}(\tau) = 2N_0 W \cdot \frac{\sin(\pi W\tau)}{\pi W\tau} . \quad (4-5)$$

The zeros of this function occur at integer multiples of W . Thus by ensuring that the sample interval is selected to correspond to the occurrence of these zeros, the samples of the complex noise sequence will be uncorrelated. Since these samples are of a zero mean Gaussian process, they are also independent. For analysis purposes, we choose the maximum required sample interval satisfying the Nyquist criterion, which corresponds to the smallest non-zero time interval that yields uncorrelated samples. The corresponding discrete-time power spectral "density" is [12]

$$S_{\tilde{N}\tilde{N}}(e^{j\Omega}) = 2N_0 F_s , \quad -\pi < \Omega \leq +\pi , \quad \Omega = \omega T_s . \quad (4-6)$$

Thus after sampling, the noise power is uniformly distributed, and therefore considered to be "white", over the Nyquist interval. With a spectral density of $2N_0$ Watts/Hz over the frequency interval $-W/2 < f \leq +W/2$ Hz, we find that the power of the complex noise waveform is $2N_0 W = 2N_0 F_s$. This corresponds to twice the variance, σ^2 , of both the in-phase and quadrature components. The resultant noise-contaminated complex

DTFM signal is represented as the random process

$$X_+(nT_s) = X_i(nT_s) + j \cdot X_q(nT_s), \quad (4-7)$$

where

$$X_i(nT_s) = i(nT_s) + N_i(nT_s) \quad (4-8)$$

and

$$X_q(nT_s) = q(nT_s) + N_q(nT_s). \quad (4-9)$$

Again, $i(nT_s)$ and $q(nT_s)$ are as in Equations (3-2) and (3-3) respectively, with the imposed modulation as in Equation (3-4). Subsequent analyses and simulations will be based on the established signal model of Equations (4-7) through (4-9).

4.1.1 The Phase Noise Probability Density Function

Consider the instantaneous phase message estimate

$$\tilde{\phi}_i(nT_s) = \text{Arctan}\left\{\frac{X_q(nT_s)}{X_i(nT_s)}\right\}, \quad (4-10)$$

defined in an analogous fashion to Equations (3-12) and (4-2). (For notational purposes, the tilde symbol, \sim , over a phase variable will be indicative of noise-contaminated phase.)

Of interest is the resulting random phase noise sequence, $\eta(nT_s)$, a constituent of the random instantaneous phase sequence

$$\tilde{\phi}_i(nT_s) = g[\alpha(nT_s) + \eta(nT_s) + 2\pi \cdot R_e(nT_s)] , \quad (4-11)$$

where $R_e(nT_s)$ is some unknown sheet sequence error, and the true phase, $\alpha(nT_s)$, is

$$\alpha(nT_s) = 2\pi f_e nT_s + \phi(nT_s) - \theta . \quad (4-12)$$

The phase noise sequence is defined *relative to* the ideal noise-free phase as

$$\eta(nT_s) = g[\tilde{\phi}_i(nT_s) - \alpha(nT_s)] . \quad (4-13)$$

Equivalently the phase noise can be defined relative to the ideal noise-free instantaneous phase as

$$\eta(nT_s) = g[\tilde{\phi}_i(nT_s) - g[\alpha(nT_s)]] . \quad (4-14)$$

Geometrically, this process is depicted on the phase plane in Figure (4-2). Note that the signal vector, s_+ , can lie on any sheet, but for simplicity is shown on sheet 0.

By virtue of the independence of the random variables X_i and X_q , the joint probability density function (pdf) of X_i and X_q is easily found as the product of the corresponding Gaussian marginal pdfs. After transforming the resulting joint pdf from Cartesian to polar coordinates and integrating over the envelope variable, Middleton [3, 37] has shown the marginal pdf of the phase noise to be

$$p(\eta) = \frac{1}{2\pi} \cdot \exp(-\rho) + \frac{\sqrt{\rho} \cos(\eta)}{\sqrt{\pi}} \cdot \exp(-\rho \sin^2(\eta)) \cdot \text{Erf}(\sqrt{2\rho} \cos(\eta)) . \quad (4-15)$$

Here, the function $Erf(u)$ is the *error function*, typically defined in communication system analysis as

$$Erf(u) = \int_{-\infty}^u \frac{1}{\sqrt{2\pi}} \cdot \exp\left(-\frac{x^2}{2}\right) dx . \quad (4-16)$$

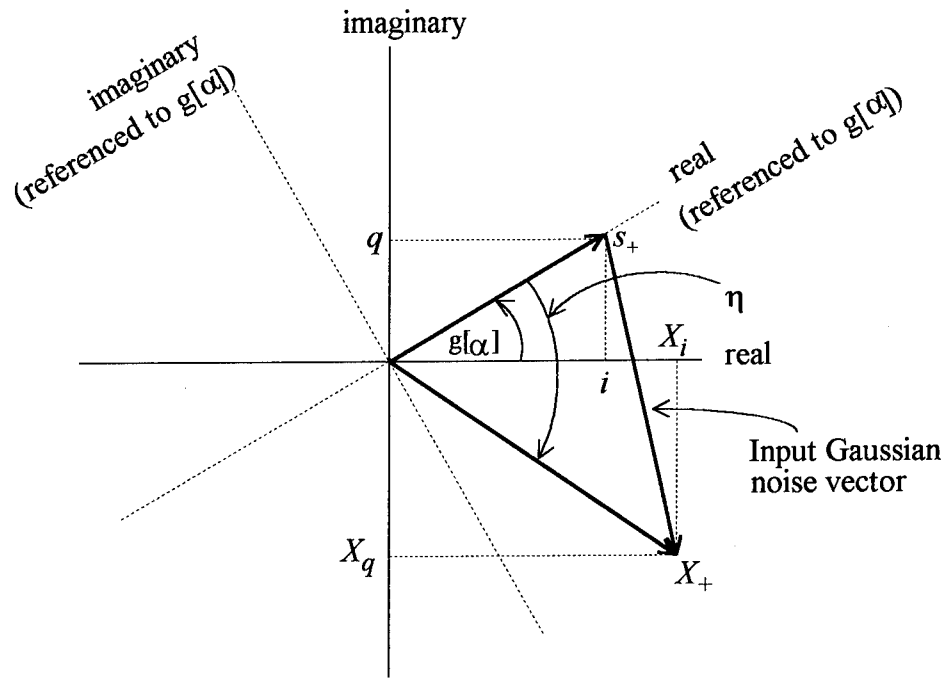


Figure (4-2). The phase plane representation of the phase noise, η , at an arbitrary time, $t = nT_s$.

The *input* (i.e., prior to phase estimation) carrier-to-noise ratio, ρ , is defined as

$$\rho = \frac{a^2}{2\sigma^2} . \quad (4-17)$$

Figure (4-3) is a plot of this phase noise pdf (herein referred to as the Middleton distribution) for various values of ρ . Note that as a result of defining the phase noise relative to the true phase, α , we have that

$$-\pi < \eta \leq +\pi . \quad (4-18)$$

It is also readily apparent that since the input noise sequence is independent from sample to sample, the output (i.e., after phase estimation) phase noise sequence will also be independent from sample to sample. Therefore the resulting phase noise power spectral density will also be uniform over the Nyquist interval, $\frac{-F_s}{2} < f \leq \frac{+F_s}{2}$. This is an additional motivation for basing performance comparisons in the phase angle domain rather than the phase-difference domain, the latter of which results in correlated consecutive samples.

We observe that as the carrier-to-noise ratio increases, η decreases such that we can use the approximations

$$\sin^2(\eta) \approx \eta^2 , \text{ and } \cos(\eta) \approx 1 .$$

In this case, the Middleton distribution of Equation (4-15) approaches a zero mean Gaussian distribution of variance $(\sigma/a)^2$. At the other extreme, for values of ρ approaching zero, the Middleton distribution approaches that of a uniform distribution in the interval $(-\pi, \pi]$.

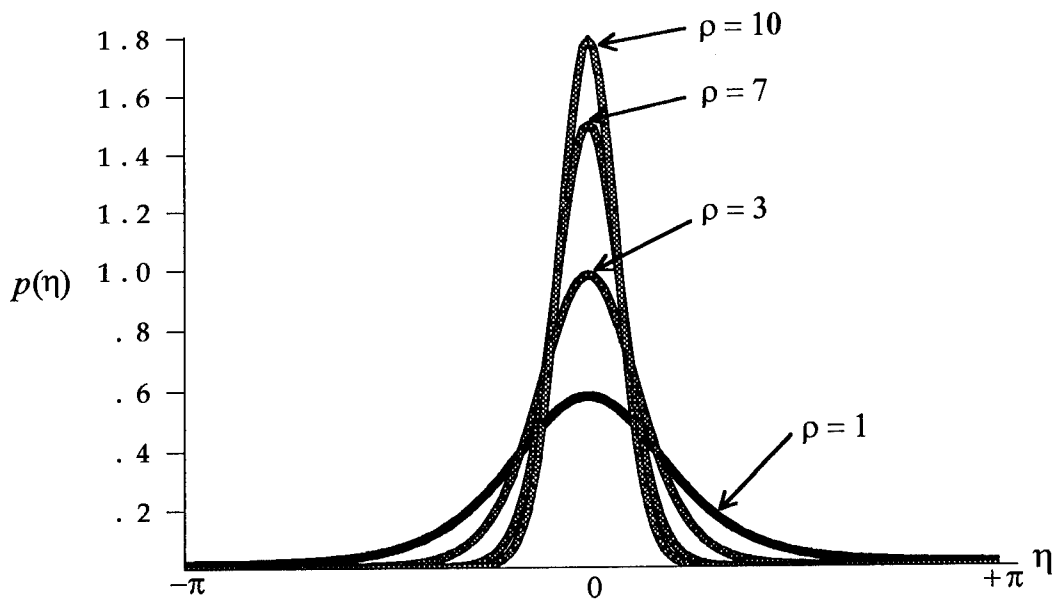


Figure (4-3). The Middleton probability density function of the phase noise, η , at various values of the carrier-to-noise ratio, ρ .

4.1.2 The Phase Cycle-Slip

In addition to the additive phase noise, η , which is present in our instantaneous phase estimate, we are also concerned with errors in the determination of the phase plane sheet on which the signal vector lies. In this research, we will not be concerned with locally constant errors in the determination of this integer value, rather, we will be concerned with *changes* in this error between consecutive sample intervals. (Note that it is these changes in this error sequence which lead to errors in the resulting backward difference instantaneous frequency sequence.) A change in the error of the phase plane sheet determination over a sample time interval will be referred to as a *phase cycle-slip*.

Recall that our true phase angle is as in Equation (4-12),

$$\alpha(nT_s) = 2\pi f_e n T_s + \phi(nT_s) - \theta ,$$

corresponding to the phase of the noise-free signal vector, $s_+(nT_s)$. Expressed in terms of the phase plane sheet sequence, $r(nT_s)$, and the sheet 0 residual phase constituents, we have

$$\alpha(nT_s) = g[\alpha(nT_s)] + 2\pi \cdot r(nT_s) , \quad r \in \text{integers} . \quad (4-19)$$

As described in Chapter 2, the integer sequence, $r(nT_s)$, identifies the sheet number on which the signal vector lies. Note that a change in r from time $t = [n-1]T_s$ to time $t = nT_s$ does not constitute a phase cycle-slip. It is simply representative of the progression of the signal vector across the $+\/-\pi$ boundary of the phase plane, during this time interval.

We will be interested in identifying the estimate of the sequence $r(nT_s)$, derived from the phase message estimate, and knowledge of the true phase sequence, $\alpha(nT_s)$. The baseline discriminator process applied to the noise-contaminated DTFM signal results in the instantaneous frequency estimate

$$\tilde{\phi}'_d(nT_s) = F_s \cdot g_E [\tilde{\phi}_i(nT_s) - \tilde{\phi}_i([n-1]T_s)] , \quad (4-20)$$

with $\tilde{\phi}_i(nT_s)$ defined as in Equation (4-10). In likeness to Equation (4-3) we can define our noise-contaminated phase message estimate as

$$\tilde{\phi}_d(nT_s) = T_s \cdot \left\{ \sum_{k=0}^n \tilde{\phi}'_d(kT_s) + \phi_d(-T_s) \right\}, \quad (4-21)$$

which will be used to identify the corresponding sheet sequence estimate, $\hat{R}(nT_s)$. Thus a phase cycle-slip occurs whenever there is a change, from time $t = [n-1]T_s$ to $t = nT_s$, in the integer valued error sequence,

$$R_e(nT_s) = \hat{R}(nT_s) - r(nT_s). \quad (4-22)$$

4.1.3 The Phase Noise and Phase Cycle-Slip Performance Statistics

To predict the performance of the discriminator phase message estimate of Equation (4-21) via simulation, it is necessary to introduce measurement-derived statistics which are representative of the phase noise and phase cycle-slip errors. This section presents the simulation technique used to determine the phase noise sample sequence from knowledge of the true phase sequence. Subsequently, the sheet sequence estimate is presented, which can be used to determine phase cycle-slip occurrences.

Observe that in the simulation process, the true phase as described by Equation (4-12) is known, since it is needed to generate the in-phase and quadrature pairs, $\{i(nT_s), q(nT_s)\}$, for the finite set of indices $n = 0, 1, 2, \dots, (\text{NPTS}-1)$. For simplicity, each vector component generated by the sine and cosine functions is left as normalized to unity, i.e., $a = 1$. Each simulation run begins with the addition of this finite-length complex signal sequence and a newly generated complex Gaussian noise sequence of zero mean and variance $2\sigma^2$. The new noise sequence, $\{N_i(nT_s), N_q(nT_s)\}$, $n = 0, 1, 2, \dots, (\text{NPTS}-1)$, generated for each simulation run, has the properties described in Section 4.1, namely :

- 1) N_i and N_q are zero mean, Gaussian uncorrelated random variables of variance σ^2 at any particular time, $t = nT_s$, and
- 2) $\{N_i(nT_s), N_q(nT_s)\}$ and $\{N_i(mT_s), N_q(mT_s)\}$ are uncorrelated for all indices with the exception of $m = n$.

The addition of the signal and noise finite length sequences results in the noise-contaminated sequence, $\{X_i(nT_s), X_q(nT_s)\}$, $n = 0, 1, 2, \dots, (NPTS - 1)$, generated at the beginning of a simulation run, having a fixed carrier-to-noise ratio equal to $1/(2\sigma^2)$.

During a simulation run, the real sequence

$$d(nT_s) = T_s \cdot \tilde{\Phi}'_d(nT_s), \quad n = 0, 1, 2, \dots, (NPTS - 1) \quad (4-23)$$

is generated using a backward difference numerical FM discrimination method. This allows us to calculate our phase message estimate simply as

$$\tilde{\Phi}_d(nT_s) = \sum_{k=0}^n d(kT_s), \quad n = 0, 1, 2, \dots, (NPTS - 1). \quad (4-24)$$

Consider first, the determination of a phase noise performance measure. Just as the zero-mean Gaussian distribution is completely characterized by its variance, the Middleton phase noise pdf in Equation (4-14) is completely characterized by its variance, $V\{\eta\}$. The phase noise variance is a decreasing function of ρ , and is bounded at the upper extreme by the variance of a uniform distribution in $(-\pi, \pi]$, and at the lower extreme by the variance, $(\sigma/a)^2$, of a Gaussian distribution. Thus we are interested in an estimate of the variance of the phase noise, as one of the performance measures.

Knowledge of the true phase, $\alpha(nT_s)$, allows us to consider determining a sample function of the phase noise sequence

$$\begin{aligned}\eta(nT_s) &= g[\tilde{\phi}_i(nT_s) - g[\alpha(nT_s)]] \\ &= g[\tilde{\phi}_d(nT_s) - \alpha(nT_s)] .\end{aligned}\quad (4-25)$$

Here, we have taken advantage of the fact that

$$\tilde{\phi}_i(nT_s) = g[\tilde{\phi}_d(nT_s)] \quad (4-26)$$

as shown in Appendix B, and the modulo 2π arithmetic property presented in Equation (3-49). From a practical viewpoint, this means that we can determine the finite length phase noise sequence, $\eta(nT_s)$, from Equation (4-25) as

$$\eta(nT_s) = g_E[\tilde{\phi}_d(nT_s) - \alpha(nT_s)] , n = 0, 1, 2, \dots, (NPTS - 1) . \quad (4-27)$$

As an estimate of the variance of the phase noise, we define the performance statistic

$$\hat{E}_p = \frac{1}{NPTS} \cdot \sum_{k=0}^{NPTS-1} [\eta(kT_s) - \bar{\eta}]^2 , \quad (4-28)$$

where $\bar{\eta}$ is an estimate of the mean of the phase noise and is defined as

$$\bar{\eta} = \frac{1}{NPTS} \cdot \sum_{k=0}^{NPTS-1} \eta(kT_s) . \quad (4-29)$$

With the ability to obtain a phase noise sample function and knowledge of the true phase, we now consider the phase cycle-slip performance measurement.

In Appendix B, we have represented the noise-contaminated phase message estimate as

$$\tilde{\phi}_d(nT_s) = \alpha(nT_s) + \eta(nT_s) + 2\pi \cdot R_e(nT_s), \quad (4-30)$$

where $R_e(nT_s)$ is as described in the appendix, an integer valued sheet sequence error.

From Equation (4-30) and the phase noise sequence of Equation (4-27), knowledge of the true phase sequence allows us to identify the sheet sequence estimate as

$$2\pi \cdot \hat{R}(nT_s) = \{\tilde{\phi}_d(nT_s) - \eta(nT_s)\} - g_E[\tilde{\phi}_d(nT_s) - \eta(nT_s)], \quad n = 0, 1, 2, \dots, (NPTS - 1). \quad (4-31)$$

In practice, the calculation in Equation (4-31) is found to be sensitive to computer representation/roundoff errors when α is an odd multiple of $+/-\pi$, and can lead to $+/-2\pi$ errors when used in conjunction with Equation (4-22) to determine a sample function of the sheet sequence error, $R_e(nT_s)$. Therefore, although Equations (4-22) and (4-31) yield further insight into the nature of the phase sheet sequence error, we select an alternate method of determining $R_e(nT_s)$. An equivalent calculation for practical purposes is

$$2\pi \cdot R_e(nT_s) = \tilde{\phi}_d(nT_s) - \alpha(nT_s) - \eta(nT_s), \quad n = 0, 1, 2, \dots, (NPTS - 1), \quad (4-32)$$

directly from Equation (4-30). By counting the number of negative transitions, $NCOUNT$, and positive transitions, $PCOUNT$, in the error sequence found in Equation (4-32), we have a measure of phase cycle-slip performance for each simulation run. Alternatively, we can form the ratio

$$\hat{p}_{cs} = \frac{NCOUNT + PCOUNT}{NPTS} = \frac{TCOUNT}{NPTS}, \quad (4-33)$$

as an estimate of the probability of a phase cycle-slip occurring at any particular sample of the phase message estimate. Here, $TCOUNT$, is the total number of transitions, either positive or negative.

Taken together, the phase cycle-slip count and the phase noise variance estimate form a set of measures which can be used to predict the performance of the baseline numerical FM discrimination process. This technique is not unlike that of Rice's [6], in which both "cycle-skips" and output signal-to-noise ratio analytical measures are used to summarize continuous-time FM discriminator performance. However, in a similar fashion to Develet's analysis of angle demodulation [20, 39], we have chosen to stay in the phase-domain with both performance measures.

4.2 Recovery of the Sheet Sequence, $r(nT_s)$, in the Presence of AWGN

We have previously introduced methods of obtaining phase noise variance and phase cycle-slip performance measures for the backward difference numerical FM discrimination technique, via experimental computer simulations. In these simulations, noise sample function sequences obtained from a Gaussian random process are added to the ideal complex DTFM signal, for subsequent analyses. We will now be concerned with the theoretical phase cycle-slip performance prediction in more detail, for comparison to the simulation results. The noise-contaminated signal model is as presented in Section 4.1.

Consider the accumulation process of Equation (4-21), which is used as our noise-contaminated phase message estimate. From this we can write

$$\begin{aligned}\tilde{\phi}_d(nT_s) &= \tilde{\phi}_d([n-1]T_s) + T_s \cdot \tilde{\phi}'_d(nT_s) \\ &= \tilde{\phi}_d([n-1]T_s) + g[\tilde{\phi}_i(nT_s) - \tilde{\phi}_i([n-1]T_s)].\end{aligned}\quad (4-34)$$

Using Equation (4-26) and modulo 2π arithmetic, Equation (4-34) is rewritten as

$$\begin{aligned}\tilde{\phi}_d(nT_s) &= \tilde{\phi}_d([n-1]T_s) + g[g[\tilde{\phi}_d(nT_s)] - g[\tilde{\phi}_d([n-1]T_s)]] \\ &= \tilde{\phi}_d([n-1]T_s) + g[\tilde{\phi}_d(nT_s) - \tilde{\phi}_d([n-1]T_s)].\end{aligned}\quad (4-35)$$

After application of Equation (4-30) and modulo 2π arithmetic in Equation (4-35), rearrangement of terms yields

$$\eta(nT_s) = v(nT_s) - 2\pi \cdot \{R_e(nT_s) - R_e([n-1]T_s)\}, \quad (4-36)$$

where

$$v(nT_s) = \eta([n-1]T_s) + g[\alpha'_d(nT_s) + \eta'_d(nT_s)] - \alpha'_d(nT_s). \quad (4-37)$$

The terms $\alpha'_d(nT_s)$ and $\eta'_d(nT_s)$ are defined as the backward differences

$$\alpha'_d(nT_s) = \alpha(nT_s) - \alpha([n-1]T_s) \quad (4-38)$$

and

$$\eta'_d(nT_s) = \eta(nT_s) - \eta([n-1]T_s). \quad (4-39)$$

Equation (4-36) is a key result in that it allows us to determine the probability of a phase cycle-slip occurring at a particular time $t = nT_s$. This equation indicates that when $v(nT_s)$ exceeds π in magnitude, a phase cycle-slip identified as

$$2\pi \cdot R_{cs}(nT_s) = 2\pi \cdot \{R_e(nT_s) - R_e([n-1]T_s)\} \quad (4-40)$$

will occur as a "compensation" such that equality with $\eta(nT_s)$ holds. The result is that the phase noise, $\eta(nT_s)$, remains on sheet 0 of the modulation referenced phase plane as defined, and as indicated in Equation (4-18).

Figure (4-4) is representative of the various pdfs which arise at a particular time, $t = nT_s$, in the formation of the random process $v(nT_s)$. For simplicity we use the notation $\alpha'_d = \alpha'_d(nT_s)$, and $\eta_- = \eta([n-1]T_s)$, $\eta = \eta(nT_s)$, $v = v(nT_s)$, for these random variables.

Figures (a) through (c) are for the case where the quantity $(\eta_- - \alpha'_d)$ is greater than zero.

Similarly, figures (d) through (f) are for the case where the quantity $(\eta_- - \alpha'_d)$ is less than zero.

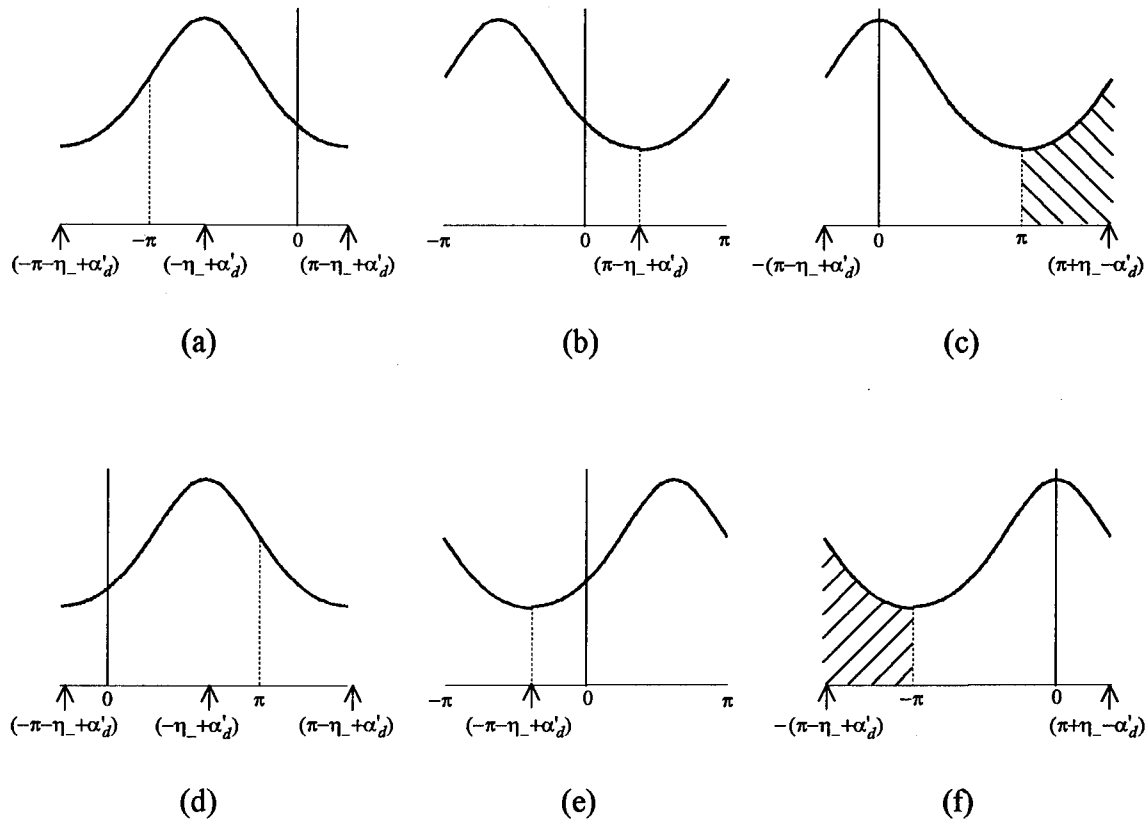


Figure (4-4). Representative pdfs arising in the formation of $v(nT_s)$.

Case 1: $(\eta_- - \alpha'_d) > 0$

- a) The pdf of $(\eta - \eta_- + \alpha'_d)$ given η_- and α'_d .
- b) The pdf of $g[\eta - \eta_- + \alpha'_d]$ given η_- and α'_d .
- c) The pdf of $v = \eta_- - \alpha'_d + g[\eta - \eta_- + \alpha'_d]$ given η_- and α'_d , $p_>(v|\eta_-, \alpha'_d)$.

Case 2 : $(\eta_- - \alpha'_d) < 0$

- d) The pdf of $(\eta - \eta_- + \alpha'_d)$ given η_- and α'_d .
- e) The pdf of $g[\eta - \eta_- + \alpha'_d]$ given η_- and α'_d .
- f) The pdf of $v = \eta_- - \alpha'_d + g[\eta - \eta_- + \alpha'_d]$ given η_- and α'_d , $p_<(v|\eta_-, \alpha'_d)$.

From the representative pdfs of figures (c) and (f), it is possible to determine the probability of a phase cycle-slip under various modulation conditions. The three cases of interest will be the unmodulated carrier with a perfectly tuned receiver, the unmodulated carrier with an off-tuned receiver, and finally, the angle modulated carrier with an off-tuned receiver. The following sections will cover each of these cases, presenting both the theoretically predicted and the corresponding simulation results.

4.2.1 Case I : The Unmodulated Carrier and Perfectly Tuned Receiver

We begin with the case where the carrier is unmodulated and there exists no tuning error, i.e., the case where $\alpha(nT_s) = \theta$. In this case, $\alpha'_d = -\theta - (-\theta) = 0$. Consider the determination of the probability that v exceeds π , which corresponds to the occurrence of a positive phase cycle-slip compensation, $2\pi R_{cs}$, at some particular time $t = nT_s$. We represent this probability as $p_{pcs} = \Pr\{v > \pi\}$. Similarly we represent the probability of a negative phase cycle-slip as $p_{ncs} = \Pr\{v < -\pi\}$. The probability of a phase cycle-slip occurrence (either positive or negative) is simply

$$p_{cs} = p_{ncs} + p_{pcs} . \quad (4-41)$$

This is true regardless of the modulation scenario, since the occurrence of a positive phase cycle-slip, the occurrence of a negative phase cycle-slip, and the occurrence of no phase cycle-slip, form a set of mutually exclusive and exhaustive events.

Due to the symmetry of the Middleton phase noise pdf, and due to the fact that the backward difference, α'_d , is equal to zero, it is readily apparent that the probabilities of a

negative phase cycle-slip and of a positive phase cycle-slip are the same. In Figure (4-4 c), the shaded area represents the probability of a positive phase cycle-slip, given a specific value, η_- , of the random variable η_- . Integrating over all possible values of η_- we obtain

$$p_{ncs} = p_{pcs} = \Pr\{v > \pi\} = \int_0^{\pi} \int_{-\pi}^{\pi+\eta_-} p_{>}(v|\eta_-) \cdot p(\eta_-) dv d\eta_- . \quad (4-42)$$

Note that integration on the variable η_- is from 0 to π rather than $-\pi$ to π , since for values of η_- less than zero, $\Pr\{v > \pi\} = 0$. To simplify Equation (4-42) we employ the fact that

$$\eta = g[v] , \quad (4-43)$$

as implied by Equation (4-36). Thus values of v in the range π to $(\pi + \eta_-)$ map to values of η in the range $-\pi$ to $(-\pi + \eta_-)$. Taking advantage of this mapping, we rewrite Equation (4-42) as

$$p_{ncs} = p_{pcs} = \Pr\{-\pi < \eta < -\pi + \eta_-\} = \int_0^{\pi} p(\eta_-) \int_{-\pi}^{-\pi+\eta_-} p(\eta) d\eta d\eta_- . \quad (4-44)$$

Note that both η and η_- are Middleton distributed as in Equation (4-15). Given the input carrier-to-noise ratio, ρ , we can use Equation (4-44) to determine the probability of a positive phase cycle-slip, which in this special case is the same as the probability of a negative phase cycle-slip.

Before presenting a comparison of the theoretical and the experimental performance predictions for various input carrier-to-noise ratios, we consider a specific example in which the carrier-to-noise ratio is allowed to approach zero. In this example, the pdfs of η_- and η approach that of a uniform distribution in the interval $(-\pi, \pi]$. From Equation (4-44) we obtain the probability of a negative phase cycle-slip as

$$\begin{aligned} p_{ncs} &= \int_0^\pi \frac{1}{2\pi} \int_{-\pi}^{-\pi+\eta_-} \frac{1}{2\pi} d\eta_+ d\eta_- \\ &= \frac{1}{4\pi^2} \int_0^\pi \eta_- d\eta_- \\ &= \frac{1}{8} \end{aligned}$$

We conclude that with perfectly tuned reception of an unmodulated carrier in the presence of AWGN, the backward difference numerical FM discriminator will result in a negative phase cycle-slip occurring at a particular time, $t = nT_s$, with a probability approaching 1/8 as ρ approaches zero. As previously indicated, the symmetry of this example implies that the probability of a positive phase cycle-slip also approaches 1/8. From Equation (4-41), the probability of a phase cycle-slip therefore approaches 1/4.

Figures (4-5 a) through (4-5 d) present both theoretical and experimental results serving as prediction of the performance of the backward difference discriminator, with regard to phase cycle-slip occurrences. Throughout the various simulations, the sequence length, $NPTS$, is equal to 1024 samples.

Figure (a) presents the analytically predicted number of *negative* phase cycle-slips per $NPTS$ samples, as ρ is varied from -20 to +40 dB in 2 dB increments. This predicted count is found as the product of p_{ncs} and $NPTS$. Here, p_{ncs} is found by numerical integration of the integral of Equation (4-44). Figure (b) presents the corresponding experimental results, which are arrived at using the technique outlined in Section 4.1.3. Rather than presenting the results in the form of a predicted probability as in Equation (4-33), we have simply plotted the variable $NCOUNT$ versus the carrier-to-noise ratio. Note that the experimental results agree quite well with the theoretical results. It is also noted that as ρ decreases, the experimental negative phase cycle-slip count approaches values near $1024/8 = 128$, as expected.

Similarly, figures (c) and (d) respectively present the theoretically and experimentally predicted number of *positive* phase cycle-slips in a sequence of length 1024 samples. The simulations presented in figure (d) plot the variable $PCOUNT$ versus the input carrier-to-noise ratio. As expected, the performance predictions are the same as for the negative phase-cycle slip measures, in the currently treated case of the unmodulated carrier and perfectly tuned receiver.

Our attention now turns to the case where there exists a tuning error, f_e , in our DTFM signal. This error is associated with the receive end of our communication system, which is modeled as the quadrature downconverter (or its equivalent) and the backward difference discriminator. The error mechanism is therefore referred to as an off-tuned receiver.

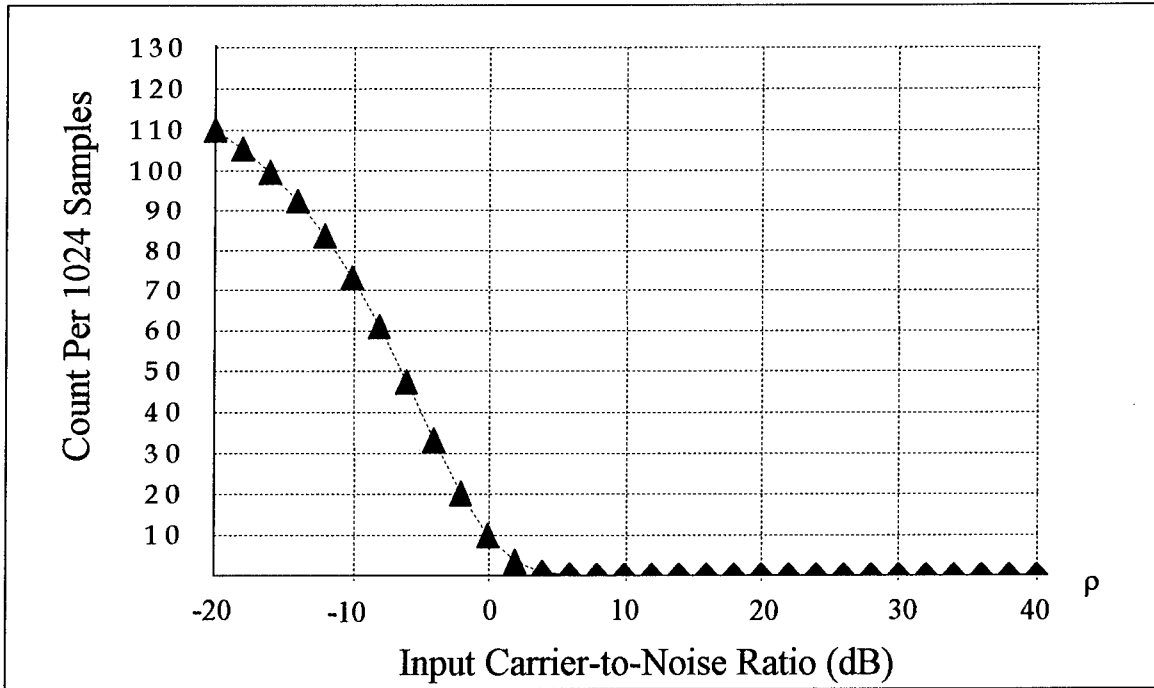


Figure (4-5 a). Analytically predicted number of *negative* phase cycle-slips vs. ρ ;
Case I : The unmodulated carrier and perfectly tuned receiver.

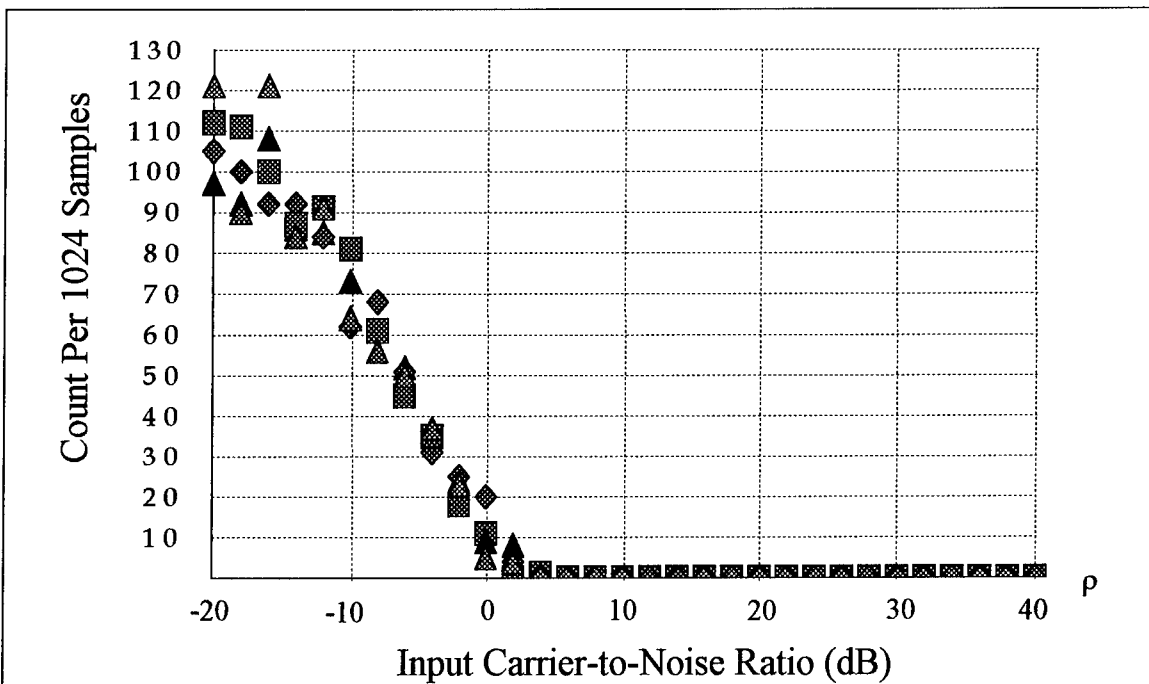


Figure (4-5 b). Experimentally predicted number of *negative* phase cycle-slips vs. ρ (4 simulation runs); Case I : The unmodulated carrier and perfectly tuned receiver.

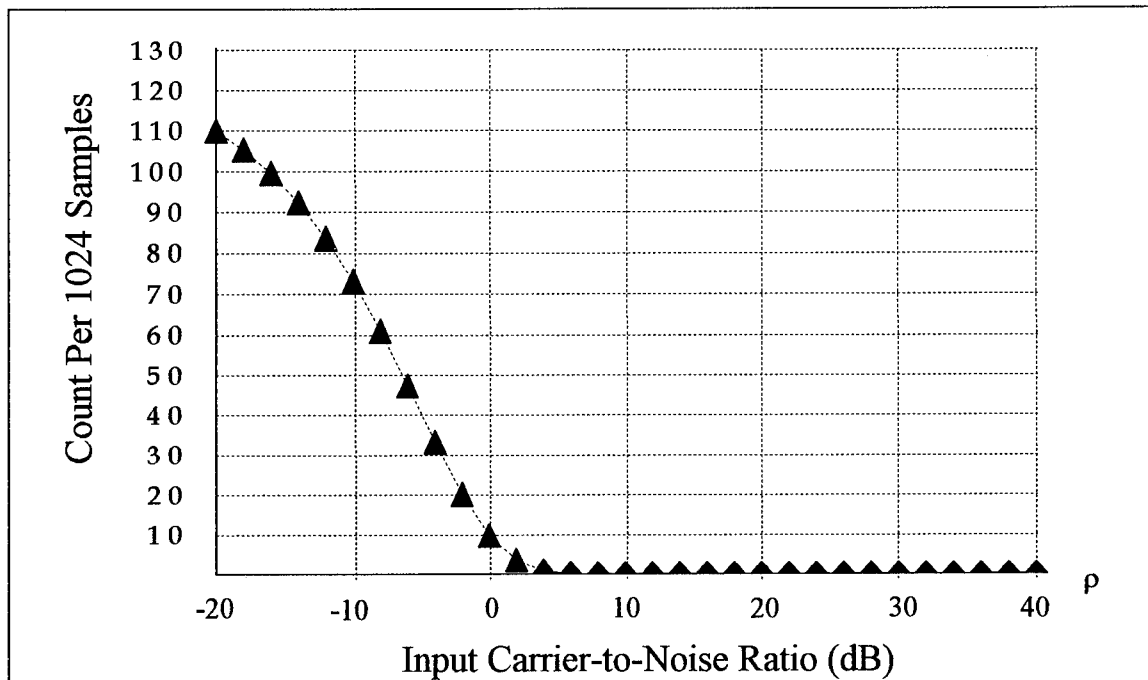


Figure (4-5 c). Analytically predicted number of *positive* phase cycle-slips vs. ρ ;
Case I : The unmodulated carrier and perfectly tuned receiver.

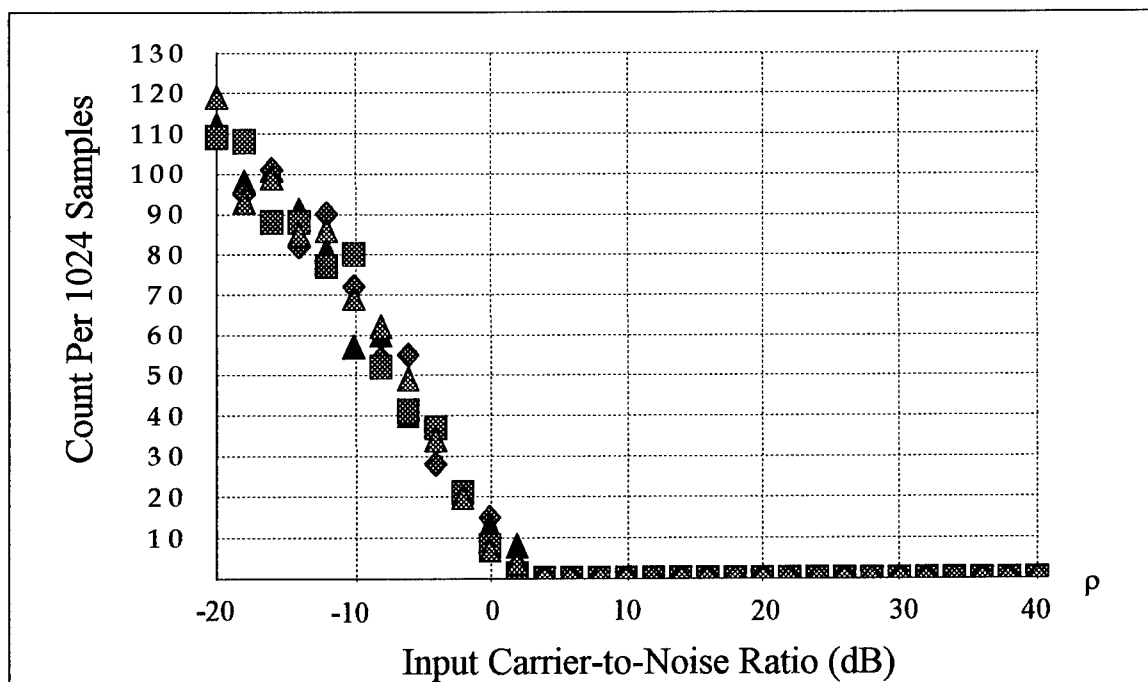


Figure (4-5 d). Experimentally predicted number of *positive* phase cycle-slips vs. ρ (4 simulation runs); Case I : The unmodulated carrier and perfectly tuned receiver.

4.2.2 Case II : The Unmodulated Carrier and Off-tuned Receiver

We now analyze the case where the carrier is unmodulated, but there exists a tuning error of f_e Hz. In this case, $\alpha'_d = (2\pi f_e n T_s - \theta) - (2\pi f_e [n - 1] T_s - \theta) = 2\pi f_e T_s$. Consider the determination of the probability that v is less than $-\pi$, which corresponds to the occurrence of a negative phase cycle-slip compensation, $2\pi R_{cs}$, at some particular time, $t = nT_s$. As before, we represent this probability as $p_{ncs} = \Pr\{v < -\pi\}$. This corresponds to the scenario where $(\eta_- - \alpha'_d)$ is less than zero, as shown in Figure (4-4 f). Integrating over all contributing values of η_- we obtain

$$p_{ncs} = \int_{-\pi - (\pi - \eta_- + \alpha'_d)}^{\alpha'_d} \int_{-\pi}^{-\pi} p_<(v|\eta_-) \cdot p(\eta_-) dv d\eta_- . \quad (4-45)$$

For the outer integral of Equation (4-45), values of η_- in the range $[-\pi, \alpha'_d]$ will result in non-zero contributions over the inner integral. Thus the limits of integration for the outer integral are established.

Likewise, for the scenario where $(\eta_- - \alpha'_d)$ is greater than zero corresponding to a positive phase cycle-slip, we write

$$p_{pcs} = \int_{\alpha'_d}^{\pi} \int_{\pi}^{\pi + \eta_- - \alpha'_d} p_>(v|\eta_-) \cdot p(\eta_-) dv d\eta_- . \quad (4-46)$$

For the outer integral of Equation (4-46), only values of η_- in the range $[\alpha'_d, \pi]$ will contribute to the overall integration.

To simplify the integrals of Equation (4-45) and (4-46) we again employ Equation (4-43). For $(\eta_- - \alpha'_d)$ less than zero, values of v in the range $-\pi$ to $-(\pi + \eta_- - \alpha'_d)$ map to values of η in the range $(\pi + \eta_- - \alpha'_d)$ to π . This allows us to rewrite Equation (4-45) as

$$p_{ncs} = \int_{-\pi}^{\alpha'_d} p(\eta_-) \int_{(\pi + \eta_- - \alpha'_d)}^{\pi} p(\eta) d\eta d\eta_- . \quad (4-47)$$

Similarly, for $(\eta_- - \alpha'_d)$ greater than zero, values of v in the range π to $(\pi + \eta_- - \alpha'_d)$ map to values of η in the range $-\pi$ to $-(\pi + \eta_- - \alpha'_d)$. Equation (4-46) is rewritten as

$$p_{pcs} = \int_{\alpha'_d}^{\pi} p(\eta_-) \int_{-\pi}^{-(\pi - \eta_- + \alpha'_d)} p(\eta) d\eta d\eta_- . \quad (4-48)$$

As in Case I, we determine the probability of a phase cycle-slip (either positive or negative) using Equation (4-41). It is interesting to note that by employing the symmetry of the Middleton pdf, a simple change of variable in Equation (4-47) along with a change in the order of integrations yields the property

$$p_{ncs}(\alpha'_d, \rho) = p_{pcs}(-\alpha'_d, \rho) . \quad (4-49)$$

In the above expression, we have explicitly indicated the dependence of these probabilities on both the tuning offset, $\alpha'_d = 2\pi f_e T_s$, and the input carrier-to-noise ratio, ρ .

Before presenting a comparison of the Case II theoretical and experimental performance predictions for various input carrier-to-noise ratios, we consider a specific example in which the carrier-to-noise ratio is allowed to approach zero. As stated previously, the pdfs of η_- and η approach that of a uniform distribution in the interval $(-\pi, \pi]$. In this example, we also allow the tuning offset to approach the positive extreme value, $\alpha'_d = +\pi$. From Equation (4-47) we obtain the probability of a negative phase cycle-slip under this condition as

$$\begin{aligned} p_{ncs} &= \int_{-\pi}^{\pi} \frac{1}{2\pi} \int_{\eta_-}^{\pi} \frac{1}{2\pi} d\eta_+ d\eta_- \\ &= \frac{1}{4\pi^2} \int_{-\pi}^{\pi} (\pi - \eta_-) d\eta_- \\ &= \frac{1}{2}. \end{aligned}$$

We conclude that with maximally positive off-tuned reception of an unmodulated carrier in the presence of AWGN, the backward difference numerical FM discriminator will result in a negative phase cycle-slip occurring at a particular time, $t = nT_s$, with a probability approaching 1/2 as ρ approaches zero. At the same time, from Equation (4-48) the probability of a positive phase cycle-slip is zero. From the property presented in Equation (4-49), this example implies that when $\alpha'_d = -\pi$, the probability of a positive phase cycle-slip also approaches 1/2 as ρ approaches zero. Likewise, from Equation (4-47) the probability of a negative phase cycle-slip is zero, when $\alpha'_d = -\pi$.

Figures (4-6 a) through (4-6 d) present both theoretical and experimental results serving as prediction of the performance of the backward difference discriminator, with regard to phase cycle-slip occurrences for Case II. Throughout the various simulations, the sequence length, $NPTS$, is again equal to 1024 samples. The tuning offset in these figures is $\alpha'_d = 2\pi f_e T_s = \pi/10$.

Figure (a) presents the analytically predicted number of *negative* phase cycle-slips per $NPTS$ samples, as ρ is varied from -20 to +40 dB in 2 dB increments. This predicted count is found as the product of p_{ncs} and $NPTS$. Here, p_{ncs} is found by numerical integration of the integral of Equation (4-47). Figure (b) presents the corresponding experimental results, which are arrived at using the technique outlined in Section 4.1.3. As in Case I, rather than presenting the results in the form of a predicted probability using Equation (4-33), we have simply plotted the variable $NCOUNT$ versus the carrier-to-noise ratio. Note that the experimental results agree quite well with the theoretical results.

Similarly, figures (c) and (d) respectively present the theoretically and experimentally predicted number of *positive* phase cycle-slips in a sequence of length 1024 samples. The simulations presented in figure (d) plot the variable $PCOUNT$ versus the input carrier-to-noise ratio. As expected, the presence of a positive tuning offset increases the chance of a negative phase cycle-slip, and decreases the chance of a positive phase cycle-slip.

Next, we will be interested in the case where there exists a tuning error, f_e , in addition to a message signal, $\phi(t)$, in our DTFM signal. This is the final and most general modulation case consistent with our established DTFM model, which will be considered.

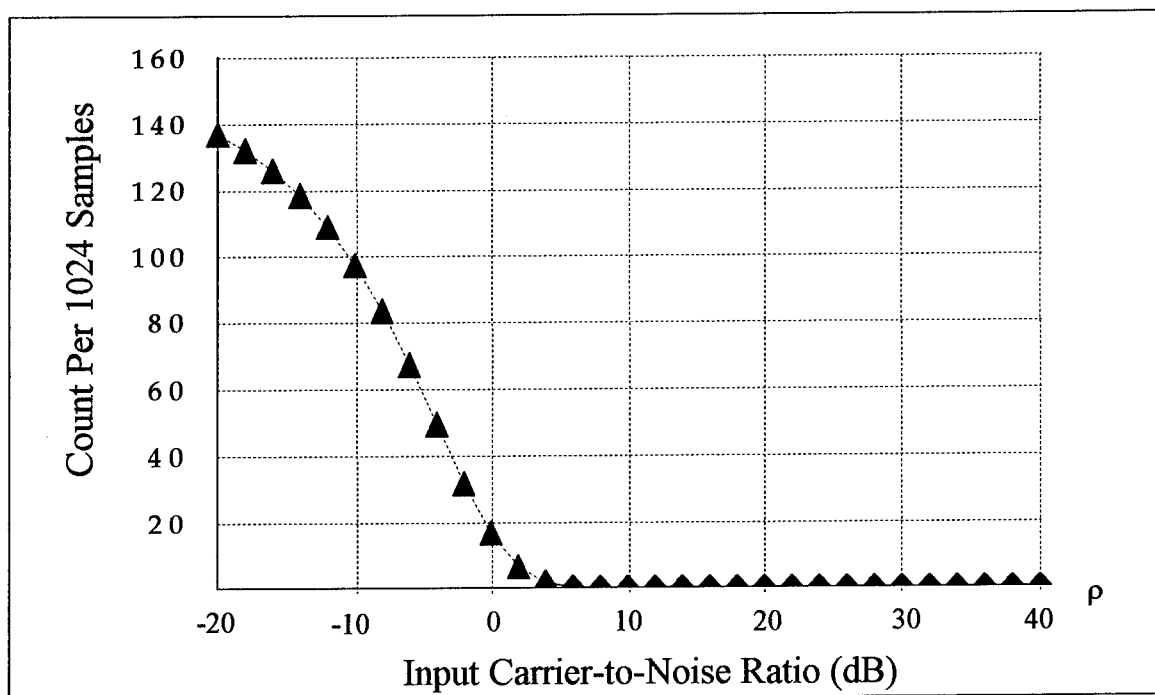


Figure (4-6 a). Analytically predicted number of *negative* phase cycle-slips vs. ρ ;
Case II : The unmodulated carrier and off-tuned receiver ($2\pi f_e T_s = \pi \delta_e = \pi/10$).

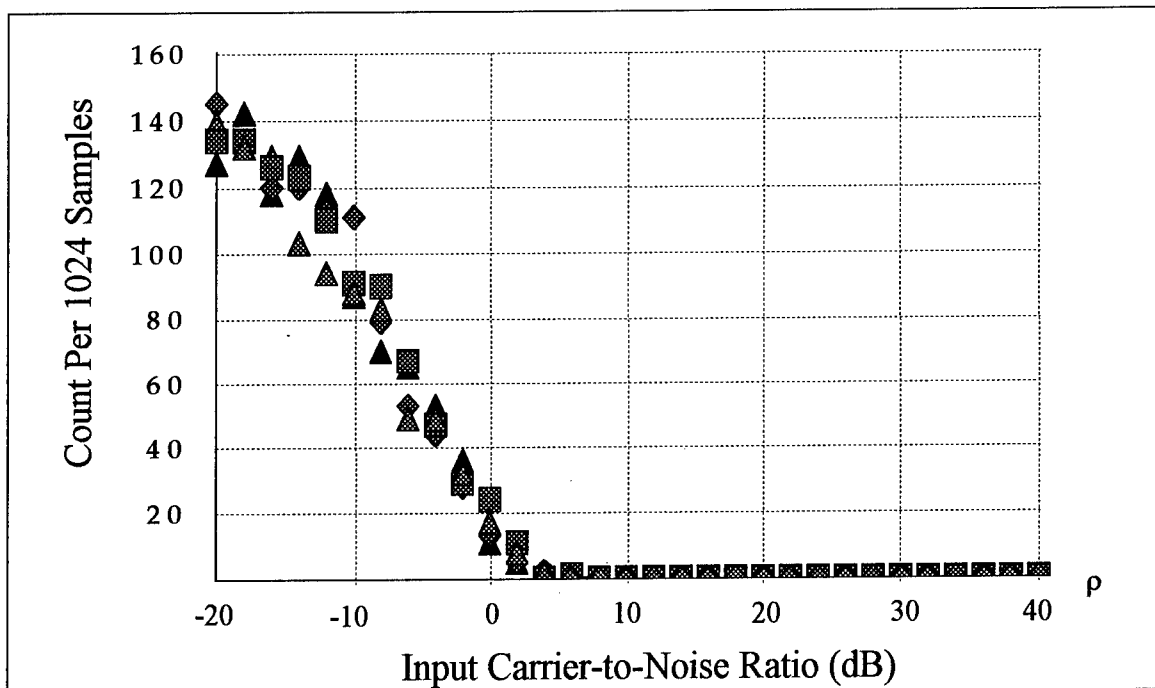


Figure (4-6 b). Experimentally predicted number of *negative* phase cycle-slips vs. ρ (4 simulation runs); Case II : The unmodulated carrier and off-tuned receiver ($2\pi f_e T_s = \pi \delta_e = \pi/10$).

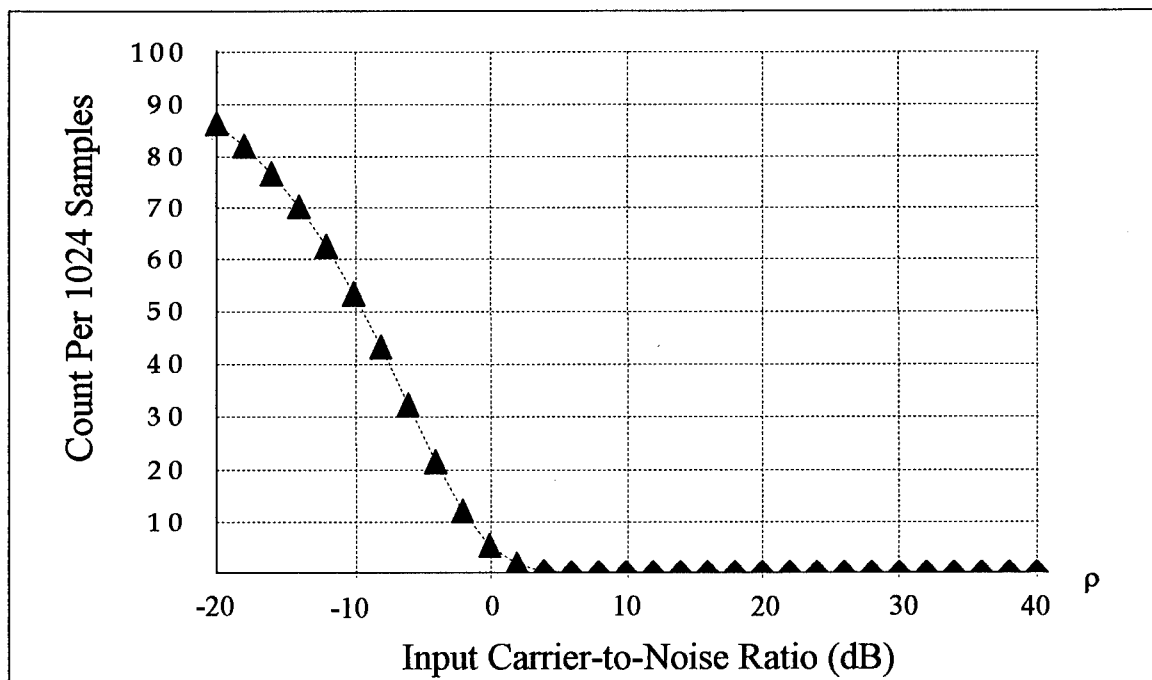


Figure (4-6 c). Analytically predicted number of *positive* phase cycle-slips vs. ρ ;
Case II : The unmodulated carrier and off-tuned receiver ($2\pi f_e T_s = \pi \delta_e = \pi/10$).

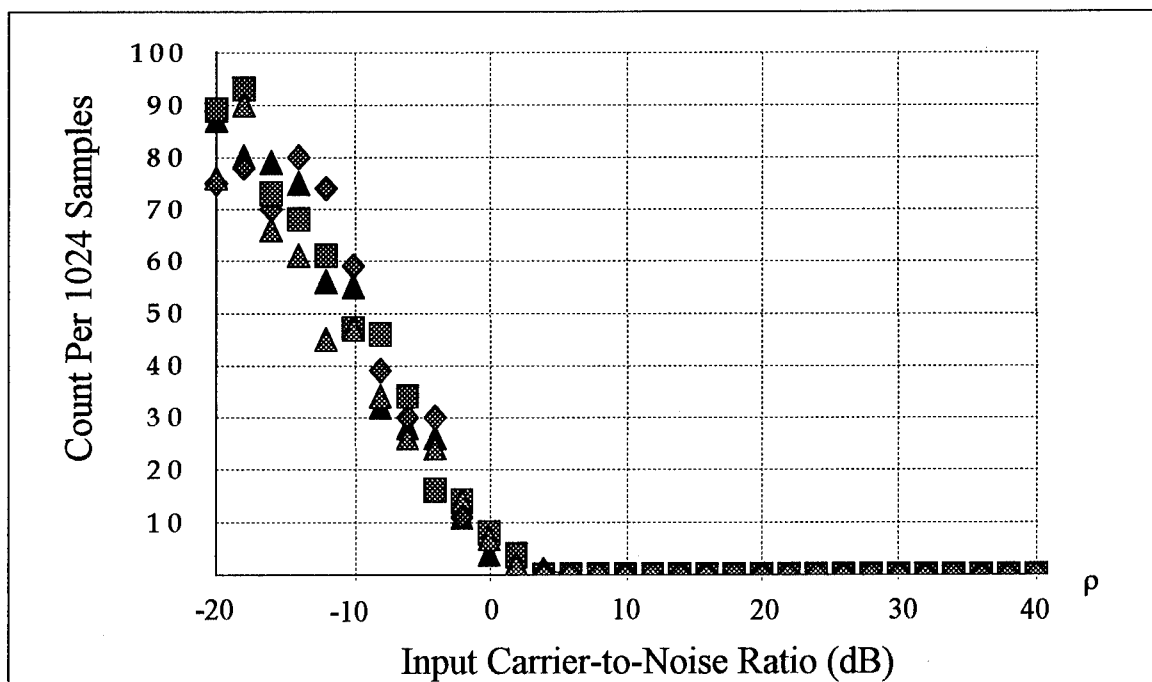


Figure (4-6 d). Experimentally predicted number of *positive* phase cycle-slips vs. ρ (4 simulation runs); Case II : The unmodulated carrier and off-tuned receiver ($2\pi f_e T_s = \pi \delta_e = \pi/10$).

4.2.3 Case III : The Angle Modulated Carrier and Off-tuned Receiver

The final case to be considered is the general case in which there exists both a tuning error and angle modulation imposed on the carrier. Demodulation of the noise-free DTFM signal in this case yields $\alpha'_d(nT_s) = 2\pi f_e T_s + \phi(nT_s) - \phi([n - 1]T_s)$. We will build upon the results of Equations (4-47) and (4-48) to arrive at phase cycle-slip probabilities for the present modulation case.

It is observed that in the noise-contaminated DTFM model which we have adopted, the distribution of phase-difference amplitude values, α'_d , is statistically independent of the distribution of each of the phase noise random variables, η and η_- . This amplitude distribution will be represented as $p_Y(y)$, where the variable Y signifies any of the possible values of the quantity $y = \alpha'_d$ at any arbitrary time, $t = nT_s$. As previously established, these amplitude values range from $-\pi$ to $+\pi$. Given the amplitude distribution, $p_Y(y)$, the probability of a negative phase cycle-slip is readily found as

$$p_{ncs} = \int_{-\pi}^{\pi} p_Y(y) \int_{-\pi}^{y} p(\eta_-) \int_{(\pi+\eta_--\alpha'_d)}^{\pi} p(\eta) d\eta d\eta_- dy . \quad (4-50)$$

Equation (4-50) can be viewed as a weighted average of Case II negative phase cycle-slip probabilities. Previous expressions for the probability of a negative phase cycle-slip are simply special cases of Equation (4-50), in which the quantity $y = \alpha'_d$ takes on a single known value.

Similarly the probability of a positive phase cycle-slip is

$$p_{pcs} = \int_{-\pi}^{\pi} p_Y(y) \int_y^{\pi} p(\eta_-)^{-(\pi - \eta_- + \alpha'_d)} \int_{-\pi}^{\eta_-} p(\eta) d\eta d\eta_- dy . \quad (4-51)$$

This can likewise be interpreted as the weighted average of Case II positive phase cycle-slip probabilities. Once again, previous expressions for the probability of a positive phase cycle-slip are simply special cases of Equation (4-51), in which the quantity $y = \alpha'_d$ takes on a single known value.

We now present the specific example in which the imposed angle modulation is sinusoidal with

$$m(nT_s) = \sin(2\pi f_m n T_s + \theta_m), \quad (4-52)$$

such that

$$\phi(nT_s) - \phi([n-1]T_s) = T_s \cdot h_D(nT_s) * \{2\pi\Delta f \cdot m(nT_s)\}. \quad (4-53)$$

In the presence of a tuning offset, employing results from Appendix A yields

$$y(nT_s) = \mu_y + a_y \sin(2\pi f_m n T_s + \theta_m - \pi \cdot \frac{f_m}{F_s}), \quad (4-54)$$

where

$$\mu_y = 2\pi f_e T_s, \quad (4-55)$$

and

$$a_y = \frac{2\Delta f}{f_m} \cdot \sin\left(\pi \cdot \frac{f_m}{F_s}\right) . \quad (4-56)$$

Random sampling of the amplitude of $y(nT_s)$ yields the distribution

$$p_Y(y) = \frac{1}{\pi a_y \sqrt{1 - \left(\frac{y - \mu_y}{a_y}\right)^2}} , \quad -a_y \leq (y - \mu_y) \leq a_y . \quad (4-57)$$

To carry out the numerical integration of Equation (4-50) and (4-51), we perform a weighted average of the inner double integrals, over a finite set of subintervals spanning the amplitude interval, $[(-a_y + \mu_y), (a_y + \mu_y)]$. The weights used are the corresponding probabilities of y being in a particular subinterval. Corresponding to each subinterval, any value of the amplitude, y , in this subinterval can be used in the calculation of the inner double integrals. Consider first the numerical calculation of Equation (4-51), the probability of the occurrence of a negative phase cycle-slip.

The approximation to Equation (4-50) which is used to find the probability of a negative phase cycle-slip is

$$p_{ncs} \approx \sum_{k=1}^{2^b-1} P_k \cdot \int_{-\pi}^y p(\eta_-) \int_{(\pi+\eta_--\alpha'_d)}^{\pi} p(\eta) d\eta d\eta_- , \quad y_k \leq y \leq y_{k+1} , \quad (4-58)$$

where the probability weights, P_k , are found as

$$P_k = \int_{y_k}^{y_{k+1}} p_Y(y) dy . \quad (4-59)$$

Here, the amplitude subintervals are a result of quantizing the modulating signal into 2^b equally spaced discrete values of y , where b is some positive integer. (In the simulations to be presented, $b = 5$.) The subintervals are $[y_k, y_{k+1}]$, $k = 1, 2, 3, \dots, (2^b - 1)$, with y_1 corresponding to $(-a_y + \mu_y)$ and $y_{2^b - 1}$ corresponding to $(a_y + \mu_y)$. In the sinusoidal modulation example, with $p_y(y)$ defined as in Equation (4-57), the weights become

$$P_k = \frac{1}{\pi} \cdot [\sin^{-1}\left(\frac{y_{k+1} - \mu_y}{a_y}\right) - \sin^{-1}\left(\frac{y_k - \mu_y}{a_y}\right)]. \quad (4-60)$$

For a numerically calculated upper bound on Equation (4-50) we employ Equation (4-58) with $y = y_{k+1}$, since $\Pr\{\nu < -\pi\}$ is an increasing function of y . Similarly, a lower bound on the probability of a negative phase cycle-slip is determined using Equation (4-58), by setting $y = y_k$.

Likewise, an approximation to the probability of the occurrence of a positive phase cycle-slip described by Equation (4-51) is

$$p_{pcs} \approx \sum_{k=1}^{2^b-1} P_k \cdot \int_y^{\pi} p(\eta_-) \int_{-\pi}^{-(\pi-\eta_-+\alpha_d')} p(\eta) d\eta d\eta_-, \quad y_k \leq y \leq y_{k+1}. \quad (4-61)$$

The weights, P_k , remain as in Equation (4-59). For a numerically calculated upper bound on Equation (4-51), we employ Equation (4-61) with $y = y_k$, since $\Pr\{\nu > \pi\}$ is a decreasing function of y . Similarly, a lower bound on the probability of a positive phase cycle-slip is determined using Equation (4-61) by setting $y = y_{k+1}$.

Figures (4-7) and (4-8) present both the theoretically and experimentally predicted phase cycle-slip performance measures, for two distinct Case III modulation scenarios. The first scenario is presented in Figures (4-7 a) through (4-7 d), with the relative message sampling rate, γ , set at 17.067, and the DTFM message index, δ_m , set at 0.2930. Figure (a) presents the upper and lower bounds on the analytically predicted number of negative phase cycle-slips. The corresponding experimental results are presented in figure (b), and are in agreement with the analytically predicted performance. Similarly, figure (c) presents the analytically predicted positive phase cycle-slip occurrences, while figure (d) presents the experimental results. Again, the analytical and experimental performance predictions are in agreement with each other.

Likewise, Figures (4-8 a) through (4-8d) present the theoretical and experimental phase cycle-slip performance predictions for the modulation scenario where γ remains set at 17.067, but δ_m is changed to 0.5859. As expected, increasing the DTFM modulation index has the effect of increasing the probability of a phase cycle-slip. Figure (a) presents the upper and lower bounds on the analytically predicted number of negative phase cycle-slips. The corresponding experimental results are presented in figure (b), and are in agreement with the analytically predicted performance. Similarly, figure (c) presents the analytically predicted positive phase cycle-slip occurrences, while figure (d) presents the experimental results. As seen in these figures, the analytical and experimental performance predictions are in agreement with each other.

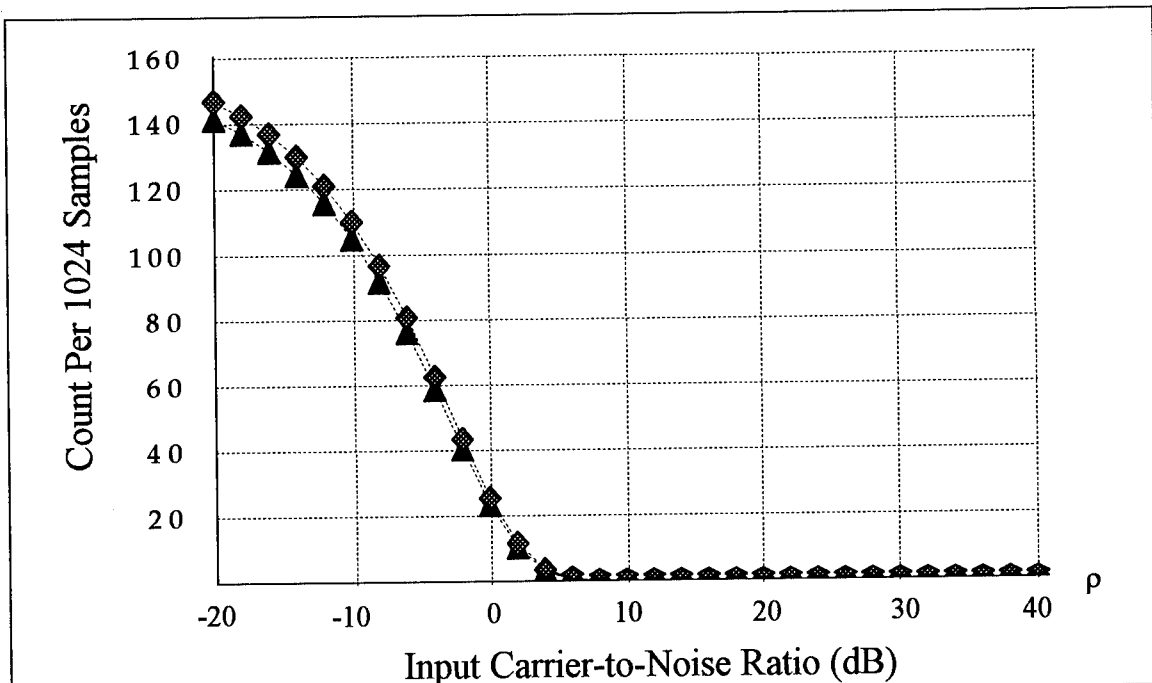


Figure (4-7 a). Analytically predicted number of *negative* phase cycle-slips vs. ρ ;
Case III : The angle modulated carrier and off-tuned receiver ($2\pi f_e T_s = \pi\delta_e = \pi/10$, with
sinusoidal modulation, $\gamma = 17.067$, $\delta_m = 0.2930$).

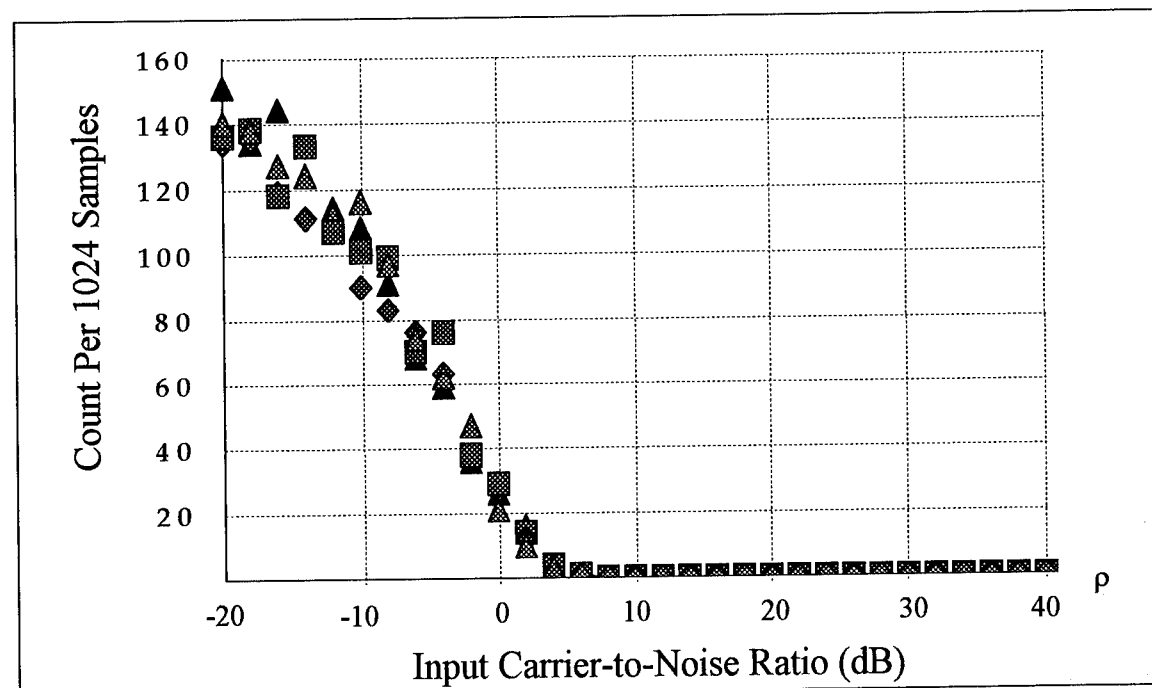


Figure (4-7 b). Experimentally predicted number of *negative* phase cycle-slips vs. ρ (4 simulation runs); Case III : The angle modulated carrier and off-tuned receiver ($2\pi f_e T_s = \pi\delta_e = \pi/10$, with sinusoidal modulation, $\gamma = 17.067$, $\delta_m = 0.2930$).

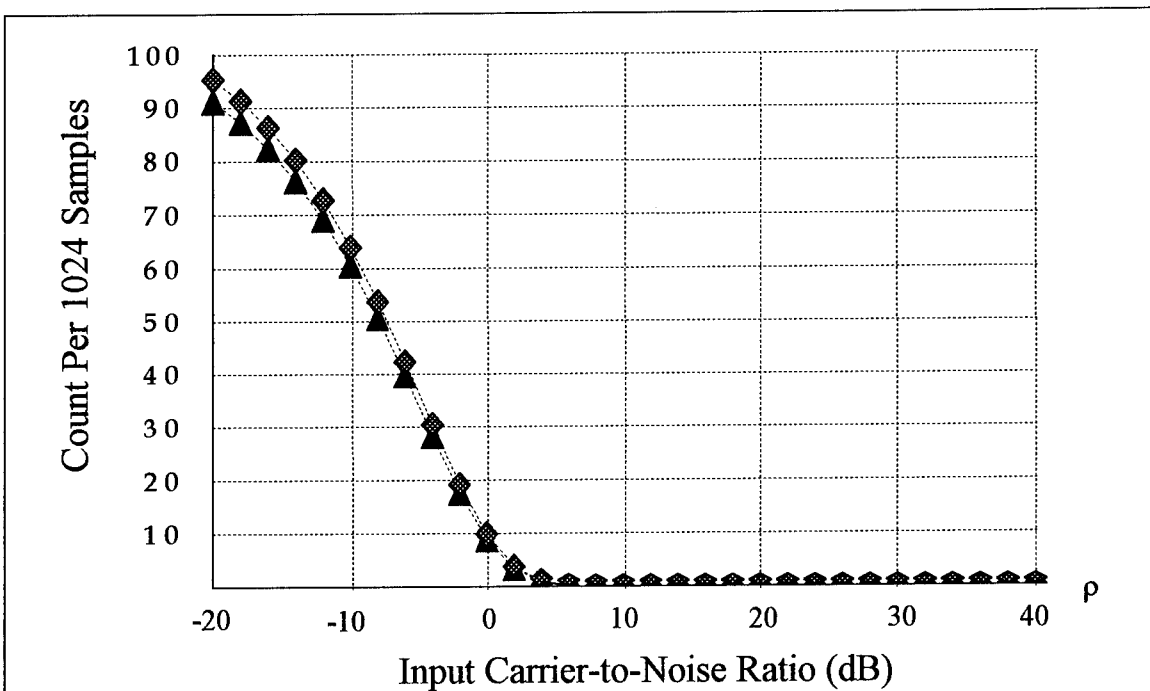


Figure (4-7 c). Analytically predicted number of *positive* phase cycle-slips vs. ρ ;
Case III : The angle modulated carrier and off-tuned receiver ($2\pi f_e T_s = \pi \delta_e = \pi/10$, with
sinusoidal modulation, $\gamma = 17.067$, $\delta_m = 0.2930$).

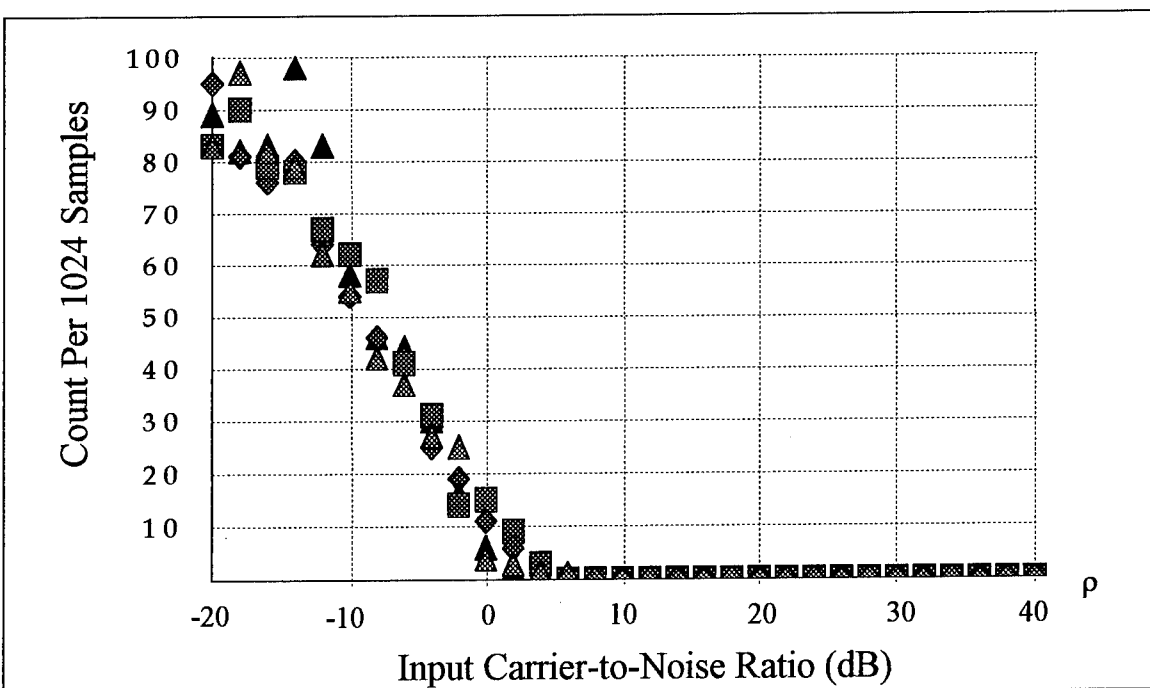


Figure (4-7 d). Experimentally predicted number of *positive* phase cycle-slips vs. ρ
(4 simulation runs); Case III : The angle modulated carrier and off-tuned receiver
($2\pi f_e T_s = \pi \delta_e = \pi/10$, with sinusoidal modulation, $\gamma = 17.067$, $\delta_m = 0.2930$).

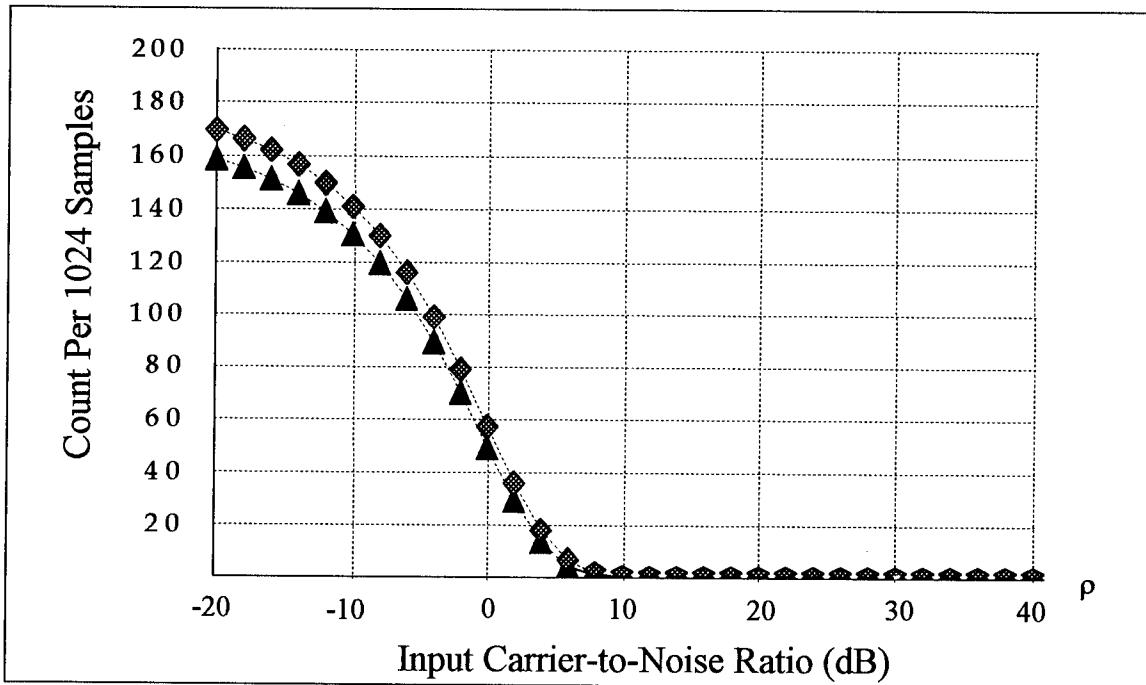


Figure (4-8 a). Analytically predicted number of *negative* phase cycle-slips vs. ρ ;
Case III : The angle modulated carrier and off-tuned receiver ($2\pi f_e T_s = \pi \delta_e = \pi/10$, with sinusoidal modulation, $\gamma = 17.067$, $\delta_m = 0.5859$).

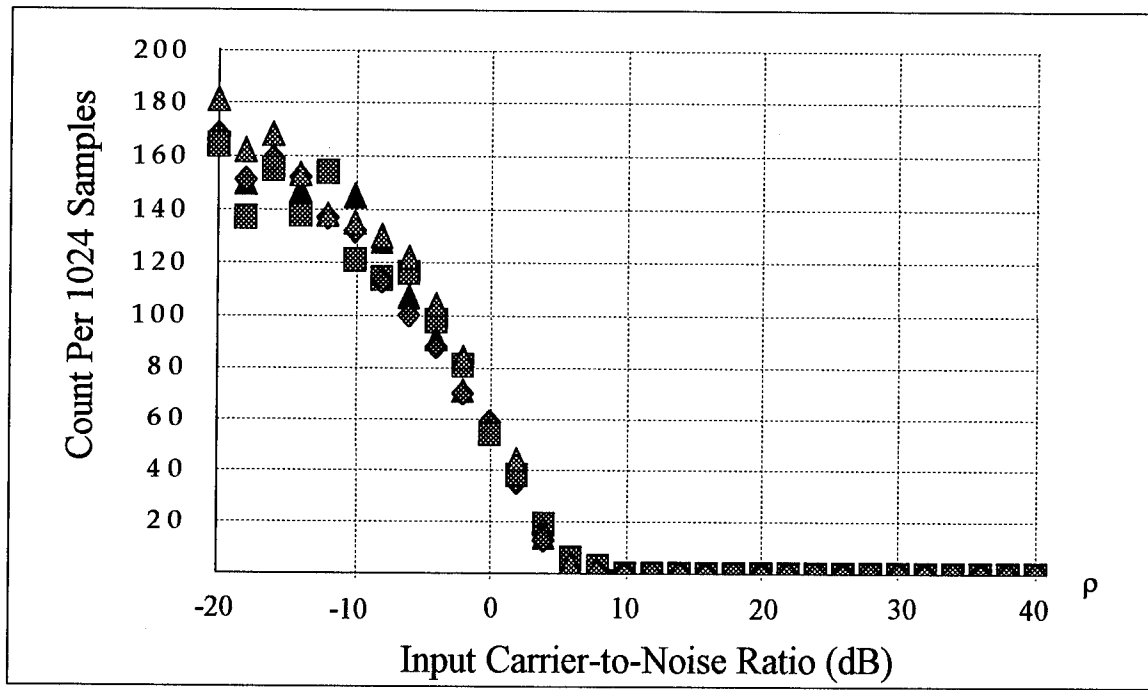


Figure (4-8 b). Experimentally predicted number of *negative* phase cycle-slips vs. ρ (4 simulation runs); Case III : The angle modulated carrier and off-tuned receiver ($2\pi f_e T_s = \pi \delta_e = \pi/10$, with sinusoidal modulation, $\gamma = 17.067$, $\delta_m = 0.5859$).

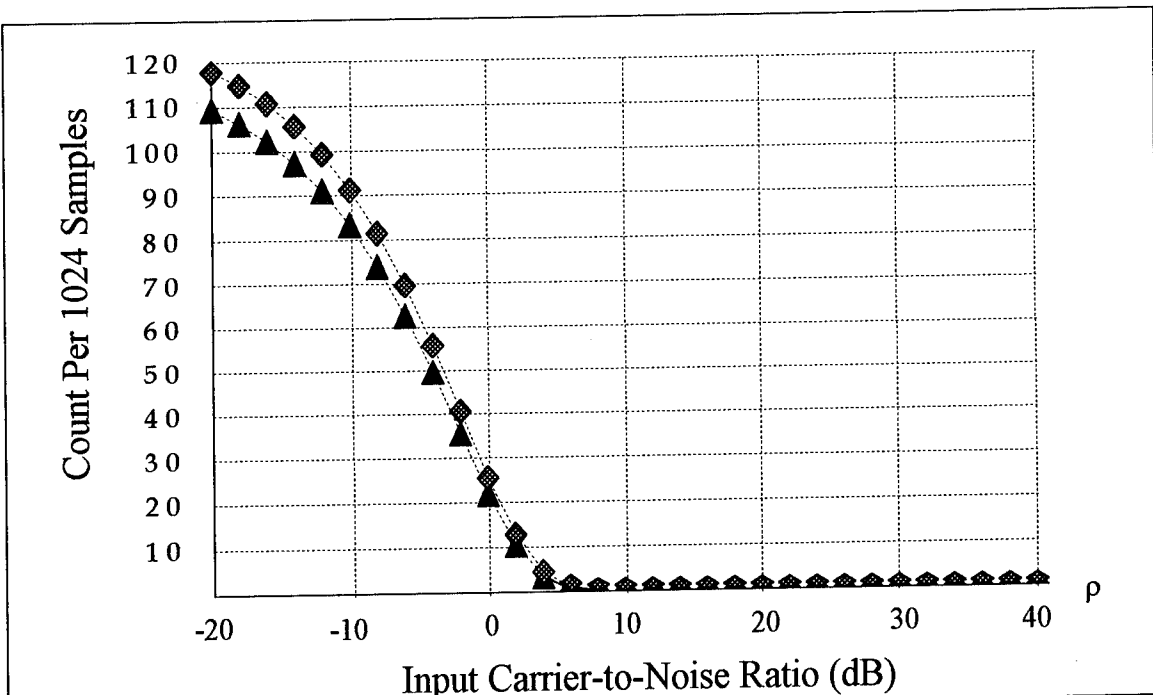


Figure (4-8 c). Analytically predicted number of *positive* phase cycle-slips vs. ρ ;
Case III : The angle modulated carrier and off-tuned receiver ($2\pi f_e T_s = \pi \delta_e = \pi/10$, with
sinusoidal modulation, $\gamma = 17.067$, $\delta_m = 0.5859$).

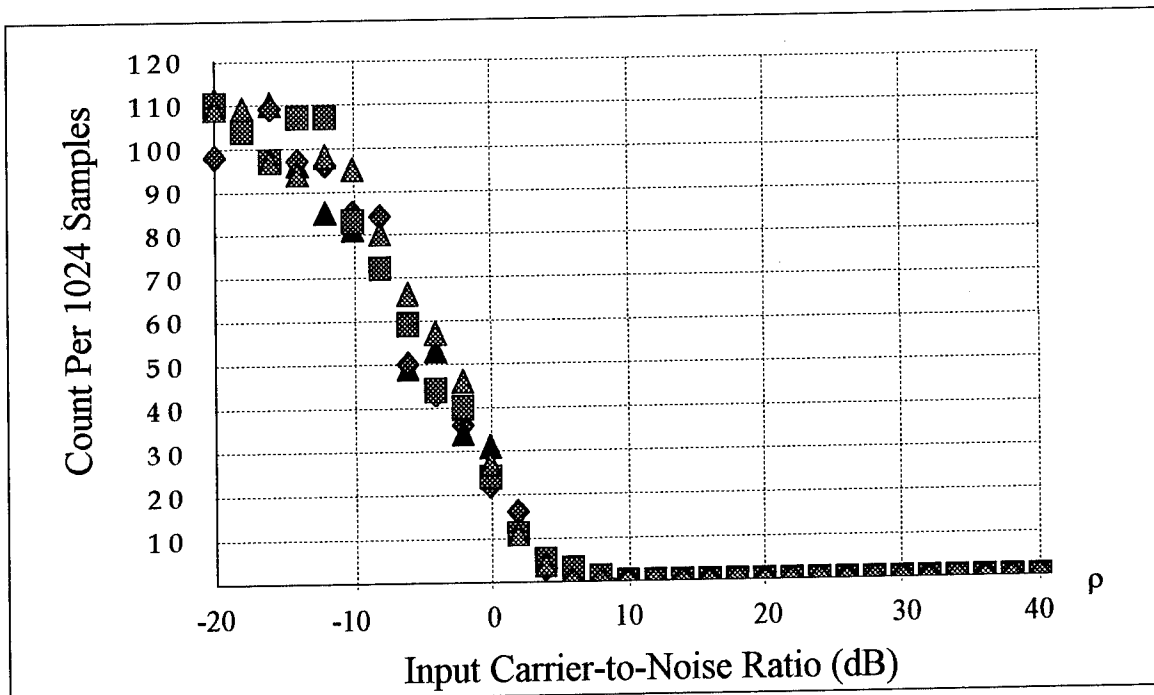


Figure (4-8 d). Experimentally predicted number of *positive* phase cycle-slips vs. ρ
(4 simulation runs); Case III : The angle modulated carrier and off-tuned receiver
($2\pi f_e T_s = \pi \delta_e = \pi/10$, with sinusoidal modulation, $\gamma = 17.067$, $\delta_m = 0.5859$).

4.3 The Mean-Square Phase Noise Performance Measure, \hat{E}_p

The emphasis in this chapter thus far has been on the phase cycle-slip performance measure. Our attention now turns toward the measured mean-square phase noise, as a phase noise variance estimate, for performance prediction purposes. Recall from Equations (4-27) through (4-28) that this measure requires the knowledge of the true phase sequence, $\alpha(nT_s)$, as in the phase cycle-slip measure. Taken together, both measures are used to predict the performance of the backward difference numerical FM discriminator in the presence of additive white Gaussian noise.

We begin by considering the special case in which the imposed angle modulation is sinusoidal as in Equation (4-52). In the presence of a tuning error, f_e , noise-free phase recovery yields

$$\alpha(nT_s) = \sum_{k=0}^n y(kT_s) = 2\pi f_e n T_s + \beta \sin(2\pi f_m n T_s + \theta_m - \frac{\pi}{2}) - \theta , \quad (4-62)$$

where β is $\Delta f / f_m$ as defined in Equation (3-73). Note that the "information-bearing" phase signal component is the term

$$\phi(nT_s) = \beta \sin(2\pi f_m n T_s + \theta_m - \frac{\pi}{2}). \quad (4-63)$$

The output noise-contaminated phase is from Equation (4-30) represented as

$$\tilde{\phi}_d(nT_s) = 2\pi f_e n T_s + \phi(nT_s) - \theta + \eta(nT_s) + 2\pi \cdot R_e(nT_s), \quad (4-64)$$

which motivates us to consider an output signal-to-noise ratio performance measure using our knowledge of $\phi(nT_s)$, and the phase noise variance estimate.

The output phase signal-to-noise ratio (for sinusoidal modulation) is defined as

$$SNR = \frac{\beta^2}{2} \cdot \frac{1}{V\{\eta\}} \cdot \gamma = \frac{\beta^2 \gamma}{2V\{\eta\}}. \quad (4-65)$$

The factor γ in the above equation represents the effect of an ideal lowpass filter of bandwidth f_m Hz, applied to the recovered phase signal. Thus the effect of the output phase noise, η , is measured over the message bandwidth. The factor $\beta^2/2$ is representative of the power of the sinusoidal modulating signal.

Figure (4-9) presents the results of both the analytically and experimentally predicted output phase SNR measure, as a function of the input carrier-to-noise ratio, ρ . Figure (a) presents the analytical results, while figure (b) presents the results of a single simulation run. For the experimental performance prediction, the numerically found phase noise variance, $V\{\eta\}$, has been replaced by its estimate, \hat{E}_p , using a simulated DTFM sequence of length NPTS = 1024 samples. In both figures, the modulation index, δ_m , takes on the values 0.0586, 0.1172, 0.2930, and 0.5860, with γ fixed at 17.067. (These values of δ_m correspond to β values of 1, 2, 5 and 10 respectively, for the current value of γ .) Note that the experimentally predicted measure is in close agreement with that of the analytically predicted measure, for the given modulation indices. It is interesting to observe that a single curve from Figure (4-9) is sufficient to serve as phase noise performance prediction; the parameter β merely shifts (increases) the ordinate by the

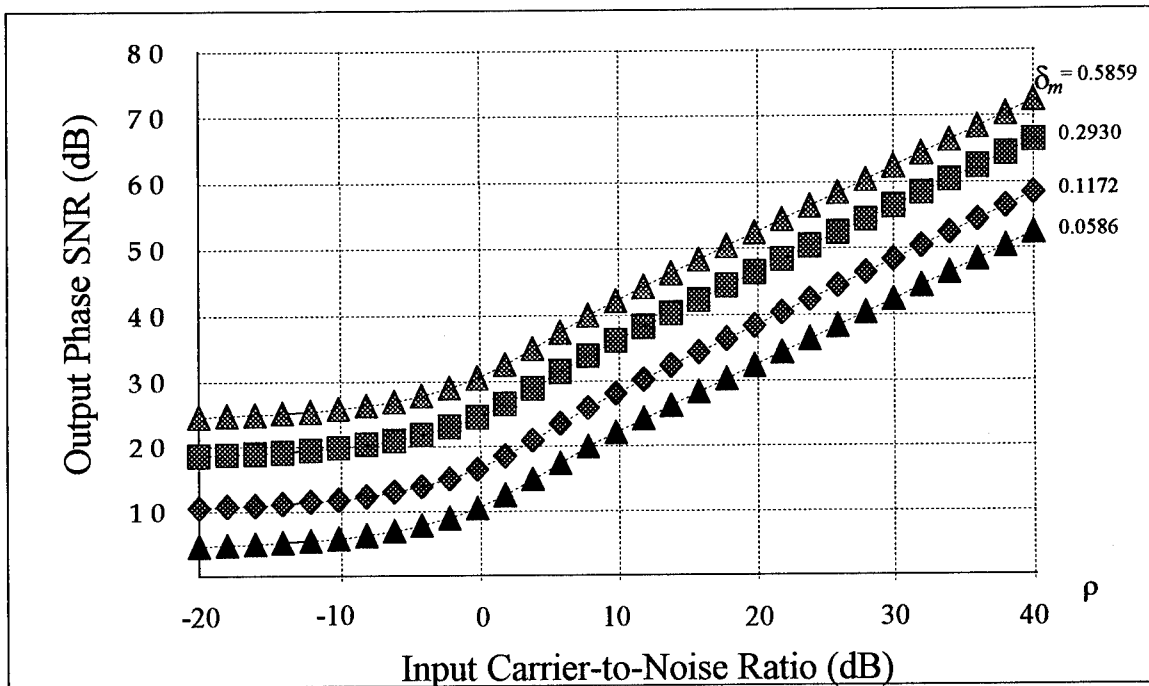


Figure (4-9 a). Analytically predicted output phase SNR in the message bandwidth; (sinusoidal modulation, $\gamma = 17.067$).

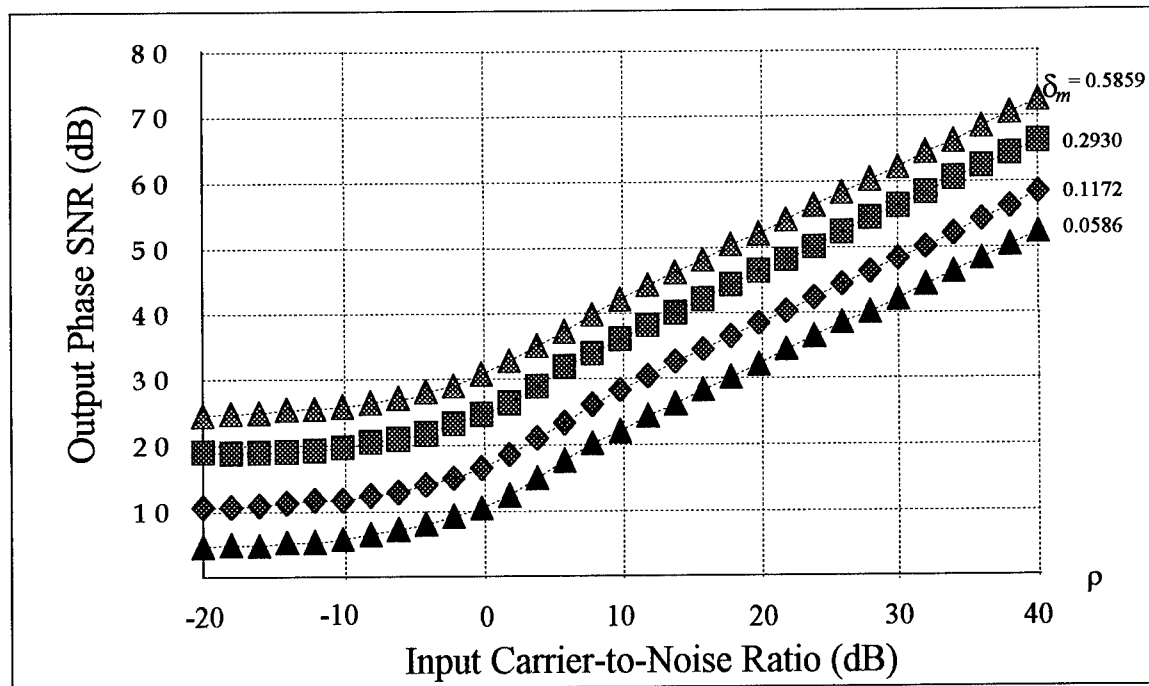


Figure (4-9 b). Experimentally predicted output phase SNR in the message bandwidth; (sinusoidal modulation, $\gamma = 17.067$).

amount $10\log\{\beta^2/2\}$. Note also, however, that as the phase noise pdf approaches a uniform distribution (for values of ρ less than 0 dB or so) the output phase SNR measure loses its meaning. In this limiting situation, the phase noise very effectively randomizes the recovered instantaneous phase and thus eliminates the signal. Due to the fact that the phase noise at time $t = nT_s$ is modeled as being statistically independent of the phase noise at time $t = [n-1]T_s$, the backward difference does not help to alleviate this effect. (In fact as indicated in [6], Rice [38], Stumpers [5], and Middleton [4], have shown that for the continuous-time case, the message signal is reduced by the factor $(1 - e^{-\rho})$.)

We make the observation that for a fixed sample rate, F_s , and fixed message bandwidth, f_m , the frequency deviation, Δf , can be increased such that for a given input carrier-to-noise ratio, the output phase signal-to-noise ratio can be enhanced. This is done, however, at the expense of increasing the probability of phase cycle-slip occurrences, as seen in Figure (4-10). In comparison to Figures (4-7) and (4-8), we see that increasing the DTFM message index, δ_m , to 0.8203 (by increasing Δf) gives rise to additional phase cycle-slips, at input carrier-to-noise ratios as high as 20 dB.

A more realistic scenario is that the sample rate is decreased in order to facilitate processing on a computing device. For a fixed message bandwidth and deviation frequency, the result is that γ decreases while δ_m increases, both towards unity. Again this is done at the expense of additional phase cycle-slips.

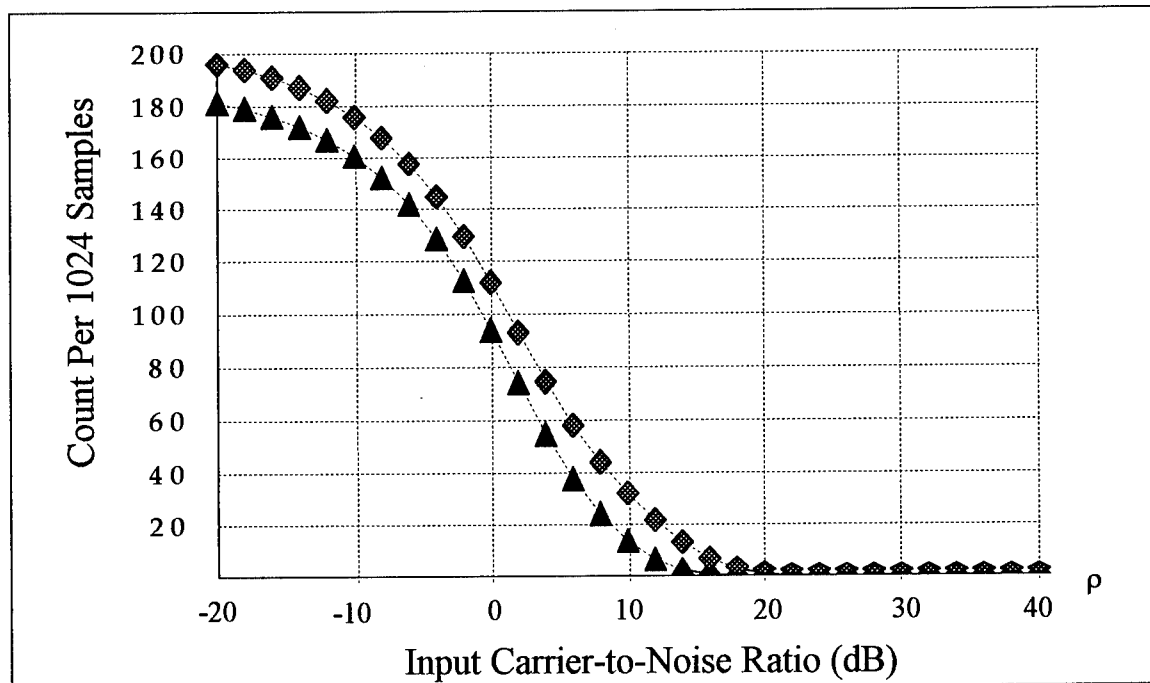


Figure (4-10 a). Analytically predicted number of *negative* phase cycle-slips vs. ρ ;
Case III : The angle modulated carrier and off-tuned receiver ($2\pi f_e T_s = \pi\delta_e = \pi/10$, with
sinusoidal modulation, $\gamma = 17.067$, $\delta_m = 0.8203$).

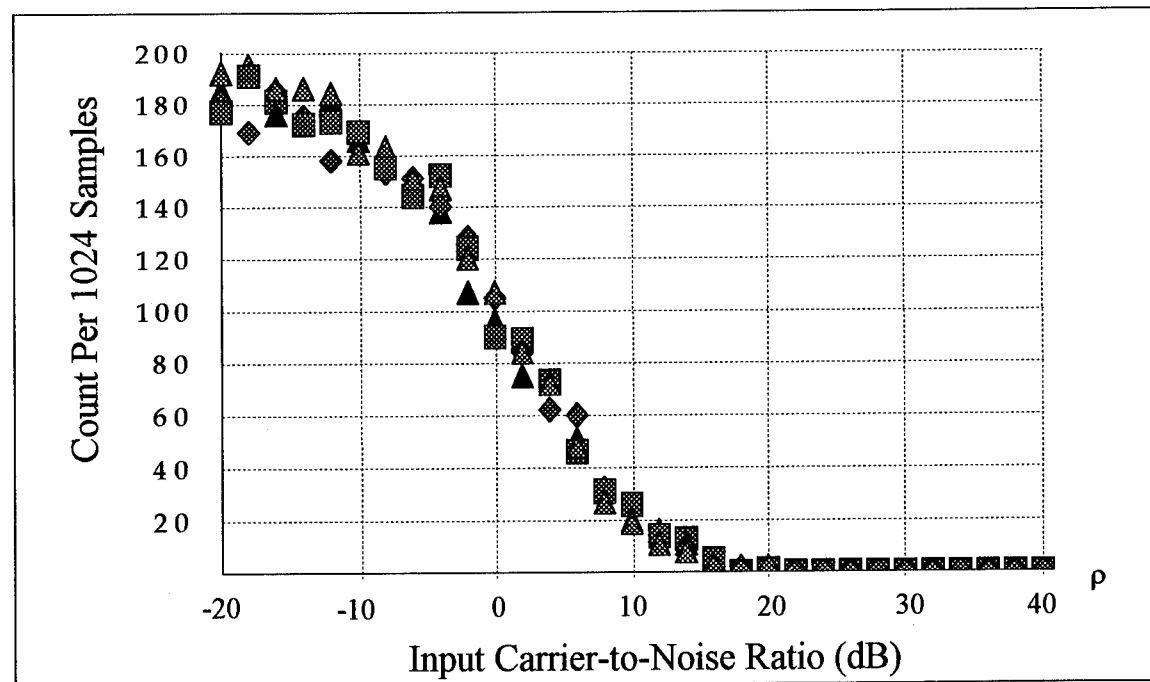


Figure (4-10 b). Experimentally predicted number of *negative* phase cycle-slips vs. ρ
(4 simulation runs); Case III : The angle modulated carrier and off-tuned receiver
($2\pi f_e T_s = \pi\delta_e = \pi/10$, with sinusoidal modulation, $\gamma = 17.067$, $\delta_m = 0.8203$).

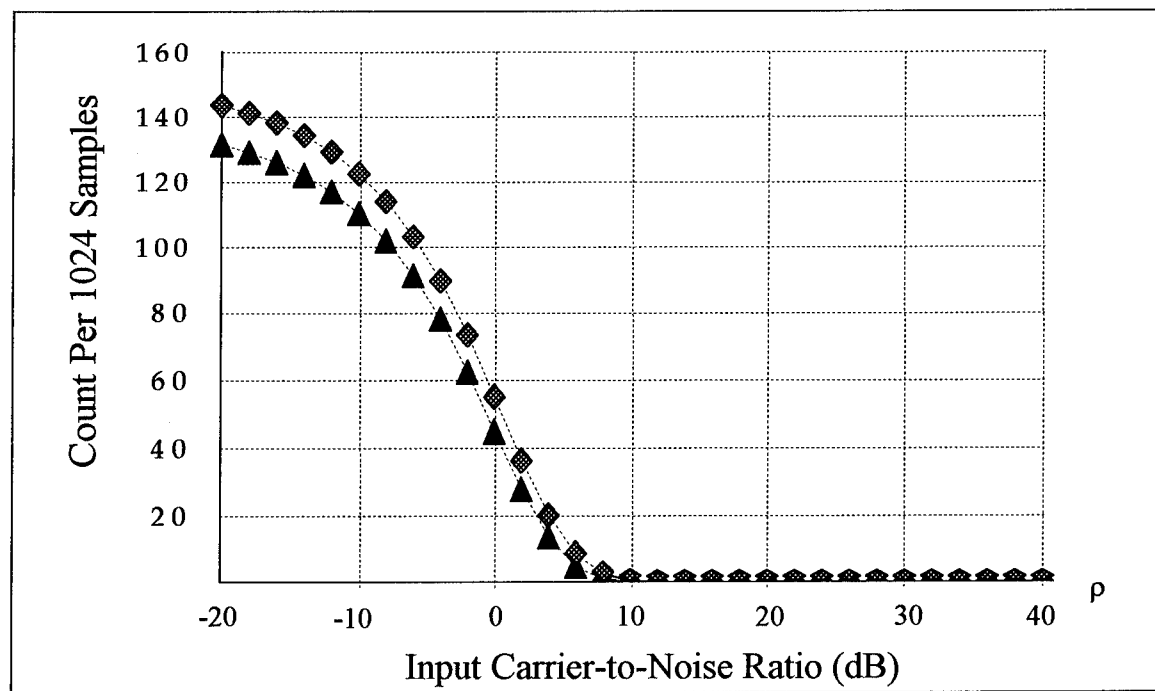


Figure (4-10 c). Analytically predicted number of *positive* phase cycle-slips vs. ρ ;
Case III : The angle modulated carrier and off-tuned receiver ($2\pi f_e T_s = \pi \delta_e = \pi/10$, with
sinusoidal modulation, $\gamma = 17.067$, $\delta_m = 0.8203$).

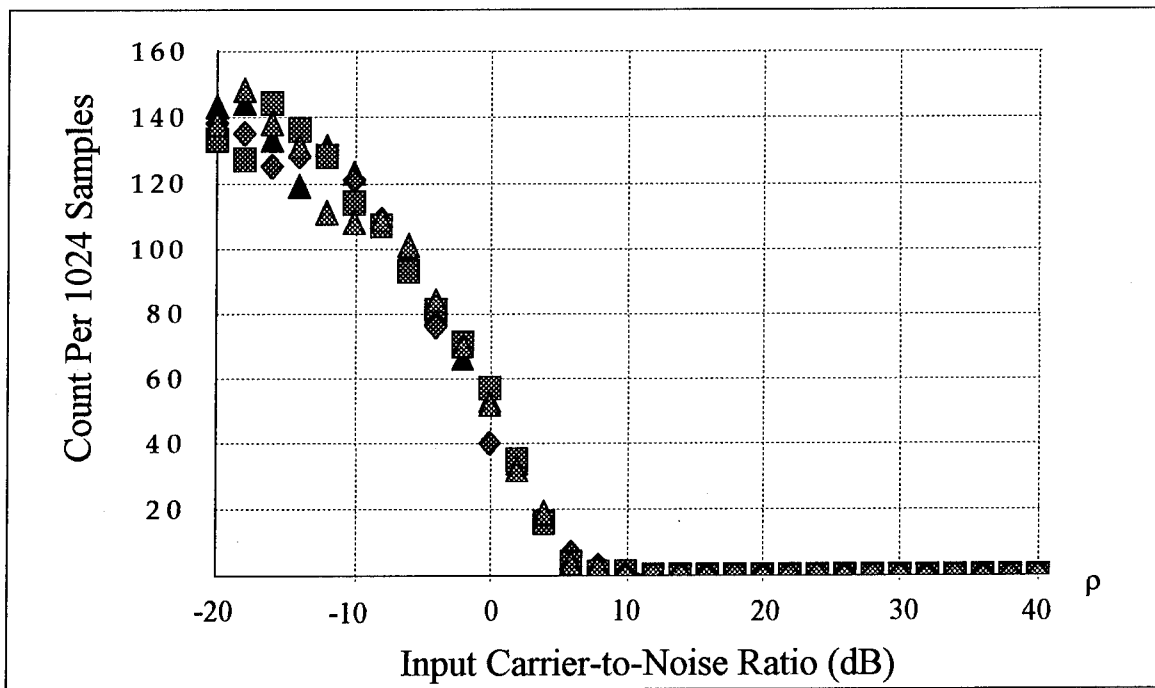


Figure (4-10 d). Experimentally predicted number of *positive* phase cycle-slips vs. ρ
(4 simulation runs); Case III : The angle modulated carrier and off-tuned receiver
($2\pi f_e T_s = \pi \delta_e = \pi/10$, with sinusoidal modulation, $\gamma = 17.067$, $\delta_m = 0.8203$).

4.4 Relating Instantaneous Frequency Aliasing and the Phase Cycle-Slip

In the absence of noise, we have previously established in Equation (3-67) the requirement to prevent instantaneous frequency aliasing due to overmodulation. With $\alpha'_d(nT_s)$ defined as in Equation (4-38), this requirement is restated as

$$-\pi < \alpha'_d(nT_s) \leq +\pi . \quad (4-66)$$

With noise as modeled in the present research, the new requirement becomes

$$-\pi < \alpha'_d(nT_s) + \eta'_d(nT_s) \leq +\pi . \quad (4-67)$$

Note that even in the latter noise-contaminated case, the requirement of Equation (4-66) remains. Thus it is best to refer to violation of Equation (4-66) as overmodulation. Violation of Equation (4-67) will be referred to as instantaneous frequency aliasing.

Further consideration of the phase cycle-slip as derived from Equation (4-37) leads us to conclude that analysis of the term

$$g[\alpha'_d(nT_s) + \eta'_d(nT_s)] ,$$

will uniquely determine when cycle-slips occur. More specifically, a phase cycle-slip is avoided under the condition

$$g[\alpha'_d(nT_s) + \eta'_d(nT_s)] = \alpha'_d(nT_s) + \eta'_d(nT_s) . \quad (4-68)$$

This condition, however, is simply a restatement of Equation (4-67). Thus the phase cycle-slip probabilities previously determined have the alternate interpretation of being the probabilities of instantaneous frequency aliasing events. Aliasing across the $+\pi$ boundary is the same as a negative phase cycle-slip, while aliasing across the $-\pi$ boundary is the same as a positive phase cycle-slip.

4.5 Concluding Remarks

As already indicated, by taking into account both the occurrences of phase cycle-slips and the output phase SNR measure, we have a method of predicting the performance of the backward difference discriminator. In the previous section we have not addressed the fact that the occurrence of a phase cycle-slip is dependent on the phase noise sequence sample function, such that these distinct noise contributions are not independent of each other. In this regard, these two noise effects should not be considered directly additive. Rather, careful consideration must be used to properly combine the effects, if so desired. Currently, we will consider it to be sufficient to leave the performance measures as separate quantities.

CHAPTER 5

**Simulation of a Method of Discriminator Performance Enhancement
for Efficient Processing of Large β DTFM Signals at Low Input CNR**

5.1 Objective

We have established in Chapter 4 the representation of the recovered phase from the backward difference discriminator, in units of radians, as

$$\tilde{\phi}_d(nT_s) = \alpha(nT_s) + \eta(nT_s) + 2\pi R_e(nT_s), \quad (5-1)$$

where

$$\alpha(nT_s) = 2\pi f_e n T_s + \phi(nT_s) - \theta. \quad (5-2)$$

Here, $2\pi f_e n T_s$ is a ramp function resulting from the tuning error, f_e , $\phi(nT_s)$ is the phase message signal, θ is an arbitrary but constant reference phase, and $\eta(nT_s)$ is the Middleton distributed phase noise process. The term $2\pi R_e(nT_s)$ is representative of the occurrence of phase cycle-slips and has the properties outlined in Chapter 4 and Appendix B. This recovered phase representation is the result of modeling the modulated input signal as the Cartesian sum of our complex DTFM signal with complex Gaussian distributed noise of uniform spectral density over the Nyquist frequency band. In this research focus will be on the reduction of phase cycle-slip occurrences, by reducing the modulation index of the noise-contaminated DTFM signal.

Of interest to us is the modulation scenario in which the original continuous-time, constant envelope, frequency modulated signal is characterized by a "large" $\Delta f/f_m$ ratio (i.e., large β). Currently we will consider the term "large" to imply that the minimum required sample rate, after conversion of the input to the generalized pre-envelope form, is such that the message signal amplitude changes by no more than 10 to 20% between

consecutive samples. (Recall that the message signal, $m(nT_s)$, is normalized in amplitude.) Note that for efficient and/or real-time processing of such a DTFM signal, it is desirable to perform computations at as low a sample rate as possible. However, as we have seen in previous results, lowering the sample rate increases the probability of the occurrence of phase cycle-slips for the given resultant value of relative message sample rate, γ . In effect, by lowering the sample rate, the DTFM modulation index, δ , increases towards its maximum allowable value of unity, beyond which the signal is considered to be over-modulated.

As indicated in Figures (4-10 a) through (4-10 d), we find that the phase cycle-slip probability increases substantially with increases in modulation index. This can be seen in comparing these results to those of Figures (4-8 a) through (4-8 d). At a 10% tuning offset, by increasing δ_m from .5859 to .8203 the phase cycle-slip count per 1024 samples increases from approximately zero, to tens of counts at values of input CNR in the range 10 to 20 dB. In this chapter, we will develop and evaluate a method of enhancing the performance of the backward difference numerical FM discriminator, using frequency feedback techniques. In particular, by simulating the noise-contaminated complex DTFM signal as in Chapter 4, observed phase cycle-slip counts and phase noise variance estimation will be used to compare the enhanced demodulator to the established backward difference discriminator baseline.

Special note is made of the fact that in this chapter, for convenience, instantaneous frequency estimates are left in units of normalized radian frequency, rather than scaling by F_s to convert to units of radians per second.

5.1.1 The FM with Feedback (FMFB) Demodulator

The continuous-time FMFB technique as proposed by Chaffee [18] and furthered by Enloe [19] and others, was originally introduced as a means of reducing the FM threshold effect for large deviation, low carrier-to-noise ratio FM systems. The basic block diagram representation of the FMFB device is presented in Figure (5-1). The related and better known phase-lock loop (PLL) device is shown by Develet [20] to be equivalent to the FMFB demodulator under the correct conditions.

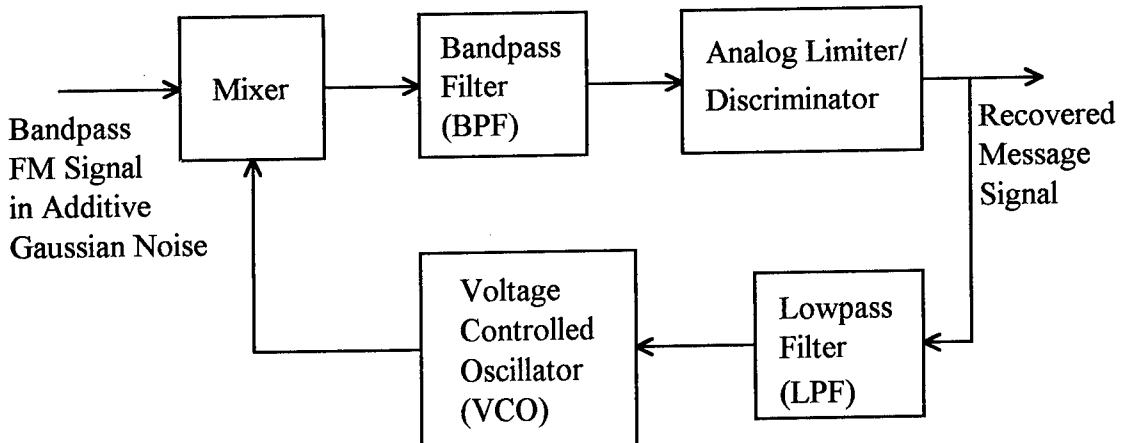


Figure (5-1). The continuous-time (analog) FM with Feedback (FMFB) demodulator.

As explained by Enloe, both the PLL and the FMFB demodulators use the *a priori* information that the ratio of frequency deviation to message signal bandwidth, $\Delta f/f_m$, is large. Referring to Figure (5-1), the function of the Voltage Controlled Oscillator (VCO) is to track the slowly varying message-signal-induced frequency excursions. At the same time, the Bandpass Filter (BPF) responds only to a much narrower band of noise centered

around these frequency excursions. The function of the Analog Limiter/Discriminator and Lowpass Filter (LPF) is to provide the necessary information to the VCO to continuously track these excursions. Note that an error in the VCO frequency relative to the input waveform will result in a proportionate control voltage, acting in a negative feedback manner, such that the error is reduced and continuously maintained near zero. Thus the discriminator is presented a narrower band of noise so that any resulting phase noise is substantially lowered at the discriminator output.

5.1.2 The Numerical FM with Feedback Demodulator

We arrive at a form of the numerical FMFB demodulator by converting to discrete-time the analog FMFB device of Figure (5-1). By additionally incorporating the generalized pre-envelope representation, we arrive at the system shown in Figure (5-2). The input to the device is the noise-contaminated generalized pre-envelope sequence, $X_+(nT_s, f_o)$. The data registers shown are simply indicative of the fact that all necessary calculations for each output estimate must be performed within the sample clock interval, T_s seconds. It is assumed that the instruction clock of the programmable device used to implement the process and the sample clock are derived from a common clock source such that an integer number of instruction cycles are available between consecutive time samples.

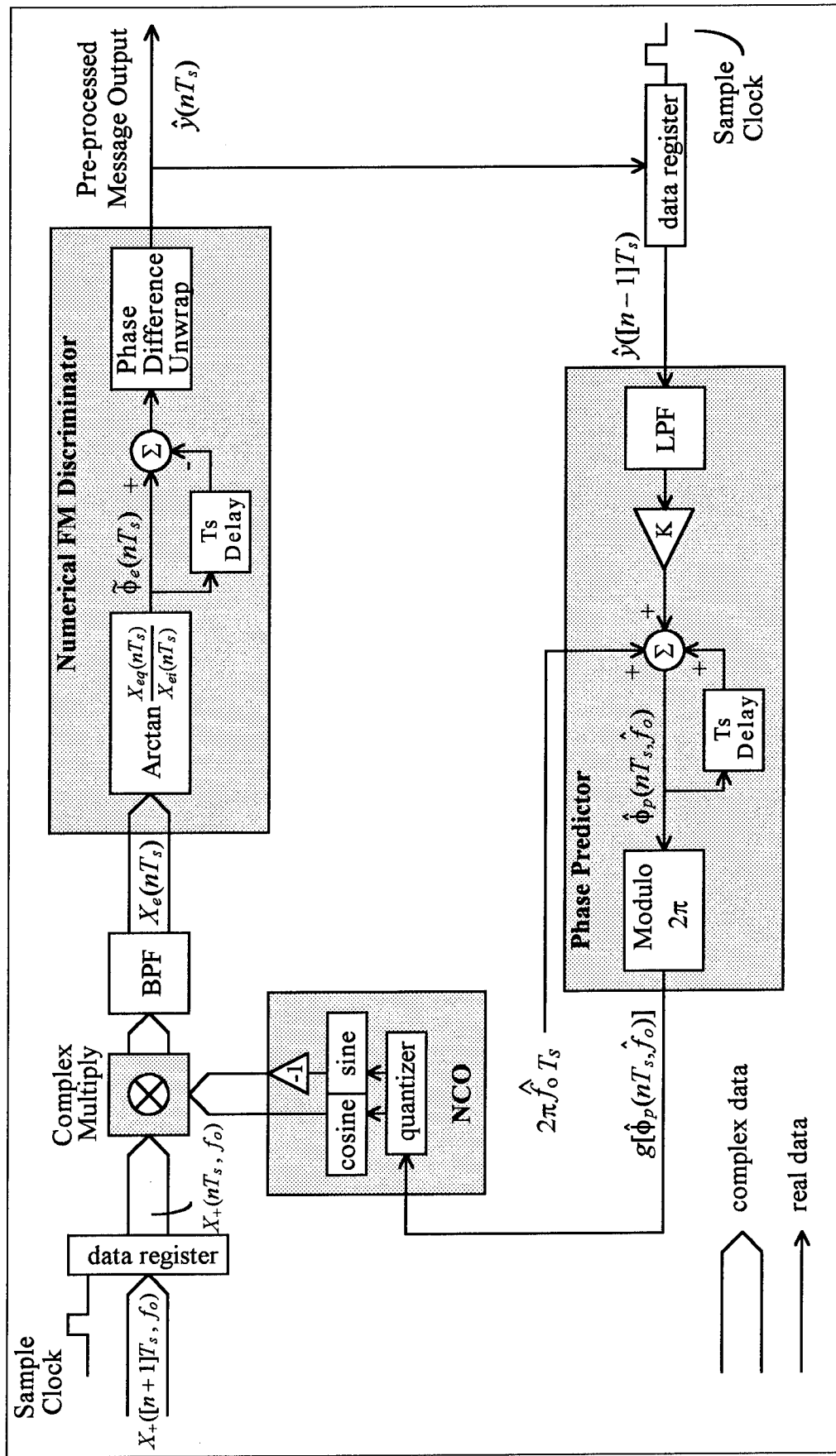


Figure 5-2). A numerical implementation of the FMFB demodulator.

For a description of its operation, we start at time $t = nT_s$ at the input to the device. The function of the Complex Multiply module is to reduce the modulation index of the input sequence by reducing the frequency deviation, Δf . With the input sequence represented as

$$X_+(nT_s, f_o) = |A_+(nT_s)| \cdot \exp\{j[2\pi f_o nT_s + \phi(nT_s) - \theta + \eta(nT_s)]\}, \quad (5-3)$$

the resultant bandpass filtered product is

$$\{X_+(nT_s, f_o) \cdot \exp\{-j\hat{\phi}_p(nT_s, \hat{f}_o)\}\}_{BPF} = |A_+(nT_s)_{BPF}| \cdot \exp\{j\tilde{\phi}_e(nT_s)\}, \quad (5-4)$$

or expressed in Cartesian form,

$$|A_+(nT_s)_{BPF}| \cdot \exp\{j\tilde{\phi}_e(nT_s)\} = \{X_{ei}(nT_s) + jX_{eq}(nT_s)\} = X_e(nT_s). \quad (5-5)$$

The notation $\{\cdot\}_{BPF}$ is representative of the effect of the complex bandpass filter in the device, shown as the BPF module. (This filter processes the result of the Complex Multiply module.) Here, $|A_+(nT_s)|$ is the noise-perturbed envelope sequence associated with $X_+(nT_s, f_o)$. Likewise, $|A_+(nT_s)_{BPF}|$ is the resulting envelope after bandpass filtering.

With the definition

$$\hat{\alpha}_+(nT_s) = K \sum_{k=0}^n \{h_{lp}(kT_s) * \hat{y}([k-1]T_s)\}, \quad (5-6)$$

the phase prediction sequence is

$$\hat{\phi}_p(nT_s, \hat{f}_o) = 2\pi \hat{f}_o nT_s + \hat{\alpha}_+(nT_s) = 2\pi [f_o - f_e] nT_s + \hat{\alpha}_+(nT_s), \quad (5-7)$$

where $h_{lp}(nT_s)$ is the impulse response of the phase predictor lowpass filter. We have also used the fact that

$$2\pi \hat{f}_o = 2\pi \cdot [f_o - f_e]. \quad (5-8)$$

The resulting residue modulation becomes

$$\tilde{\phi}_e(nT_s) = g[\{\alpha(nT_s) + \eta(nT_s) - \hat{\alpha}_+(nT_s)\}_{BPF}]. \quad (5-9)$$

The intent of the bandpass filtering operation is to pass a narrow band of frequency excursions centered around zero hertz, and to reject the noise energy outside of this band. At the same time, this filter must remain wide enough in frequency such that the residue modulation accurately represents the reduced index phase modulation. Employing the backward difference discriminator, the Numerical FM Discriminator module processes this reduced modulation index signal, producing an estimate of the original modulating signal. Although not shown, this estimate can subsequently be processed further, using for example lowpass filtering, to enhance the output signal-to-noise ratio. Thus available to the Phase Predictor module for generating the current phase prediction, are all instantaneous frequency estimates prior to the current time, $t = nT_s$. With the above calculations complete, a new sample interval begins with a sample clock transition to $t = [n+1]T_s$, and the entire process continues.

The shown form of the phase predictor consists of a fixed feedback gain factor, K, the lowpass filter, LPF, and an accumulator which acts as an integrator inverting the differentiation process of the numerical discriminator. Injection of the center frequency estimate after scaling by the sample interval, effectively sets the nominal operating frequency of the Numerically Controlled Oscillator (NCO) module. The shown NCO allows for quantization of the feedback phase prediction such that the required cosine and sine trigonometric functions can be readily implemented using look-up table techniques. The number of bits used in the quantizer determines both the size of the look-up table, and the amplitude resolution of the instantaneous phase prediction. The number of bits can be chosen to produce a resolution which is commensurate with the maximum change between consecutive samples expected in the modulation sequence .

For practical reasons, the output of the accumulator in the Phase Predictor module is retained in a modulo 2π fashion, bounding the accumulated result in the interval $(-\pi, \pi]$ and easing quantizer implementation. Overall, with proper choice of feedback gain, complex bandpass filtering and phase prediction lowpass filtering, the numerical implementation acts in an analogous manner to its continuous-time counterpart and effectively tracks instantaneous frequency excursions.

5.2 The Reconstituted Numerical FM with Feedback (RNFMB) Demodulator

We now introduce a form of demodulator device to be referred to as the Type I RNFMB demodulator, shown in Figure (5-3). This device operates just as the previously described numerical FMFB demodulator of Figure (5-2). However, from this previous description it is observed that we have available to us the instantaneous phase prediction sequence,

$$g[\hat{\phi}_p(nT_s, \hat{f}_o)] = g[2\pi\hat{f}_o nT_s + \hat{\alpha}_+(nT_s)], \quad (5-10)$$

which has been used to reduce the modulation index of the original input sequence, $X_+(nT_s, f_o)$. Since the message output is no longer taken directly from the numerical discriminator, we modify Equation (5-6) as

$$\hat{\alpha}_+(nT_s) = K \cdot \sum_{k=0}^n \{ h_{lp}(kT_s) * g[d_e([k-1]T_s)] \}, \quad (5-11)$$

where

$$d_e(nT_s) = \tilde{\Phi}_e(nT_s) - \tilde{\Phi}_e([n-1]T_s). \quad (5-12)$$

It is apparent that the rate of change of the instantaneous phase prediction sequence of Equation (5-10) represents the frequency compression that has been effected upon the original modulated signal. Thus with the appropriate time alignment as shown in the Phase-Difference Reconstitution module, this compression signal can be *recombined* with

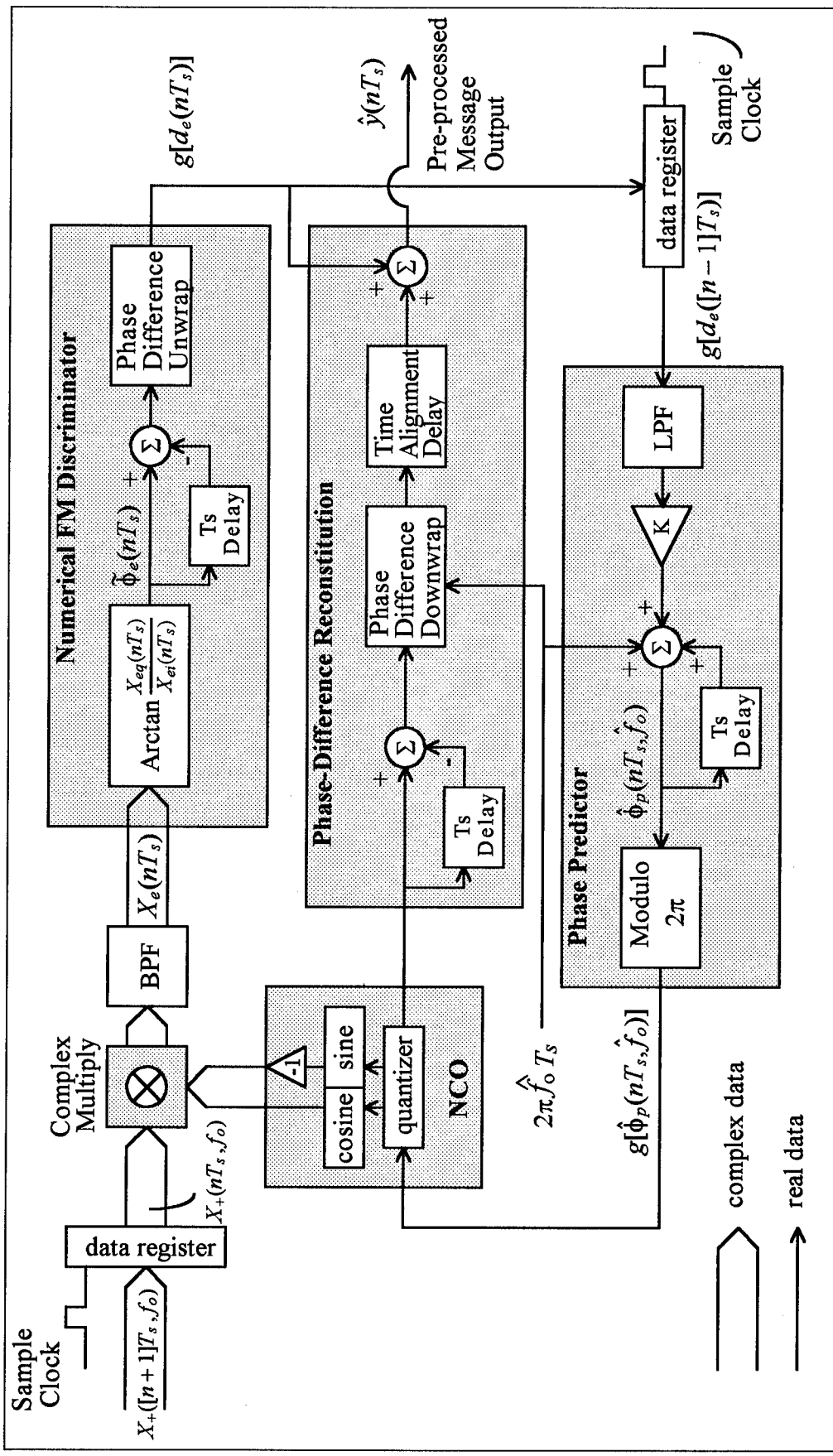


Figure (5-3). The Type I reconstituted numerical FM with feedback demodulator.

the recovered residue modulation estimate, *reconstituting* the original modulation. The time alignment takes into account the group delay of the complex bandpass filter function, BPF. The output is now identified as this reconstituted instantaneous frequency estimate.

The Type I RNFMBF device, interesting in its own right, is left for future research efforts. Currently we emphasize the analysis of a specific implementation of the Type II RNFMBF demodulator, as presented in Figure (5-4). The Type II device is distinguished from the Type I in that the signal fed back to the Phase Predictor module is now the reconstituted message estimate, rather than the residue constituent, $g[d_e(nT_s)]$. Note that for the implemented RNFMBF demodulator, as shown in the figure, both the bandpass and lowpass filter functions have been omitted for computational efficiency and reduction of complexity. By additionally designing the acquisition and demodulation process such that T_s is as large as permissible for proper message recovery, we increase the number of instructions available between consecutive samples.

In practice, we find that cost effective programmable Digital Signal Processing (DSP) devices are characterized by their ability to perform the operations of multiply-accumulate and table look-ups quite efficiently in terms of executed instructions. However, these devices typically cannot perform calculations such as division and arctangent in an efficient manner. As a consequence of these device characteristics, the presented RNFMBF demodulator becomes attractive to the communications engineer, given that the extra processing requirements can be implemented in a small percentage of the total set of instructions required for demodulation. We therefore potentially gain more instructions by increasing T_s than are invested in the additional processing. In the absence

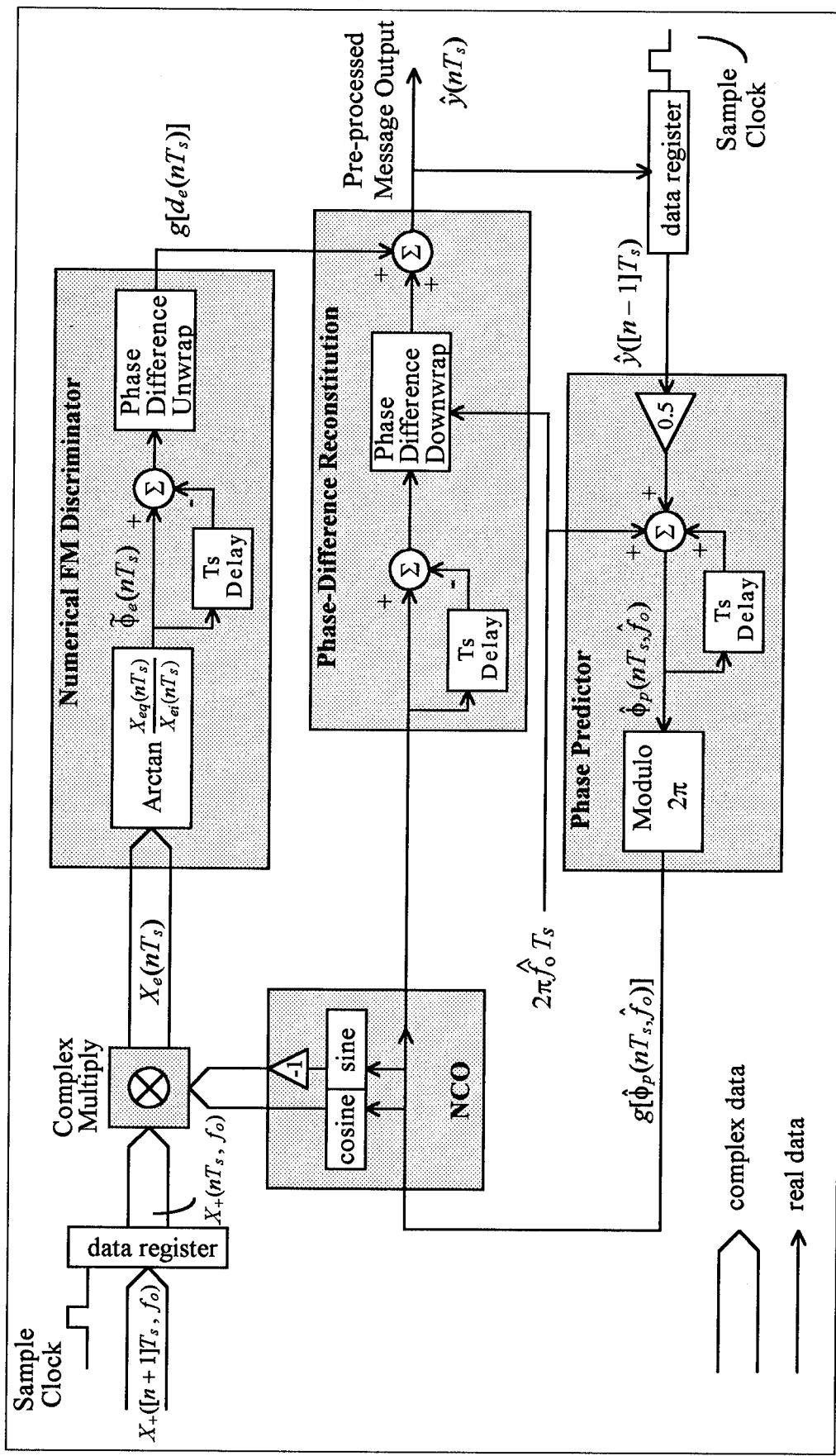


Figure 5-4. Implemented Type II reconstituted numerical FM with feedback demodulator.

of this processing advantage, analysis of the performance of the RNFMB device relative to the established baseline enhances basic understanding of the operation of numerically implemented frequency feedback techniques.

To facilitate the description of the operation of the RNFMB demodulator, we refer to the phase-domain model.

5.2.1 The Implemented RNFMB Demodulator Phase-Domain Model

The phase-domain model of the implemented RNFMB demodulator is shown in Figure (5-5), where we have made use of the z-transform time delay notation, z^{-1} .

Referring to the figure, we find that

$$g[\hat{\phi}_p(nT_s, \hat{f}_o)] = g[2\pi\hat{f}_o nT_s + 0.5 \sum_{k=0}^n \hat{y}([k-1]T_s)] \quad (5-13)$$

such that

$$\begin{aligned} \tilde{\phi}'_2(nT_s) &= g[d_2(nT_s, \hat{f}_o), \hat{f}_o] \\ &= g[g[\hat{\phi}_p(nT_s, \hat{f}_o)] - g[\hat{\phi}_p([n-1]T_s, \hat{f}_o)] - 2\pi\hat{f}_o] \\ &= g[0.5\hat{y}([n-1]T_s)] . \end{aligned} \quad (5-14)$$

Since

$$\hat{y}(nT_s) = \tilde{\phi}'_1(nT_s) + \tilde{\phi}'_2(nT_s) , \quad (5-15)$$

we find that the message output has the property

$$-2\pi < \hat{y}(nT_s) \leq +2\pi , \quad (5-16)$$

which allows us to simplify Equation (5-14) and write

$$\tilde{\phi}'_2(nT_s) = 0.5\hat{y}([n-1]T_s) . \quad (5-17)$$

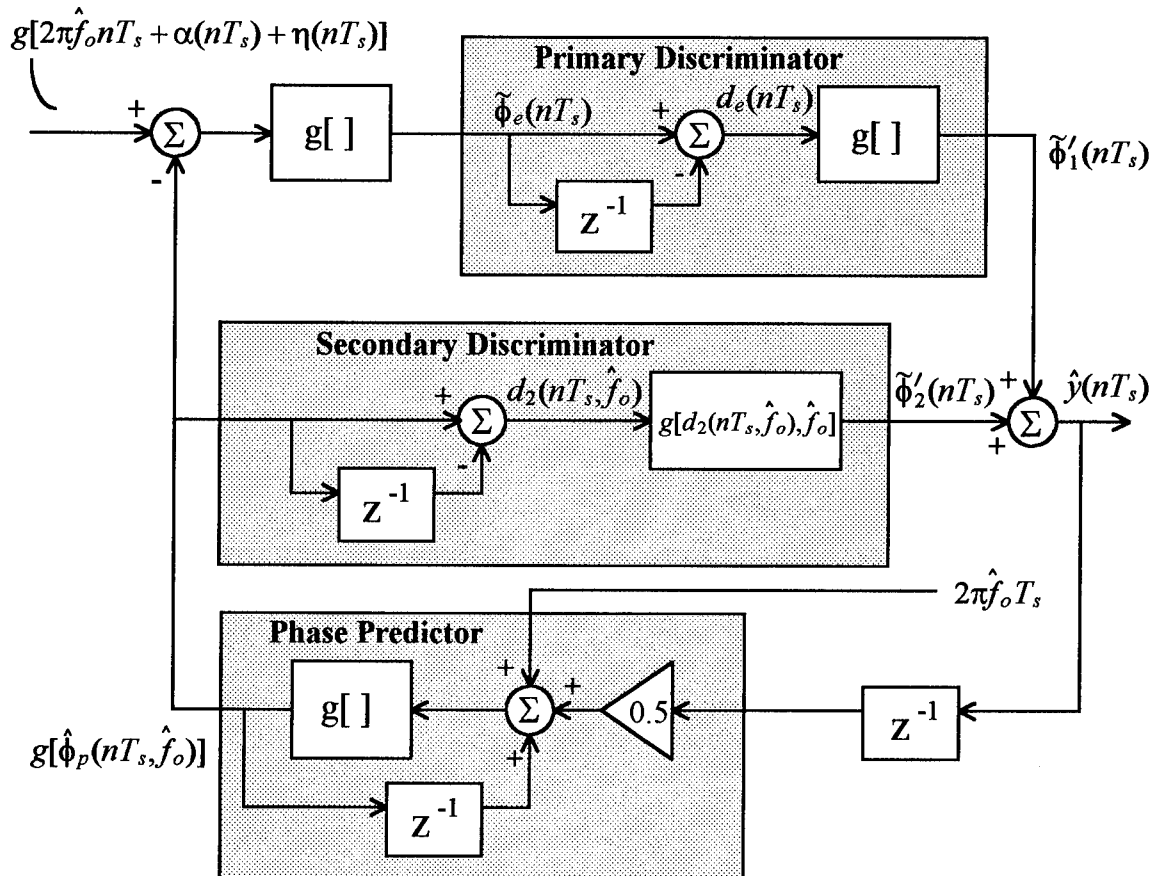


Figure (5-5). The phase-domain model of the implemented Type II RNFMB Demodulator.

With the output of the secondary discriminator established, we are now interested in determining an expression for the primary discriminator output. First we note that

$$\begin{aligned}\tilde{\phi}_e(nT_s) &= g[g[2\pi\hat{f}_o nT_s + \alpha(nT_s) + \eta(nT_s)] - g[\hat{\phi}_p(nT_s, \hat{f}_o)]] \\ &= g[\alpha(nT_s) + \eta(nT_s) - 0.5 \sum_{k=0}^n \hat{y}([k-1]T_s)] ,\end{aligned}\quad (5-18)$$

where we have made use of Equations (5-2) and (5-13). From the above and Equation (5-8) we can write

$$\tilde{\phi}'_1(nT_s) = g[\alpha'_d(nT_s) + \eta'_d(nT_s) - 0.5\hat{y}([n-1]T_s)] ,\quad (5-19)$$

where $\alpha'_d(nT_s)$ and $\eta'_d(nT_s)$ are as defined in Equations (4-38) and (4-39). Equivalently,

$$\tilde{\phi}'_1(nT_s) = \alpha'_d(nT_s) + \eta'_d(nT_s) - 0.5\hat{y}([n-1]T_s) + 2\pi R_{cs}^*(nT_s),\quad (5-20)$$

where the integer sequence, $R_{cs}^*(nT_s)$, is required to ensure that we retain the property

$$-\pi < \tilde{\phi}'_1(nT_s) \leq +\pi .\quad (5-21)$$

This integer sequence is representative of the occurrence of phase cycle-skips in the primary discriminator of the phase-domain model, and has properties that are unique to the RNFMF device. Thus when the quantity

$$\alpha'_d(nT_s) + \eta'_d(nT_s) - 0.5\hat{y}([n-1]T_s)$$

exceeds π in magnitude, a phase cycle-skip occurs as compensation to ensure validity of Equation (5-21). Combining the primary and secondary discriminator outputs as in Equation (5-15), we find from Equations (5-17) and (5-20) that the message output becomes

$$\hat{y}(nT_s) = \alpha'_d(nT_s) + \eta'_d(nT_s) + 2\pi R_{cs}^*(nT_s) . \quad (5-22)$$

Note that Equation (5-22) implies that the output phase noise is identical to that which would have been obtained using the backward difference discriminator alone. Therefore, in subsequent simulations, we expect the predicted output phase noise variance performance measure to be consistent with the baseline discriminator. At best then, we only expect enhanced performance via reduced phase cycle-skip occurrences.

Observe that with regard to the implemented RNFMB demodulator, the intent of the device is to divide the discrimination process equally between two numerical FM demodulators identified as the primary and secondary discriminators. A consequence of the fact that we are processing large β DTFM signals, is that the message signal changes in amplitude by only a small percentage between consecutive samples. This in turn results in a large relative message sampling rate, γ . This *a priori* information allows us to use the current instantaneous frequency estimate as the predicted value of the next estimate. With a feedback factor of $K = 0.5$, the frequency deviation of the signal presented to the primary discriminator is potentially reduced by 50%. We also note that with this value of K , phase cycle-skips are confined to the primary discriminator.

In the absence of a previous phase cycle-skip at time $t = [n-1]T_s$, the quantity controlling the occurrence of a cycle-skip becomes

$$\alpha'_d(nT_s) + \eta'_d(nT_s) - 0.5\hat{y}([n-1]T_s) = \alpha'_d(nT_s) - 0.5\alpha'_d([n-1]T_s) + \epsilon'_d(nT_s), \quad (5-23)$$

where

$$\epsilon'_d(nT_s) = \eta'_d(nT_s) - 0.5\eta'_d([n-1]T_s). \quad (5-24)$$

At values of input carrier-to-noise ratio, $\rho = \alpha^2/(2\sigma^2)$, greater than 10 dB or so, the phase noise is approximately Gaussian, with a variance of less than $(\sigma/a)^2$. For $\beta > 4$, this leads to pre-filtered output phase signal-to-noise ratios greater than 20 dB. This in turn implies that the primary discriminator noise term identified in Equation (5-24) is small relative to the reduced index signal,

$$\alpha'_1(nT_s) = \alpha'_d(nT_s) - 0.5\alpha'_d([n-1]T_s). \quad (5-25)$$

Using the pessimistic modulation scenario in which the message signal is sinusoidal, the relative message sampling rate can be used to bound the message prediction error. It can be shown that

$$\Delta m_{\max} = 2 \cos[\pi \cdot (\frac{\gamma-1}{2\gamma})] \quad (5-26)$$

represents this maximum message amplitude change between consecutive samples.

5.3 RNFMB Demodulation Performance Simulation Results

The Type II RNFMB demodulator of Figure (5-4) has been implemented for comparison to the performance of the established backward difference numerical discriminator baseline. Each demodulator is presented four (for a total of eight) independently generated sample functions of the noise-contaminated DTFM process, of length 1024 samples. Modulation parameters have been selected which demonstrate the typical performance of these demodulators for large β systems. Specifically, the relative message sample rate is set at $\gamma = 17.067$ at a 10% tuning offset, with a message index of $\delta_m = .8203$. This choice of parameters coincides with a β value of 14.

These parameters were chosen to ensure that the maximum message amplitude change between consecutive samples as indicated in Equation (5-26), is less than 20%. This is consistent with our clarification of the term "large β ". In the presented simulations, the selected γ value yields a maximum message amplitude change of 18.4%. The selected parameters also represent a progression from the performance results previously given in Chapter 4 for the backward difference discriminator.

Once again, we present both the probability of occurrence of phase cycle-slips and phase noise variance estimates as performance measures. However, special note is made with regard to the phase cycle-slip counts. As already indicated, the RNFMB demodulator produces a phase cycle-skip sequence which can potentially change by more than 2π between consecutive samples. This fact has been taken into account in the simulations to be presented, such that phase cycle changes greater than 2π are specifically looked for during the counting process. In the simulations presented, no such phase cycle

changes were observed at or above 0 dB input carrier-to-noise ratio. Therefore, we properly refer to the phase cycle changes observed for the RNFMB demodulator, as phase cycle-slips.

Figures (5-6 a) through (5-6 d) present the observed number of both negative and positive phase cycle-slips for the backward difference and RNFMB demodulators. In particular we note the significantly enhanced performance of the RNFMB device indicated in Figure (5-6 b) over that of the baseline discriminator results in Figure (5-6 a). For values of input carrier-to-noise ratio between 10 and 20 dB, the RNFMB device produces no observed cycle-slips, whereas the non-enhanced backward difference demodulator produces tens of cycle-slips.

Estimates of phase noise variance were also made, and converted to output phase signal-to-noise ratios in the message signal bandwidth, as in Chapter 4. In comparing the results of the backward difference discriminator of Figure (5-7 a) with the RNFMB demodulator of Figure (5-7 b), we note no observable difference. This is consistent with the resultant phase noise indicated in Equation (5-22) for the RNFMB demodulator, and theoretical results obtained for the backward difference discriminator in Appendix B.

We conclude that the RNFMB demodulator is a viable method of performance enhancement for the backward difference numerical FM discriminator, under the appropriate modulation conditions. Specifically we have demonstrated the ability of the RNFMB demodulator to operate at combined low sample rate and low input carrier-to-noise ratios for large β systems.

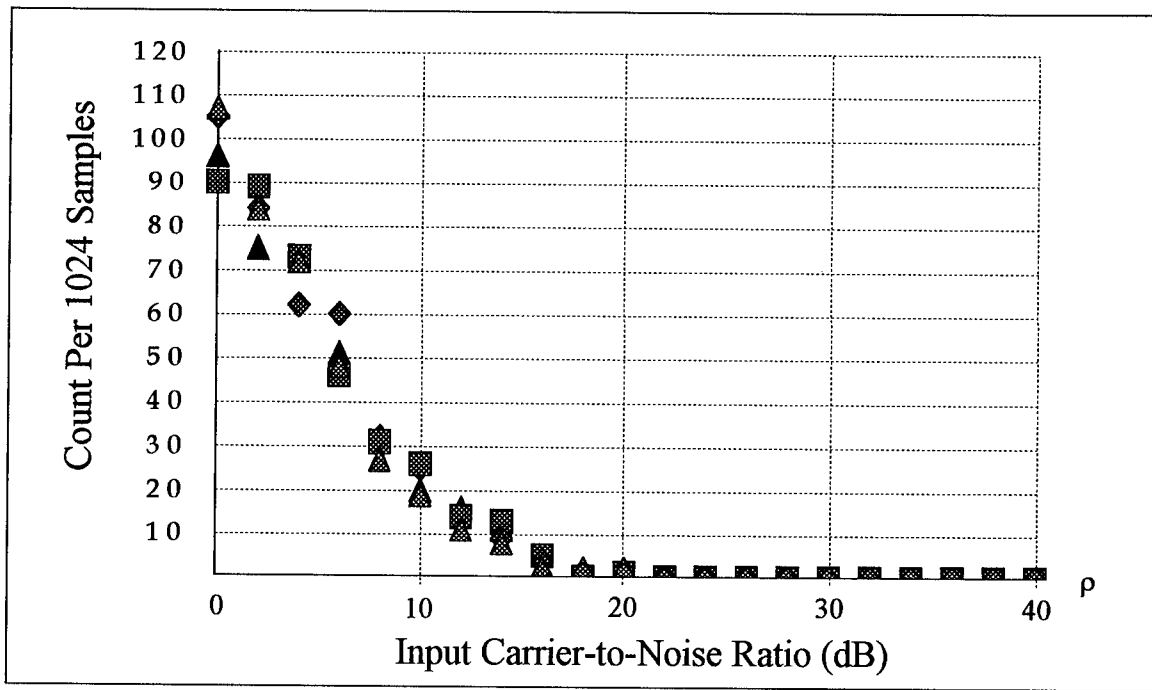


Figure (5-6 a). Experimentally predicted number of *negative* phase cycle-slips vs. ρ (4 simulation runs); Backward Difference Discriminator, ($2\pi f_e T_s = \pi\delta_e = \pi/10$, with sinusoidal modulation, $\gamma = 17.067$, $\delta_m = 0.8203$).

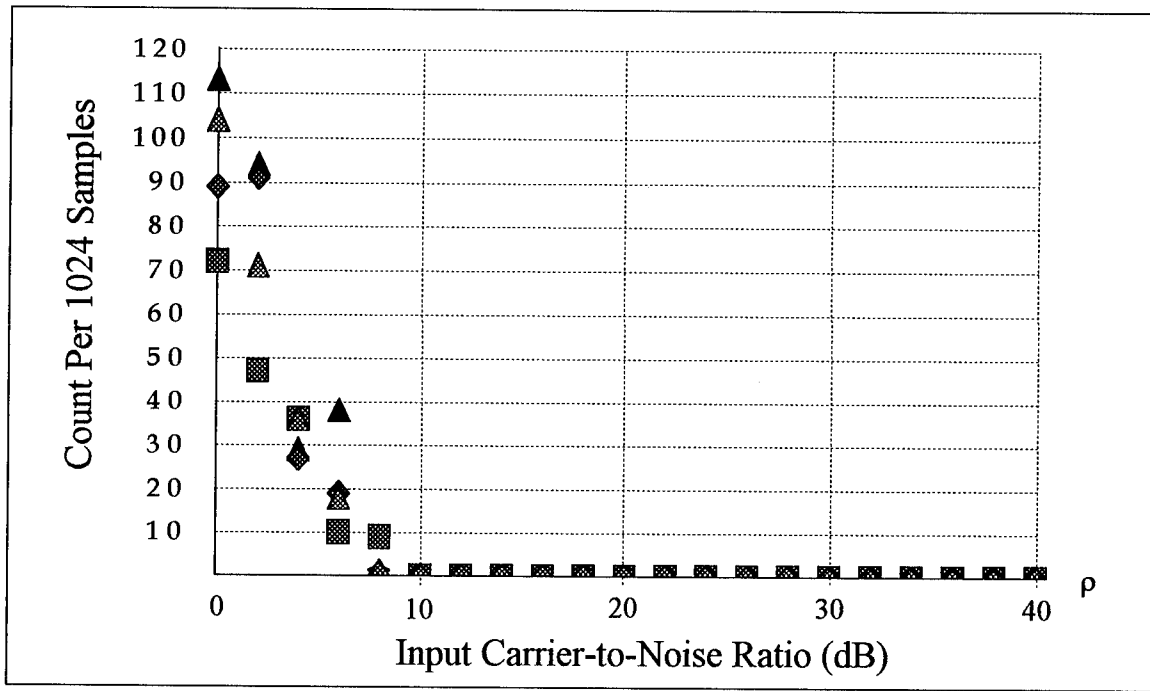


Figure (5-6 b). Experimentally predicted number of *negative* phase cycle-slips vs. ρ (4 simulation runs); RNFMF Demodulator, ($2\pi f_e T_s = \pi\delta_e = \pi/10$, with sinusoidal modulation, $\gamma = 17.067$, $\delta_m = 0.8203$).

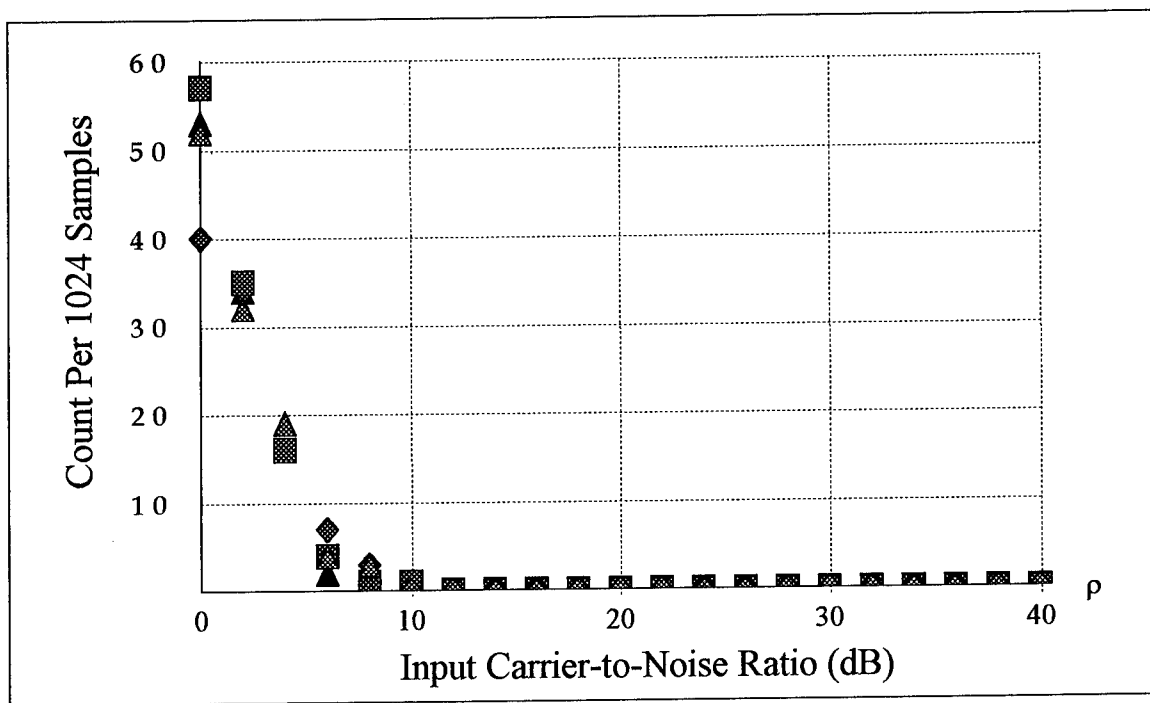


Figure (5-6 c). Experimentally predicted number of *positive* phase cycle-slips vs. ρ (4 simulation runs); Backward Difference Discriminator, ($2\pi f_e T_s = \pi\delta_e = \pi/10$, with sinusoidal modulation, $\gamma = 17.067$, $\delta_m = 0.8203$).

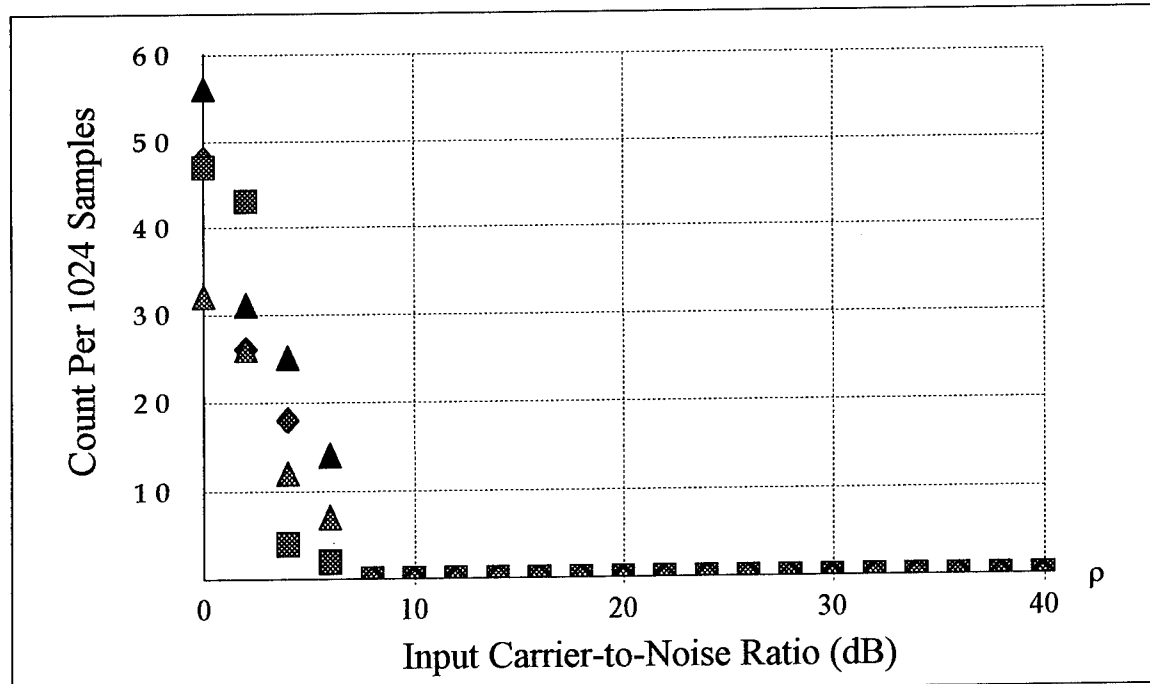


Figure (5-6 d). Experimentally predicted number of *positive* phase cycle-slips vs. ρ (4 simulation runs); RNFMFB Demodulator, ($2\pi f_e T_s = \pi\delta_e = \pi/10$, with sinusoidal modulation, $\gamma = 17.067$, $\delta_m = 0.8203$).

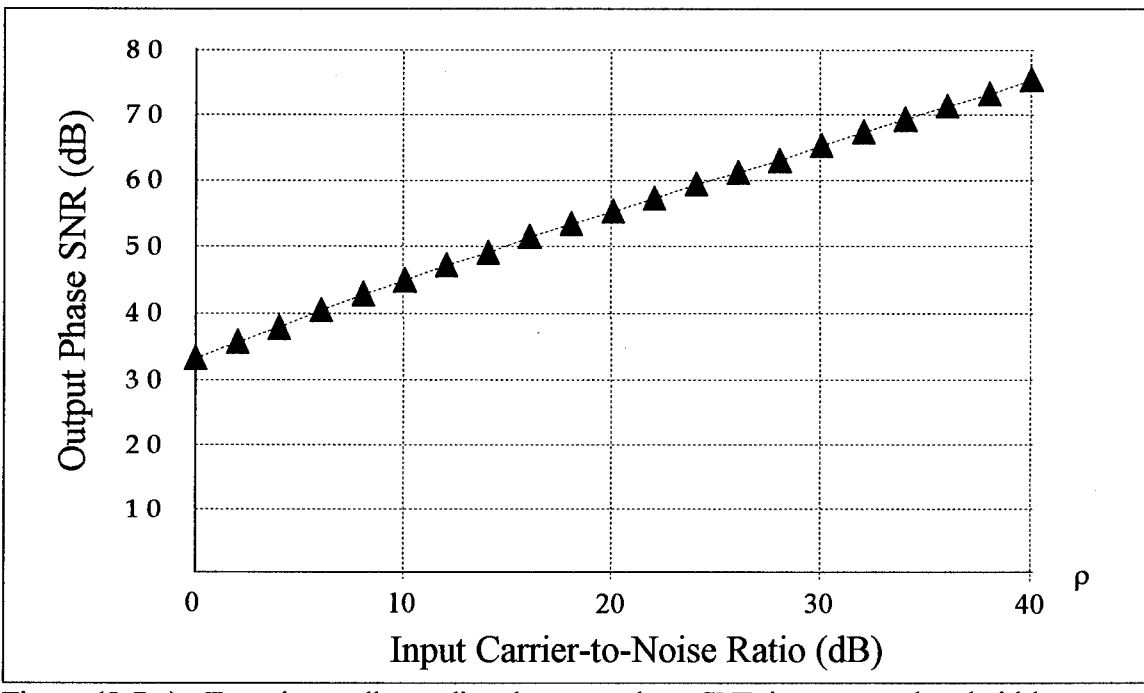


Figure (5-7 a). Experimentally predicted output phase SNR in message bandwidth;
Backward Difference Discriminator (sinusoidal modulation, $\gamma = 17.067$, $\delta_m = .8203$).

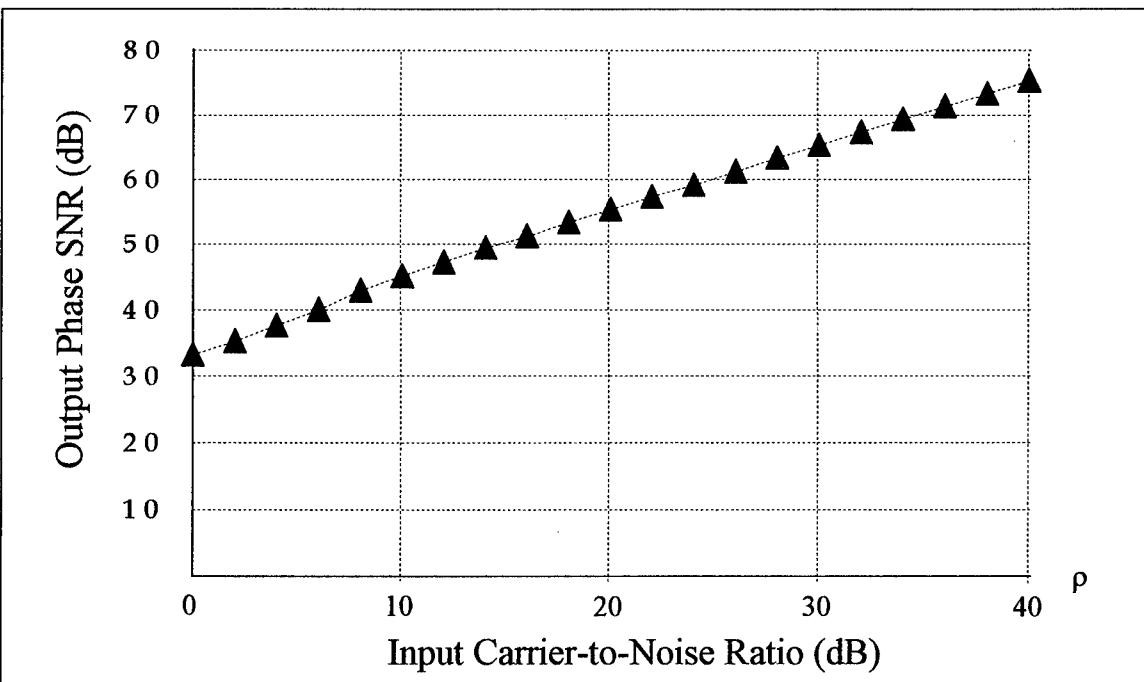


Figure (5-7 b). Experimentally predicted output phase SNR in message bandwidth;
RNFMB Demodulator (sinusoidal modulation, $\gamma = 17.067$, $\delta_m = .8203$).

CHAPTER 6

Conclusions and Areas of Future Research

6.1 Conclusions

In this research, a performance analysis has been performed regarding a class of numerical FM demodulators operating in the presence of additive, spectrally uniform, Gaussian noise. Both theoretical and computer simulation techniques have been employed, and have given consistent performance prediction results. The class of numerical demodulators which have been analyzed apply the backward difference estimate of the time derivative of the phase, to estimate the instantaneous frequency of an angle-modulated complex exponential sequence. Several computationally different approaches to backward difference numerical FM demodulation have been shown to produce equivalent results. Basic concepts regarding the representation and processing of complex-valued, uniformly sampled, discrete-time sequences have been reviewed. These concepts lead to the generalization of the pre-envelope, involving a circular frequency rotation of the complex envelope. The generalized pre-envelope along with the development and representation of the modulo 2π process, $g[\alpha, f_o]$, together reveal themselves to be fundamental in the understanding of the discrete-time FM (DTFM) signal and backward difference demodulation. Subsequently, a method of enhancing the performance of the numerical demodulation process using frequency feedback is presented. A form of this numerical FM with feedback (FMFB) demodulator is introduced and referred to as the reconstituted numerical FM with feedback (RNFMFB) demodulator. Simulation results are presented for a specific implementation of this demodulator operating in the presence of noise. Performance enhancement is demonstrated for large $\Delta f/f_m$ ratios at low sample rates, and low carrier-to-noise ratios.

Regarding the backward difference numerical FM demodulation process, the presence of additive white Gaussian noise is shown to create an additive Middleton distributed phase noise term, along with randomly occurring $+/-2\pi$ phase cycle changes or phase cycle-slips. These phase cycle-slips increase in rate of occurrence with an increase in the modulation index, and are equivalent to noise-induced instantaneous frequency aliasing. The determination of the rate of occurrence of these slips when the message waveform is known, is one performance prediction measure used in this analysis. Experimental results obtained via simulation of the noisy DTFM signal agree with the analytically predicted phase cycle-slip occurrence rates. The second performance prediction measure is the estimate of phase noise variance. Experimental measurements of this variance estimate also gave results in agreement with the true variance of the Middleton distribution. These performance measures, the phase cycle-slip probability estimate and the phase noise variance estimate, together establish a baseline performance summary as associated with backward difference numerical FM demodulation techniques.

The sampling rate requirements of the DTFM signal have been addressed. Two parameters, the relative message sampling rate, γ , and the DTFM modulation index, δ , are required when presenting the analysis of waveforms composed of modulated complex exponentials. Proper selection of these parameters ensures proper recovery of the original message from the complex exponential signal.

6.2 Areas of Future Research

In this research we have intentionally separated the phase cycle-slip error mechanism from the Middleton phase noise process, to elucidate device behavior and to lead to a method of performance enhancement. With careful consideration, these measures can be combined to form a measure of mean square error, leading to the use of optimal receiver design and analysis techniques [40-42]. Whether working in the phase or instantaneous frequency domain, it may further be appropriate to include pre-emphasis/de-emphasis filtering in the communication system model. More generally, wherever additional information regarding the message signal is available a priori, it is often useful to modify the system model accordingly. In addition to presenting results in the context of optimal receiver design and analysis using a minimum mean square error criterion, the non-ideal effects of bandpass filtering on complex envelope generation can be addressed. Although methods of generating the complex generalized pre-envelope from the received band-limited signal have been presented, of interest would be the effects of filtering in both the static and tracking filter cases. These filter effects are particularly important when the receiver employs frequency feedback techniques.

Various methods exist in the literature which help to alleviate the onset of phase cycle-slips, which tend to occur (and increase rapidly) as the input carrier-to-noise ratio decreases. In particular, the phase-lock loop device has been a popular choice for communications engineers. Also of interest, however, have been methods of demodulation which employ frequency feedback techniques. Further research on the development and application of the RNFMB demodulator can be performed.

Specifically, the inclusion of complex bandpass filtering prior to discrimination, and lowpass filtering in the feedback path are expected to be extremely useful in various applications, including co-channel interference mitigation. The ability to separately control the distinct function of these filters makes the FMFB device attractive to communication engineers. In addition, methods of incorporating additional knowledge regarding the message signal into the phase prediction process can be addressed.

Other areas of future research include the potential application of these results to the problem of phase unwrapping of frequency domain responses in homomorphic processing applications [12, 43], the use of the central difference derivative approximation, data signal recovery [44], and low sample rate demodulation of over-modulated DTFM signals.

APPENDIX A

The Backward Difference Approximation to Time Differentiation

A.1 Acquisition of a Bandlimited Signal and its Corresponding Derivative

Consider the two methods of acquiring both the sampled version of a bandlimited signal, $x(t)$, and the sampled version of its time derivative, $x'(t)$, as shown in Figure (A-1). The sampling time interval, T_s , is chosen such that the sampling rate, $F_s = 1/T_s$, is greater than twice the highest frequency component of $x(t)$. As indicated in the figure the integer, n , is an index which identifies a particular sampling instant via the product, $t = nT_s$. The input, $x(t)$, has a Fourier transform such that

$$|X(f)| \geq 0, \quad 0 \leq |f| \leq W \\ = 0, \quad \text{else.} \quad (\text{A-1})$$

Note that both systems are considered to be linear and time-invariant.

A.2 The Frequency Response of the Time Derivative Process

For System A the ideal time derivative, $y(t)$, is known to have the Fourier transform [29]

$$Y(f) = j2\pi f \cdot X(f), \quad (\text{A-2})$$

which is also zero outside the interval $0 \leq |f| \leq W$, since $X(f)$ is zero outside this interval. This system requires synchronized sampling of both the input signal, and its corresponding derivative.

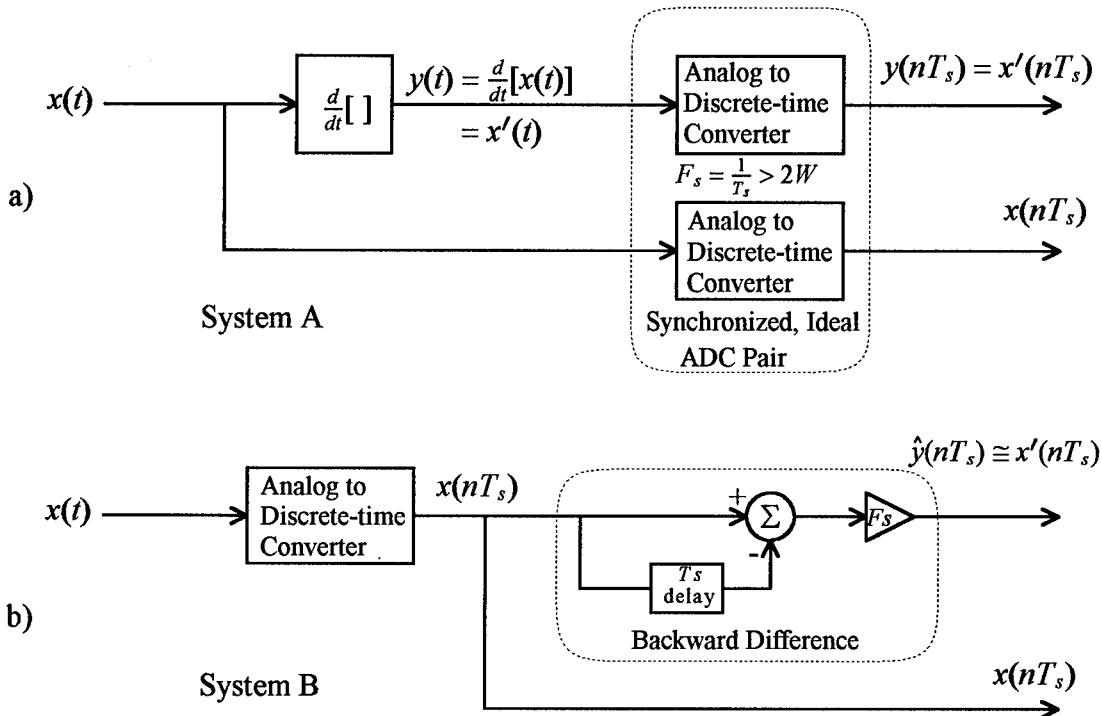


Figure (A-1). Two methods of acquiring a bandlimited signal, $x(t)$, and its corresponding time derivative. a) A continuous-time method employing an analog time derivative and synchronized Analog to Discrete-time Converter (ADC) pair. b) The discrete-time backward difference approximation, employing a single ADC and difference of consecutive samples.

We can represent $x(nT_s)$ as the superposition of infinitesimally small complex sinusoids of the form [12]

$$\frac{1}{2\pi} \cdot X(e^{j\Omega}) \cdot e^{j\Omega n} d\Omega ,$$

as in the Fourier integral

$$x(nT_s) = \frac{1}{2\pi} \int_{-\pi}^{+\pi} X(e^{j\Omega}) e^{j\Omega n} d\Omega . \quad (\text{A-3})$$

Note that Ω ranges over an interval of length 2π , and $X(e^{j\Omega})$ determines the relative (complex) amount of each complex sinusoidal component. Here, $\Omega = \omega T_s$ radians, and $\omega = 2\pi f$ radians/second¹. Likewise, $y(nT_s)$ can be represented in the above manner.

The frequency response of System A is represented as $H_A(e^{j\Omega})$, where

$$Y(e^{j\Omega}) = H_A(e^{j\Omega}) \cdot X(e^{j\Omega}) . \quad (\text{A-4})$$

We can determine $H_A(e^{j\Omega})$ by considering the response of System A to the input

$$x(t) = e^{j\omega t} , \quad (\text{A-5})$$

where $\omega = \Omega / T_s$. In this case we find that

$$\begin{aligned} y(nT_s) &= \left\{ \frac{d}{dt} [e^{j\omega t}] \right\} \Big|_{t=nT_s} \\ &= \{ j\omega e^{j\omega t} \} \Big|_{t=nT_s} \\ &= [j\frac{\Omega}{T_s}] e^{j\Omega n} . \end{aligned} \quad (\text{A-6})$$

Thus $H_A(e^{j\Omega})$ can be identified in Equation (A-6) as

¹ To be consistent with the usual meaning of the variable ω , the variable Ω must have units of radians. (This differs from the usage of these variables in reference [12].) When T_s is equal to 1 second, Ω and ω happen to have the same value and it is tempting to consider them as having the same units, but strictly speaking, the units remain as given.

$$\begin{aligned}
H_A(e^{j\omega T_s}) &= H_A(e^{j\Omega}) \\
&= j \frac{\Omega}{T_s} \\
&= j\omega , \quad -\pi < \omega T_s \leq +\pi .
\end{aligned} \tag{A-7}$$

Note that this frequency response differs from that implied by Equation (A-2), since $H_A(e^{j\Omega})$ is implicitly periodic in Ω , with period 2π . However, since $x(t)$ is bandlimited and properly sampled, the effect of these two distinct responses, over the range of ω of interest, is the same.

The magnitude frequency response of System A is

$$\begin{aligned}
|H_A(e^{j\omega T_s})| &= \sqrt{H_A(e^{j\omega T_s}) \cdot H_A(e^{-j\omega T_s})} \\
&= |\omega| , \quad -\pi < \omega T_s \leq +\pi .
\end{aligned} \tag{A-8}$$

The phase response is identified as

$$\begin{aligned}
\angle H_A(e^{j\omega T_s}) &= \frac{-\pi}{2} , \quad -\pi < \omega T_s < 0 \\
&= 0 , \quad \omega T_s = 0 \\
&= \frac{+\pi}{2} , \quad 0 < \omega T_s \leq +\pi .
\end{aligned} \tag{A-9}$$

A.3 The Frequency Response of the Backward Difference Approximation

In a similar manner, the transfer function of System B is represented as $H_B(e^{j\Omega})$,

where

$$\hat{Y}(e^{j\Omega}) = H_B(e^{j\Omega}) \cdot X(e^{j\Omega}) . \quad (\text{A-10})$$

We can determine $H_B(e^{j\Omega})$ by considering the response of System B to the input identified by Equation (A-5). For System B we find that

$$\begin{aligned} \hat{y}(nT_s) &= \frac{1}{T_s} \{x(nT_s) - x([n-1]T_s)\} \\ &= \frac{1}{T_s} \{e^{j\Omega n} - e^{j\Omega[n-1]}\} \\ &= \frac{1}{T_s} \{1 - e^{-j\Omega}\} \cdot e^{j\Omega n} . \end{aligned} \quad (\text{A-11})$$

From Equation (A-11) we can readily identify the response of System B as

$$\begin{aligned} H_B(e^{j\omega T_s}) &= H_B(e^{j\Omega}) \\ &= \frac{1}{T_s} \cdot \{1 - e^{-j\Omega}\} \\ &= \frac{1}{T_s} \cdot \{1 - e^{-j\omega T_s}\}, \quad -\pi < \omega T_s \leq +\pi . \end{aligned} \quad (\text{A-12})$$

Equation (A-12) further simplifies to

$$H_B(e^{j\omega T_s}) = \frac{2}{T_s} \sin(\omega T_s/2) \cdot e^{j(\pi-\omega T_s)/2} , \quad -\pi < \omega T_s \leq +\pi . \quad (\text{A-13})$$

The magnitude frequency response of system B is

$$\begin{aligned}|H_B(e^{j\omega T_s})| &= \frac{2}{T_s} \sqrt{\sin^2(\omega T_s/2)} \\ &= \frac{1}{T_s} \sqrt{2 - 2 \cos(\omega T_s)} , \quad -\pi < \omega T_s \leq +\pi .\end{aligned}\quad (\text{A-14})$$

and its phase response is identified as

$$\begin{aligned}\angle H_B(e^{j\omega T_s}) &= (\pi - \omega T_s)/2 - \pi, \quad -\pi < \omega T_s < 0 \\ &= 0 , \quad \omega T_s = 0 \\ &= (\pi - \omega T_s)/2 , \quad 0 < \omega T_s \leq +\pi .\end{aligned}\quad (\text{A-15})$$

With the frequency responses of the ideal time differentiator and the backward difference having been determined, it is possible to determine how closely the difference approximation resembles the ideal differentiator.

A.4 The Equivalent Distortion Response

We can consider the frequency response of System B in Figure (A-1) as the product of the ideal response of System A, and a distortion response, $H_D(e^{j\omega})$, as shown in Figure (A-2).

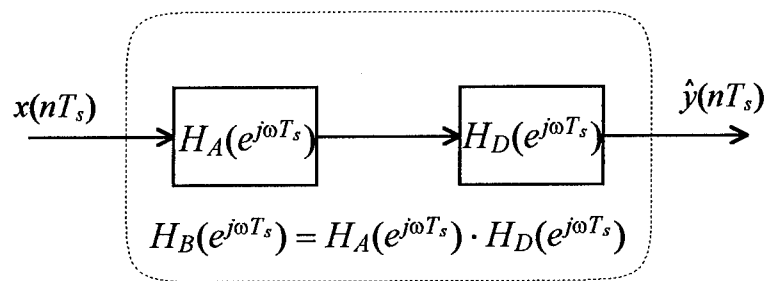


Figure (A-2). A discrete-time filter which has the same frequency response as System B shown in Figure (A-1).

It is readily seen that the distortion response is

$$H_D(e^{j\omega T_s}) = \frac{H_B(e^{j\omega T_s})}{H_A(e^{j\omega T_s})}. \quad (\text{A-16})$$

From Equation (A-7) with $j = e^{j\pi/2}$, along with Equation (A-13) we find that

$$\begin{aligned} H_D(e^{j\omega T_s}) &= \frac{\sin(\omega T_s/2) \cdot e^{j(\pi-\omega T_s)/2}}{\frac{\omega T_s}{2} \cdot e^{j\frac{\pi}{2}}} \\ &= \text{sinc}(\omega T_s/2) \cdot e^{-j(\omega T_s/2)}, \quad -\pi < \omega T_s \leq +\pi, \quad (\text{A-17}) \end{aligned}$$

where $\text{sinc}(x)$ is defined as $\sin(x) / x$. Since $\text{sinc}(x)$ is positive over the interval $-\pi/2 < x < +\pi/2$, the magnitude frequency response is identified as

$$|H_D(e^{j\omega T_s})| = \text{sinc}(\omega T_s/2), \quad -\pi < \omega T_s \leq +\pi, \quad (\text{A-18})$$

and is periodic in $\Omega = \omega T_s$, with period 2π . The phase of this equivalent distortion response is

$$\angle H_D(e^{j\omega T_s}) = -\omega T_s/2, \quad -\pi < \omega T_s \leq +\pi. \quad (\text{A-19})$$

Equation (A-19) places in evidence the fact that the backward difference approximation introduces a half-sample-interval time lag relative to the input function and relative to the ideal derivative of this input. Although this time delay is not a distortion per se, knowledge of the existence of this delay may affect design considerations in some applications. Thus the distortion phase response is linear, and not generally considered to be a problem.

The magnitude frequency response of the distortion is, in fact, not particularly bad either. As seen in Figure (A-3), the magnitude response of System B has the effect of attenuating higher frequencies as compared to the magnitude response of the ideal differentiator of System A. Figure (A-4) shows the magnitude and phase response of the equivalent distortion, $H_D(e^{j\Omega})$.

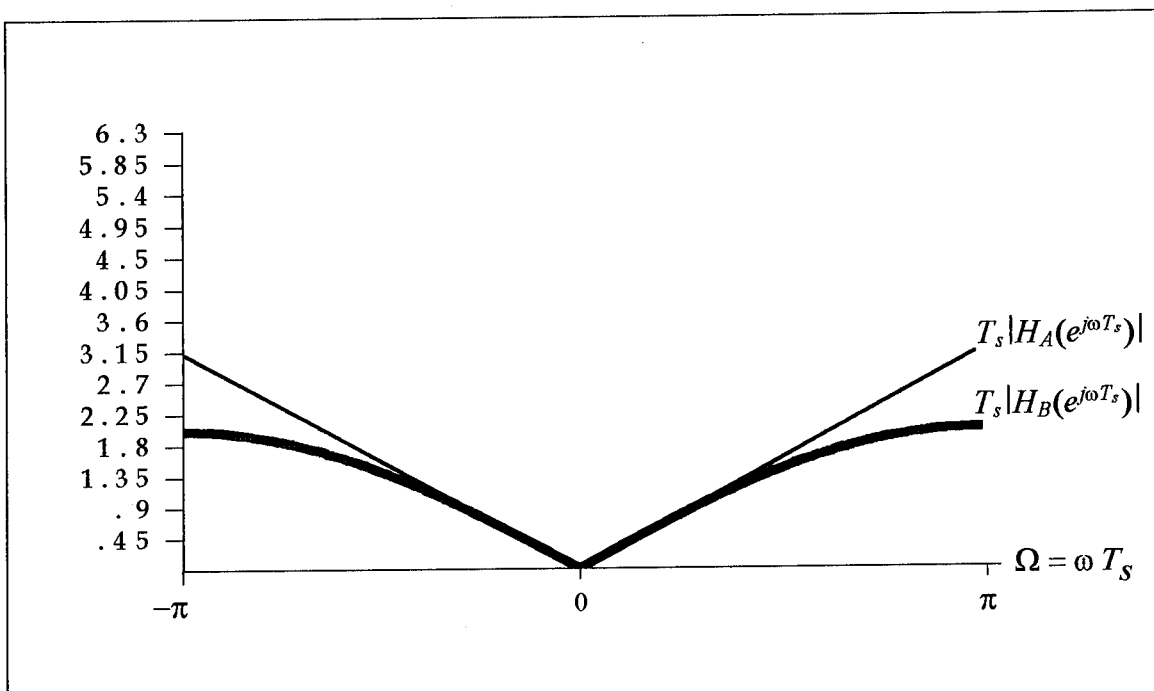


Figure (A-3). One period of the magnitude frequency responses, $T_s|H_A(e^{j\omega T_s})|$ and $T_s|H_B(e^{j\omega T_s})|$.

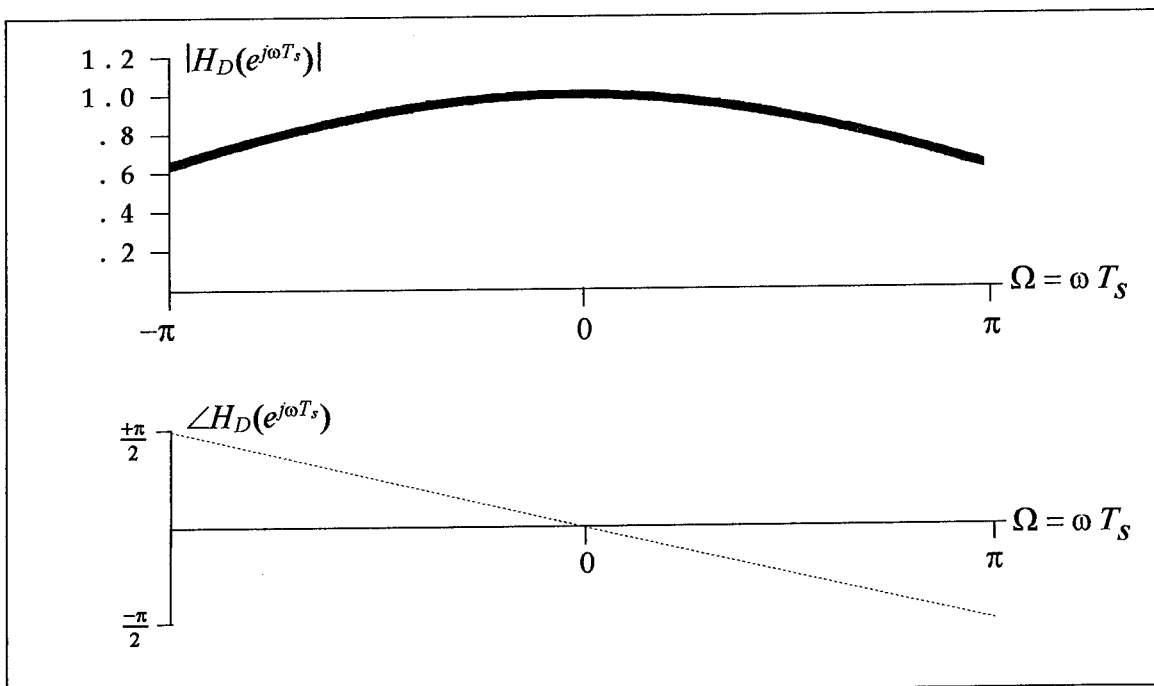


Figure (A-4). One period of the frequency response of the distortion, $H_D(e^{j\omega T_s})$.

APPENDIX B

The Backward Difference Phase Estimate Representation

B.1 The Effects of the Presence of Phase Noise

We are interested in justifying the representation of our noise-contaminated phase estimate as the sum of the original phase, $\alpha(nT_s)$, the Middleton distributed phase noise, $\eta(nT_s)$, and a sheet sequence phase error, $2\pi R_e(nT_s)$. Also of interest are any constraints or properties of the integer sequence, $R_e(nT_s)$, that may arise.

From Figure (4-2), it is apparent that the recovered instantaneous phase estimate can be represented as

$$\begin{aligned}\tilde{\phi}_i(nT_s) &= g[g[\alpha(nT_s)] + \eta(nT_s)] \\ &= g[\alpha(nT_s) + \eta(nT_s)].\end{aligned}\quad (\text{B-1})$$

(Here, the modulo 2π arithmetic property presented in Equation (3-49) has once again been utilized, and will be employed without reference throughout the remainder of this appendix.) By definition we have from Equations (4-20) and (4-21) that

$$\tilde{\phi}'_d(nT_s) = F_s \cdot g_E [\tilde{\phi}_i(nT_s) - \tilde{\phi}_i([n-1]T_s)] \quad (\text{B-2})$$

and

$$\tilde{\phi}_d(nT_s) = T_s \cdot \left\{ \sum_{k=0}^n \tilde{\phi}'_d(kT_s) + \phi_d(-T_s) \right\}. \quad (\text{B-3})$$

Thus from Equations (B-1) and (B-2) we can write

$$\begin{aligned}\tilde{\phi}'_d(nT_s) &= F_s \cdot g[g[\alpha(nT_s) + \eta(nT_s)] - g[\alpha([n-1]T_s) + \eta([n-1]T_s)]] \\ &= F_s \cdot g[\alpha'_d(nT_s) + \eta'_d(nT_s)] ,\end{aligned}\quad (\text{B-4})$$

where $\alpha'_d(nT_s)$ and $\eta'_d(nT_s)$ are as defined in Equations (4-38) and (4-39) respectively. In the absence of noise, to prevent instantaneous frequency aliasing, we have from Chapter 3 the requirement

$$-\pi < \alpha'_d(nT_s) \leq +\pi . \quad (\text{B-5})$$

The phase noise, η , has been defined such that

$$-\pi < \eta(nT_s) \leq +\pi ,$$

which results in the property

$$-2\pi < \eta'_d(nT_s) < +2\pi . \quad (\text{B-6})$$

Combining Equations (B-5) and (B-6) we have that

$$-3\pi < \alpha'_d(nT_s) + \eta'_d(nT_s) < +3\pi . \quad (\text{B-7})$$

From Equation (B-7) we can write

$$\alpha'_d(nT_s) + \eta'_d(nT_s) = g[\alpha'_d(nT_s) + \eta'_d(nT_s)] - 2\pi R'_e(nT_s) , \quad -1 \leq R'_e(nT_s) \leq +1 . \quad (\text{B-8})$$

Note that for any particular time, $t = nT_s$, we have that $R'_e(nT_s) \in \{-1, 0, 1\}$.

If we had available to us the quantity $\alpha'_d(nT_s) + \eta'_d(nT_s)$, along with initial phase conditions, we could form the accumulation

$$\begin{aligned}\tilde{\Phi}_{goal}(nT_s) &= \sum_{k=0}^n \{\alpha'_d(kT_s) + \eta'_d(kT_s)\} + \{\alpha(-T_s) + \eta(-T_s)\} \\ &= \alpha(nT_s) + \eta(nT_s).\end{aligned}\quad (\text{B-9})$$

In lieu of Equation (B-9), we use what is available and form

$$\tilde{\Phi}_d(nT_s) = \sum_{k=0}^n g[\alpha'_d(kT_s) + \eta'_d(kT_s)] + \tilde{\Phi}_i(-T_s), \quad (\text{B-10a})$$

where

$$\tilde{\Phi}_i(-T_s) = g[\alpha(-T_s) + \eta(-T_s)]. \quad (\text{B-10b})$$

Combining Equations (B-8) through (B-10) we have that

$$\tilde{\Phi}_{goal}(nT_s) = \tilde{\Phi}_d(nT_s) - 2\pi \sum_{k=0}^n R'_e(kT_s), \quad -1 \leq R'_e(kT_s) \leq +1. \quad (\text{B-11})$$

Defining $R_e(nT_s)$ such that $R'_e(nT_s) = R_e(nT_s) - R_e([n-1]T_s)$, we arrive at

$$\tilde{\Phi}_{goal}(nT_s) = \tilde{\Phi}_d(nT_s) - 2\pi R_e(nT_s), \quad (\text{B-12})$$

where the integer sequence $R_e(nT_s)$ has the property that

$$-1 \leq R_e(nT_s) - R_e([n-1]T_s) \leq +1 . \quad (B-13)$$

From Equations (B-9) and (B-12) we can write

$$\tilde{\phi}_d(nT_s) = \alpha(nT_s) + \eta(nT_s) + 2\pi R_e(nT_s) . \quad (B-14)$$

It is also readily apparent from Equations (B-1) and (B-14) that

$$\tilde{\phi}_i(nT_s) = g[\tilde{\phi}_d(nT_s)] . \quad (B-15)$$

This fact is utilized in Section 4.1.3 to help establish a pair of experimental statistics as measures of backward difference phase estimate performance prediction.

Thus our noise-contaminated backward difference phase estimate is represented as the sum of the original phase, $\alpha(nT_s)$, the Middleton distributed phase noise, $\eta(nT_s)$, and a sheet sequence phase error, $2\pi R_e(nT_s)$. The sheet sequence error, $R_e(nT_s)$, has the property that it either remains unchanged between consecutive time samples, or changes by +/-1. Therefore we refer to the sequence

$$2\pi R_{cs}(nT_s) = 2\pi R'_e(nT_s) = 2\pi \cdot \{R_e(nT_s) - R_e([n-1]T_s)\} \quad (B-16)$$

as a phase cycle-slip sequence, since it indicates the occurrences of +/-2π phase changes at any particular time, $t = nT_s$.

REFERENCES

- [1] E. H. Armstrong, "A Method of Reducing Disturbances in Radio Signaling by a System of Frequency Modulation," *Proc. IRE*, vol. 24, pp. 689-740, 1935.
- [2] J. R. Carson, T. C. Fry, "Variable Frequency Electric Circuit Theory with Applications to the Theory of Frequency-Modulation," *Bell Systems Tech. J.* vol. 16, 513, 1937.
- [3] D. Middleton, "Some General Results in the Theory of Noise through Nonlinear Devices," *Quart. Appl. Math.*, vol. 5, pp. 445-498, 1948.
- [4] D. Middleton, "The Spectrum of Frequency-Modulated Waves after Reception in Random Noise I, II," *Quart. Appl. Math.*, vol. 7, pp. 129-174, 1949; vol. 8, pp. 59-80, 1950.
- [5] F. L. H. M. Stumpers, "Theory of Frequency-Modulation Noise," *Proc. IRE*, vol. 36, pp. 1081-1092, 1948.
- [6] S. O. Rice, "Noise in FM Receivers," *Time Series Analysis*, ed. M. Rosenblatt, pp. 395-422, John Wiley & Sons, New York, 1963.
- [7] R. G. Wiley, H. Schwarzlander, D. D. Weiner, "Demodulation Procedure for Very Wide-Band FM," *IEEE Trans. Commun.*, vol. COM-25, No. 3, March 1977.
- [8] K. D. Kammeyer, "On the Design of an Efficient Digital Broadcast FM Receiver," *EURASIP Proc. European Signal Processing Conference*, Signal Processing II: Theories and Applications, pp. 355-358, 1983.
- [9] H. Cramer, M. R. Leadbetter, *Stationary and Related Stochastic Processes*, John Wiley & Sons, New York, 1967.
- [10] D. Gabor, "Theory of Communication," *Proc. IEE*, vol. 93 part III, pp. 429-457, 1946.
- [11] H. Urkowitz, *Signal Theory and Random Processes*, Artech House, 1983.
- [12] A. V. Oppenheim, R. W. Schafer, *Discrete Time Signal Processing*, Prentice-Hall, 1989.
- [13] A. H. Nuttall, "On the Quadrature Approximations to the Hilbert Transform of Modulated Signals," *Proc. IEEE*, pp. 1458-1459, Oct. 1966.

- [14] H. W. Schussler, J. Weith, "On the Design of Recursive Hilbert-Transformers," *Proc. IEEE Int'l Conf. ASSP (ICASSP)*, pp. 876-879, April 1987.
- [15] P. A. Regalia, S. K. Mitra, "Quadrature Mirror Hilbert Transformers," *Digital Signal Processing - 87*, pp. 775-782, 1987.
- [16] W. Rosenkranz, "Quadrature Sampling of FM-Bandpass Signals - Implementation and Error Analysis," *Digital Signal Processing - 87*, pp. 377-381, 1987.
- [17] B. Boashash, G. Jones, P. O'Shea, "Instantaneous Frequency of Signals: Concepts, Estimation Techniques and Applications," *SPIE vol 1152, Advanced Algorithms and Architectures for Signal Processing IV*, pp. 382-400, 1989.
- [18] J. G. Chaffee, "The Application of Negative Feedback to Frequency-Modulation Systems," *Bell Sys. Tech. J.*, vol. 18, pp. 403-437, July 1939.
- [19] L. H. Enloe, "Decreasing the Threshold in FM by Frequency Feedback," *Proc. IRE*, vol. 50, pp. 18-30, January 1962.
- [20] J. A. Develet Jr., "Statistical Design and Performance of High-Sensitivity Frequency-Feedback Receivers," *IEEE Trans. on Military Electronics*, pp. 281-284, October 1963.
- [21] W. Rosenkranz, "Design and Optimization of a Digital FM Receiver Using DPLL Techniques," *Proc. IEEE Int'l Conf. ASSP (ICASSP)*, pp. 592-595, March 1985.
- [22] L. M. Robinson, "Tanlock: A Phase-Lock Loop of Extended Tracking Capability," *Proc. IRE Conv. Military Electronics*, February 1962.
- [23] J. C. Lee, C. K. Un, "Performance Analysis of Digital Tanlock Loop," *IEEE Trans. Commun.*, vol. COM-30, No. 10, pp. 2398-2411, October 1982.
- [24] S. Ono, T. Aoyama, M. Hagiwara, M. Nakagawa, "Implementation of a New Type DSP PLL Using High Performance DSP DSSP-1," *Proc. IEEE Int'l Conf. ASSP (ICASSP)*, pp. 2195-2198, April 1986.
- [25] B. Boashash, L. B. White, "Instantaneous Frequency Estimation and Automatic Time-Varying Filtering," *Proc. IEEE Int'l Conf. ASSP (ICASSP)*, pp. 1221-1224, April 1990.
- [26] F. D. Natali, "AFC Tracking Algorithms," *IEEE Trans. Commun.*, vol. COM-32, No. 8, August 1984.
- [27] W. R. LePage, *Complex Variables and the Laplace Transform for Engineers*, Dover Publications, 1961.

- [28] R. V. Churchill, *Introduction to Complex Variables and Applications*, 2nd Ed., McGraw-Hill, 1960.
- [29] S. Haykin, *Communication Systems*, 2nd Ed., John Wiley & Sons, New York, 1983.
- [30] F. G. Stremler, *Introduction to Communication Systems*, 2nd Ed., Addison-Wesley, 1982.
- [31] H. Nyquist, "Certain Topics in Telegraph Transmission Theory," *AIEE Trans.*, pp. 617-644, 1928.
- [32] C. E. Shannon, "Communication in the Presence of Noise," *Proc. IRE*, vol. 37, pp. 10-21, June 1949.
- [33] A. J. Jerri, "The Shannon Sampling Theorem - Its Various Extensions and Applications; A Tutorial Review," *Proc. IEEE*, vol. 65, No. 11, pp. 1565-1596, November 1977.
(See also : A. J. Jerri, Correction to above paper, *Proc. IEEE*, vol. 67, No. 4, p. 695, April 1979.)
- [34] D. Slepian, "On Bandwidth," *Proc. IEEE*, vol. 64, No. 3, pp. 292-300, March 1976.
- [35] E. Bedrosian, "A Product Theorem for Hilbert Transforms," *Proc. IEEE*, vol. 51, pp. 868-869, 1963.
- [36] K. S. Shanmugan, A. M. Breipohl, *Random Signals Detection, Estimation and Data Analysis*, John Wiley & Sons, New York, 1988.
- [37] D. Middleton, *An Introduction to Statistical Communication Theory*, McGraw-Hill, New York, 1960. (reprint ed.: Peninsula Publ., Los Alto CA, 1987.)
- [38] S. O. Rice, "Statistical Properties of a Sine Wave plus Random Noise," *Bell Systems Tech. J.*, vol. 27, pp. 109-157, 1948.
- [39] J. A. Develet, "A Threshold Criterion for Phase-Lock Demodulation," *Proc. IEEE*, pp. 349-356, February 1963.
(See also : Develet, J. A., Correction to "A Threshold Criterion for Phase-Lock Demodulation," *Proc. IEEE*, p. 580, April 1963.)
- [40] H. L. Van Trees, *Detection, Estimation, and Modulation Theory; Part II: Nonlinear Modulation Theory*, John Wiley & Sons, New York, 1971.

- [41] S. Kay, "Statistically / Computationally Efficient Frequency Estimation," *Proc. IEEE Int'l Conf. ASSP (ICASSP)*, pp. 2292-2295, April 1988.
- [42] S. W. Lang, B. R. Musicus, "Frequency Estimation from Phase Differences," *Proc. IEEE Int'l Conf. ASSP (ICASSP)*, pp. 2140-2143, May 1989.
- [43] J. M. Triboulet, "A new Phase Unwrapping Algorithm," *IEEE Trans. ASSP*, vol. ASSP-25, No. 2, April 1977.
- [44] H. Meyr, M. Oerder, A. Polydoros, "On Sampling Rate, Analog Prefiltering, and Sufficient Statistics for Digital Receivers," *IEEE Trans. Commun.*, vol. 42, No. 12, December 1994.

***MISSION
OF
ROME LABORATORY***

Mission. The mission of Rome Laboratory is to advance the science and technologies of command, control, communications and intelligence and to transition them into systems to meet customer needs. To achieve this, Rome Lab:

- a. Conducts vigorous research, development and test programs in all applicable technologies;
- b. Transitions technology to current and future systems to improve operational capability, readiness, and supportability;
- c. Provides a full range of technical support to Air Force Materiel Command product centers and other Air Force organizations;
- d. Promotes transfer of technology to the private sector;
- e. Maintains leading edge technological expertise in the areas of surveillance, communications, command and control, intelligence, reliability science, electro-magnetic technology, photonics, signal processing, and computational science.

The thrust areas of technical competence include: Surveillance, Communications, Command and Control, Intelligence, Signal Processing, Computer Science and Technology, Electromagnetic Technology, Photonics and Reliability Sciences.